INFORMATION TO USERS

This reproduction was made from a copy of a document sent to us for microfilming. While the most advanced technology has been used to photograph and reproduce this document, the quality of the reproduction is heavily dependent upon the quality of the material submitted.

The following explanation of techniques is provided to help clarify markings or notations which may appear on this reproduction.

1. The sign or "target" for pages apparently lacking from the document photographed is "Missing Page(s)". If it was possible to obtain the missing page(s) or section, they are spliced into the film along with adjacent pages. This may have necessitated cutting through an image and duplicating adjacent pages to assure complete continuity.

2. When an image on the film is obliterated with a round black mark, it is an indication of either blurred copy because of movement during exposure, duplicate copy, or copyrighted materials that should not have been filmed. For blurred pages, a good image of the page can be found in the adjacent frame. If copyrighted materials were deleted, a target note will appear listing the pages in the adjacent frame.

3. When a map, drawing or chart, etc., is part of the material being photographed, a definite method of "sectioning" the material has been followed. It is customary to begin filming at the upper left hand corner of a large sheet and to continue from left to right in equal sections with small overlaps. If necessary, sectioning is continued again—beginning below the first row and continuing on until complete.

4. For illustrations that cannot be satisfactorily reproduced by xerographic means, photographic prints can be purchased at additional cost and inserted into your xerographic copy. These prints are available upon request from the Dissertations Customer Services Department.

5. Some pages in any document may have indistinct print. In all cases the best available copy has been filmed.

University Microfilms International
300 N. Zeeb Road
Ann Arbor, MI 48106

Rogers, John Rice

ABERRATIONS OF UNOBSCURED REFLECTIVE OPTICAL SYSTEMS

The University of Arizona PH.D. 1983

PLEASE NOTE:

In all cases this material has been filmed in the best possible way from the available copy. Problems encountered with this document have been identified here with a check mark __√__.

1. Glossy photographs or pages _____
2. Colored illustrations, paper or print _____
3. Photographs with dark background _____
4. Illustrations are poor copy _____
5. Pages with black marks, not original copy _____
6. Print shows through as there is text on both sides of page _____
7. Indistinct, broken or small print on several pages ✓
8. Print exceeds margin requirements _____
9. Tightly bound copy with print lost in spine _____
10. Computer printout pages with indistinct print _____
11. Page(s) _____ lacking when material received, and not available from school or author.
12. Page(s) _____ seem to be missing in numbering only as text follows.
13. Two pages numbered _____. Text follows.
14. Curling and wrinkled pages _____
15. Other _____

ABERRATIONS OF UNOBSCURED REFLECTIVE OPTICAL SYSTEMS

by

John Rice Rogers

A Dissertation Submitted to the Faculty of the

COMMITTEE ON OPTICAL SCIENCES (GRADUATE)

In Partial Fulfillment of the Requirements
For the Degree of

DOCTOR OF PHILOSOPHY

In the Graduate College

THE UNIVERSITY OF ARIZONA

1 9 8 3

THE UNIVERSITY OF ARIZONA
GRADUATE COLLEGE

As members of the Final Examination Committee, we certify that we have read the dissertation prepared by John Rice Rogers

entitled Aberrations of unobscured reflective optical systems

and recommend that it be accepted as fulfilling the dissertation requirement for the Degree of Doctor of Philosophy.

Roland V. Shack	Date 4/1/83
P N Slater	Date 4/1/83
Robert R Shannon	Date 4/1/83
	Date
	Date

Final approval and acceptance of this dissertation is contingent upon the candidate's submission of the final copy of the dissertation to the Graduate College.

I hereby certify that I have read this dissertation prepared under my direction and recommend that it be accepted as fulfilling the dissertation requirement.

Robert R Shannon
Dissertation Director

4 April 83
Date

STATEMENT BY AUTHOR

This dissertation has been submitted in partial fulfillment of requirements for an advanced degree at The University of Arizona and is deposited in the University Library to be made available to borrowers under rules of the Library.

Brief quotations from this dissertation are allowable without special permission, provided that accurate acknowledgment of source is made. Requests for permission for extended quotation from or reproduction of this manuscript in whole or in part may be granted by the head of the major department or the Dean of the Graduate College when in his judgment the proposed use of the material is in the interests of scholarship. In all other instances, however, permission must be obtained from the author.

SIGNED: John R. Rogers

ACKNOWLEDGMENTS

I would like to thank my advisor, Robert R. Shannon, for his guidance and teaching during the course of my study at the Optical Sciences Center.

A debt of thanks is owed also to Roland V. Shack, with whom I had many helpful discussions on the subject of the vector aberration theory.

I am grateful for the help of Kevin P. Thompson, who took the time to explain his work to me during the hectic final weeks of the preparation of his own dissertation.

John E. Stacy gave me much assistance in matters relating to programming, including the use of some of his ACCOSV "MACRO" files.

My thanks to Sharon Hickey for her diligence in typing the manuscript.

An acknowledgment is owed to the Jet Propulsion Laboratory for funding the research and for providing the necessary computer resources.

Finally, to Martha, I would like to express my gratitude for her support and encouragement during the preparation of this manuscript.

TABLE OF CONTENTS

		Page
	LIST OF ILLUSTRATIONS	vii
	LIST OF TABLES	ix
	ABSTRACT	x
1.	INTRODUCTION	1
	Scope of the Dissertation	2
	Historical Background	4
	Terminology	6
	Structure of the Dissertation	7
2.	GAUSSIAN PROPERTIES	9
	Local Axis	9
	Special Case: Schmidt Systems	10
	Object Parameters	10
	Image Tilt	11
	Keystone Distortion	13
	Anamorphism	22
	Refraction Equations	24
	Pupil Parameters	24
3.	CANONICAL PARAMETERS	28
	Object Parameters	29
	Pupil Parameters	33
	Refraction Equations	37
	Transfer Equations	46
	Conversion from Canonical to Real-Space Parameters	48

TABLE OF CONTENTS -- Continued

		Page
4.	SEIDEL ABERRATIONS	54
	Theoretical Background	54
	Base Sphere Contributions	55
	Aspheric Contributions	55
	Special Cases	55
	Vector Form of Aberrations	56
	Summation of Aberration Fields	57
	Computational Technique	66
	Special Cases	70
	Calculation of the Wave Aberration Coefficients	73
5.	EFFECTS OF GAUSSIAN DISTORTIONS ON THE ABERRATIONS	78
	Effects of Pupil Distortions	80
	Spherical Aberration	86
	Coma	88
	Astigmatism and Field Curvature	88
	Distortion	91
	Effects of Object Distortions	92
	Discussion	94
6.	PROJECTION OF THE IMAGE ONTO THE DETECTOR PLANE	98
	Gaussian Properties	98
	Aberrational Properties	104
7.	ANALYSIS OF UNOBSCURED REFLECTIVE OPTICAL SYSTEMS	109
	Gaussian Properties and Distortion	109
	Aberrational Properties	114
8.	OPTIMIZATION OF UNOBSCURED REFLECTIVE OPTICAL SYSTEMS	125
	Initial Optimization Attempts	126
	Geometrical Interpretation of the Theory	127
	Coma	127
	Astigmatism	131
	Application to a Two Mirror System	137
	Application to a Three Mirror System	140

TABLE OF CONTENTS -- Continued

Page

9. FIELD AVERAGED WAVEFRONT VARIANCE 152

Calculation 153
Applications 160
Discussion 161

10. SUMMARY AND CONCLUSIONS 163

Suggestions for Further Research 164

APPENDIX A: DERIVATION OF THE FIELD AVERAGED MEAN SQUARE WAVEFRONT VARIANCE 166

Term 1 167
Term 2 169
Term 3 169
Term 4 172
Term 5 177

SELECTED BIBLIOGRAPHY 179

LIST OF ILLUSTRATIONS

Figure		Page
2.1.	Computation of Image Tilt Angle	12
2.2.	Variation in Magnification with Object Position	15
2.3.	Rotation of Coordinate Axes	19
2.4.	Transfer of Keystone Distortion	23
3.1.	Geometry of a Tilted and Decentered Object	30
3.2.	Geometry of a Tilted Pupil	34
3.3.	Relating Image Space and Object Space Ray Angles	39
3.4.	Relating Pupil Angles from Object to Image Space	44
4.1.	Vectoral Coordinates of the Object and Pupil	58
4.2.	Computation of Real Object Decentration Angle	69
4.3.	Geometry for Pupil Expansion	71
4.4.	Pupil Coordinates used by ACCOSV	75
5.1.	Relating Local and OAR Pupil Coordinates	82
5.2.	Relating Gaussian and Local Pupil Coordinates	84
6.1.	Separation of Gaussian Image and Detector Plane	99
6.2	Projecting the Gaussian Image onto the Detector Plane	101
6.3.	Projecting the Aberrations onto the Detector Plane	107
7.1.	Layout of System 1	110
7.2.	Anamorphic and Keystone Distortion of a Regular Grid	111
7.3.	Distortion Plot for System 1	113
7.4.	Distortion Plot for System 2	115

LIST OF ILLUSTRATIONS -- Continued

Figure		Page
7.5.	Layout of System 3	116
7.6.	Ray Fans for System 3 at $H_y = 0$, $H_x = 0$	117
7.7.	Ray Fans for System 3 at $H_y = 0$, $H_x = 1$	118
7.8.	Field-Difference Fans for System 3	120
7.9.	Distortion Plot for System 3	121
7.10.	Layout of System 4	123
7.11.	Ray Fans for System 4 at $H_y = 0$, $H_x = 0$	124
8.1.	Magnitudes of Two Coma Fields	129
8.2.	Locating the Resultant Coma Node	130
8.3.	Magnitudes of Two Quadratic Astigmatism Fields	132
8.4.	Locating the Resultant Astigmatism Node	133
8.5.	Magnitude of Binodal Astigmatism	135
8.6.	Orientation Plot for Binodal Astigmatism	136
8.7.	Node Locations and Magnitudes for System 4	141
8.8.	Aberration Magnitudes for System 4	142
8.9.	Aberration Magnitudes for a possible Tertiary Mirror	144
8.10.	Aberration Magnitudes for the preferred Tertiary Mirror	148
8.11.	Layout of Final Three Mirror System	149
8.12.	Spot Diagrams for Three Mirror System	150

LIST OF TABLES

Table		Page
2.1	Refraction Equations for the Object Parameters	25
2.2	Refraction Equations for the Pupil Parameters	27
3.1	Equations defining the Canonical Parameters	38
3.2	Refraction Equations for the Canonical Parameters	47
3.3	Transfer Equations for the Canonical Parameters	49
3.4	Conversion from Canonical to Real Space Parameters	52
4.1	Conversion from ACCOSV to Wave Aberration Coefficients	77
5.1	Aberrational Consequences of Gaussian Distortions of the Pupil	93
5.2	Aberrational Consequences of Gaussian Distortions of the Object	95
8.1	Aberration Coefficients for System 3	138
8.2	Aberration Coefficients for System 4	145
8.3	Signs of Coma and Astigmatism for Tertiary Mirrors of Several Types	146

ABSTRACT

The primary distinction between an ordinary optical system and one which is both unobscured and reflective is that the elements of the latter must be tilted or decentered with respect to one another. In general, this results in an optical system which has no axis of rotational symmetry, and therefore the classical aberration theory of symmetric systems is no longer applicable. Furthermore, the image becomes anamorphic and keystone distorted, due to the relative tilt between the object and the optical surfaces.

The first part of this work is the development of a semi-analytic treatment of the properties (through third order) of systems possessing large tilts and decentrations. The Gaussian properties of both the image and pupil are described in terms of tilt, decentration, magnification, keystone distortion, and anamorphic distortion parameters. In computing these parameters, it is important to take into account the transferred components of the parameters, which are due to the Gaussian properties of the preceding surfaces. The third order properties are computed using the fact that each optical surface, together with its associated entrance pupil, form an optical subsystem which possesses an axis of approximate symmetry. About this axis, the aberration contributions of that surface may be described in the classical wave

aberration expansion. The coefficients in this expansion may be corrected for the non-circular appearance of both the object and pupil, using the parametric description of their Gaussian form. Because the field of view of the system is not aligned with this axis, the node or center of the aberration field is displaced from the center of the field of view. The aberration fields due to the various surface contributions are then combined vectorally to yield the resultant aberration field in the image plane.

Using aberration coefficients derived from the transverse ray error terms of the lens design program ACCOSV, the vector theory is applied to the analysis of several optical systems, and the accuracy of the theory verified by comparison with raytrace data. As a demonstration of the usefulness of the theory to an optical designer, a three mirror unobscured system was designed using a methodology derived from the theory. At each step, the design options are explained, and the probable results are discussed. The residual aberrations of the resulting system are studied, and the selection of anotner design starting point is discussed from the point of view of the theory.

Finally, the field average of the mean square wavefront variance is developed from the third-order theory, and applied as a figure of merit to two systems. The advantages and limitations of this figure of merit are discussed.

CHAPTER 1

INTRODUCTION

Presently, in the fields of astronomy and remote sensing, there is an increasing interest in unobscured all-reflecting optical systems. The tendency toward all-reflecting systems is necessitated by the trend toward imaging systems operating in the ultraviolet and infrared regions of the spectrum, where the number of glasses available for transmission elements is limited. Even in applications using the visible region of the spectrum, the reflecting system's freedom from chromatic aberrations is a significant advantage. Unfortunately, the obscuration caused by the secondary element or film plane in a classical, axially symmetric reflecting telescope causes several significant undesirable effects. The primary image is restricted to be smaller than the central obscuration, thus limiting the field of view of the telescope. The diffraction caused by the central obscuration decreases the resolution in the intermediate spatial frequencies, even in the absence of aberrations; furthermore, the resolution at high spatial frequencies is increased. (Although this latter effect may seem to be an advantage, it is sometimes a disadvantage if the image is to be sampled with a periodic array of detectors due to the phenomenon known as aliasing.) Only by tilting or decentering the elements sufficiently to move the subsequent elements out of the way of the incoming beam can the designer simultaneously

avoid the problems caused by the obscuration and still have an entirely reflecting system.

In general, the resulting system no longer has an axis of rotational symmetry. This reduction in symmetry causes a significant increase in the complexity of the image behavior. Buchdanl (1970) shows that while a rotationally symmetric optical system possesses five primary or "third order" aberrations, a system having only two meridional planes of symmetry has 19 third order aberrations and a system with no symmetry at all has 35 such terms. Clearly, an analytic aberration theory to describe systems of this type would be of limited use due to its inherent complexity. For this reason, the imagery of such systems is usually described by interpretation of ray trace data at sample points in the image field.

Among unobscured optical systems, the class of systems consisting of tilted and decentered elements which are individually rotationally symmetric is of particular interest, for these surfaces are the easiest to manufacture. Additionally, the theory of rotationally symmetric optical systems may be extended in a straightforward manner to include this class of systems.

Scope of the Dissertation

This work is the development of a semi-analytic theory covering the image properties of systems composed of rotationally symmetric elements which have been tilted or decentered in one plane only, so that the system has one meridional plane of symmetry. (This latter restriction is made in order to simplify the description of the Gaussian properties of the systems; the Seidel aberration theory developed in

Chapter 3 requires no such symmetry.) The term semi-analytic is used to describe this treatment, for it is based on both analytical formulation and ray trace data for two "real" rays. Although the impetus for this work comes from the need to design unobscured all-reflecting optical systems, the work is applicable to systems containing refracting components as well. It is assumed that the reader is familiar with the properties of rotationally symmetric optical systems, through third order.

The rationale in developing a primarily analytic theory rather than one based on the interpretation of ray trace data is based on several reasons. 1) An analytic theory requires far less computational time than one based on real rays. 2) The field dependence for each aberration is given explicitly by the theory, eliminating the need to sample the image field. (3) The theory provides the designer with image quality information in terms with which he is familiar (e.g., coma, astigmatism, etc.) providing him with useful insight into the relationships between the constructional parameters of the system (curvatures, tilt angles, etc.) and the behavior of the system. 4) An analytic description furthermore lends itself more readily to a parameterization of the image quality.

Even though a third order analysis cannot adequately describe a complicated optical system containing high order aspherics, such an analysis will still be useful in the early stages of the design of that system.

Historical Background

Early attempts to study the aberrations of non-rotationally symmetric optical systems involved the application of perturbation theory to symmetrical optical systems which were slightly disturbed. Conrady (1919) used this approach and showed that such systems would produce imagery with the same wavefront forms as coma, astigmatism, and distortion at the center of the image field. Epstein (1949) performed a similar analysis and concluded that in wide aperture, narrow field systems, small decentrations of the elements would produce coma, while in wide field systems of low numerical aperture, distortion would result. Ukita and Tsujiuchi (1954) also studied the "axial" behavior of symmetric systems with small perturbations. Ruben (1964) pointed out that the decentration of an element could be regarded as a shift of the aperture stop, and computed axial values for the third order aberrations based on the stop-shift equations of Hopkins (1950).

Another approach to the study of aberrations in general is that of tracing an exact ray through the system for some given field point, and developing an analytical expansion of the refraction and transfer equations about that ray. Weinstein (1949, 1950) used this technique to develop aberration coefficients for off-axis field points in symmetrical optical systems, and estimated that this method was four times faster than fitting curves to numerically traced data. Sands (1967) extended this approach to include field points in a region around the exact ray traced. He pointed out that although his technique was intended to

provide wide field information for a symmetrical system, it was applicable to an asymmetrical system as well. Hopkins (1976) used this same technique to compute the aberration coefficients up to seventh order for symmetric systems. Buchdahl (1954) extended this approach, developing an iterative process for computing the aberration coefficients of asymmetrical systems.

Several authors have studied the image quality of optical systems in closed form, rather than in terms of aberration coefficients. Hopkins (1946) studied the sagittal and tangential focal surfaces of optical systems using the concept that these two orientations have two distinct focal lengths. Shearer (1950) used this technique to study the imagery of cross-tilted spherical mirrors. Prasad, Mitra and Jain (1975) computed the aberrations of plane refracting surfaces on a noncollimated beam. Hofmann and Klebe (1965) derived the differential equations describing the surface profiles required to give aberration-free imagery, allowing the possibility of surface decentrations. Korsch (1974) used Fermat's principle to develop design equations for an all-reflective Schmidt system. He later (Korsch, 1980a and 1980b) developed the equations describing the surface profiles for strictly aplanatic two- and three-mirror systems.

The principle on which this work is based is that each surface possesses an axis of symmetry, about which the aberrations of that surface may be found in the normal fashion. Buchroeder (1976) used this principle to develop design techniques for tilted component optical systems. Thompson (1980) used vector algebra to combine the aberration

fields of several surfaces, obtaining a description of the aberrations (including the field dependence) to fifth order.

Two other authors deserve mention. Burch (1942) pointed out that the field aberrations may be regarded as a manifestation of the decentration of the pupil in the presence of spherical aberration. Linfoot (1946) applied this approach in reverse to calculate the aberrations of decentered aspheric plates. This technique is applicable to the computation of the aberrations of Schmidt systems.

Terminology

It is common practice among lens designers to use the terms paraxial, first order, and Gaussian interchangeably, when referring to such properties of optical systems as magnification and image position. This practice is correct when referring to symmetric systems, for these properties may be found equally well by executing a paraxial ray trace, by considering only the properties of the image which vary as the first power of the field and pupil coordinates, or by considering the cardinal points of a surface.

For nonrotationally symmetric systems, these terms are no longer interchangeable, and their misuse would lead to confusion. The term paraxial is obviously improper, for such a system has no unique axis. Referring to the properties only by their order number would be equally confusing, for in Chapter 2 we shall derive Gaussian properties depending on all powers of the field, and in Chapters 4 and 5 we shall find that some of the so-called "third order" aberrations will develop terms with first order dependences. Accordingly, those properties which are derived

from the cardinal points of a surface will be referred to as Gaussian properties, and those which arise from the ordinary third order aberrations will be called Seidel aberrations.

Structure of the Dissertation

The structure of the dissertation is as follows: Chapter 2 develops the Gaussian properties of tilted and decentered optical systems, in terms of variables describing the actual image (real-space parameters). Chapter 3 develops a set of canonical parameters which are useful for computational purposes. This treatment is an extension of Hopkins (in press). Chapter 4 develops the aberration theory resulting from the Seidel aberrations. This chapter is an extension of the work by Thompson (1980) on the aberration fields of rotationally symmetric designs suffering alignment errors. Chapter 5 addresses the interaction between the Gaussian distortions of the object and entrance pupil for a particular surface and the Seidel aberrations for that surface. In Chapter 6, the relationship between the aberration coefficients for a system and the transverse ray errors at the detector plane is developed. Chapter 7 demonstrates the application of the theory to the analysis of several systems, and the accuracy of the theory as measured against ray trace data is shown. In Chapter 8, the vector aberration concept is applied to the design of an unobscured reflective optical system. The aberrations of a two mirror starting point are discussed, and an appropriate tertiary mirror is selected to balance the aberrations. In Chapter 9, a useful parameter for describing the image behavior is developed, and its possible application as a merit function in an

automatic design procedure is discussed. Chapter 10 summarizes the work and suggestions for further research are made.

CHAPTER 2

GAUSSIAN PROPERTIES

The properties discussed in this chapter are those which may be derived using only the principal planes and focal points of the individual surfaces, and the locations of the centers of the entrance pupils for those surfaces. Aspheric departures of the surfaces and distortions of the pupils need not be considered, for they affect only the aberrations and not the Gaussian properties. The term base sphere will be used to mean the surface with its aspheric departure terms removed.

Local Axis

Central to the method employed in this work is the realization that a single surface and its entrance pupil form an optical system which is rotationally symmetric about the line joining the center of curvature of that surface and the entrance pupil for that surface. The principal planes for that surface are coincident and lie normal to the local axis at the point where it pierces the base sphere. Except for the fact that the object may be displaced from this axis and may be tilted with respect to the principal planes, the optical system defined about this axis behaves as an ordinary symmetric system.

Special case: Schmidt systems

If the entrance pupil for a surface coincides with the center of curvature, as in a Schmidt camera, the axis described above does not exist. If the entrance pupil is nearly coincident with the center of curvature, but shifted slightly in a direction transverse to the direction of propagation of the pencil of light, then a line could be drawn from the center through the pupil; however, this line would not be an appropriate optical axis for the calculation of either Gaussian or aberrational quantities. Although no Schmidt systems are analyzed in this dissertation, the appropriate axis to choose in these cases is the line joining the object and the center of curvature, for the system is rotationally symmetric about this axis with the exception that the pupil, rather than the object, is decentered and tilted.

Object Parameters

It is obvious that the decentration of an object will cause its image to be decentered, and that a tilted object will produce a tilted image. Only slightly less obvious is the fact that the tilted object appears foreshortened in the direction of its tilt, when viewed from the optical system. This effect causes the effective object size in the direction of tilt to be less than that in the orthogonal direction, and is known as anamorphism. Also related to the tilt is the fact that one end of the object is closer to the optical system than the other, causing a variation in magnification with position on the object. This effect is familiar to photographers as keystone distortion. Buchroeder (1976) derived the mathematical form of the image of a tilted, decentered

object using the principle of collineation. Here, the form of the image will be derived directly from the system parameters.

Image Tilt

Figure 2.1 shows a refracting surface together with an object/image pair which is decentered and tilted with respect to the axis. Unless otherwise noted, all figures and equations in this work will conform to the following conventions: 1) The coordinate axes will have their origin at the (coincident) principal points of the optical surface, with the z - axis aligned with the local axis. 2) The y - axis is aligned with the common direction of all tilts and decentrations. 3) Image-space quantities will be denoted by the use of a prime ('). 4). Angles representing a counter-clockwise rotation from the appropriate reference line are taken as positive.

The image tilt angle may be found simply by considering the ray which passes through all object points in the y-z plane before striking the principal plane at y_p. This ray must also pass through all the image points in this meridian. Let Y_0 and Y_0' be parameters describing the decentration of the object and image, while Z_0 and Z_0' represent their longitudinal positions, respectively. Defining T_ε to be the tangent of the object tilt angle, then

$$T_\varepsilon = \frac{Z_0}{y_p - Y_0} \tag{2.1}$$

and

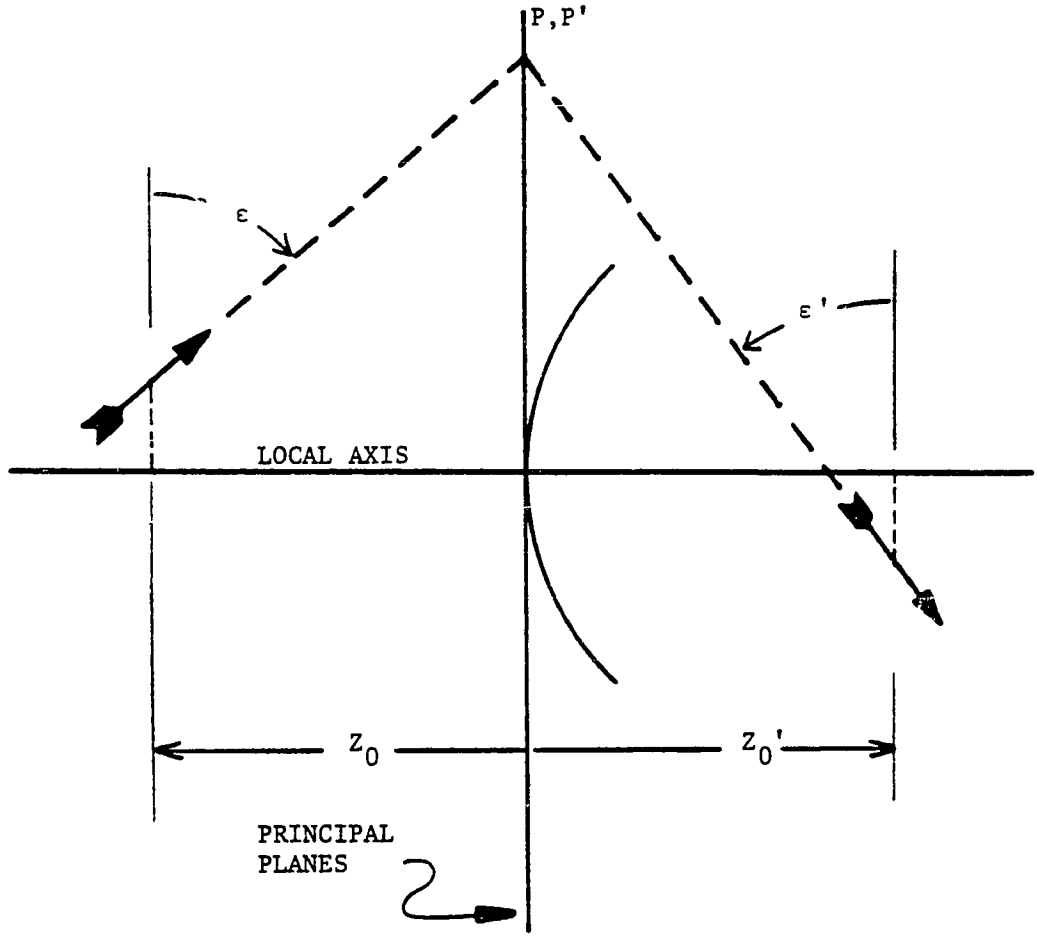

Figure 2.1. Computation of Image Tilt Angle.

$$T_\varepsilon' = \frac{Z_0'}{y_p - Y_0'}. \tag{2.2}$$

These equations may be combined to yield a conjugate relation for the tangent of the tilt angle

$$T_\varepsilon' = \frac{T_\varepsilon Z_0'}{Z_0 + T_\varepsilon(Y_0 - Y_0')}. \tag{2.3}$$

This expression becomes indeterminate when the object resides on the surface ($z = z' = 0$), in which case $T_\varepsilon' = T_\varepsilon$.

Keystone Distortion

In order to define a convenient parameter to describe keystone distortion, it is first necessary to consider the shape of the image of a tilted but undistorted object. Such an object may be described by the equations:

$$x = X_1 H_x , \tag{2.4}$$

$$y = Y_0 + Y_1 H_y \tag{2.5}$$

and

$$z = Z_0 + Z_1 H_y. \tag{2.6}$$

where H_x and H_y are the fractional object coordinates measured in the

plane of the object.

Consider now the variation in magnification with longitudinal position. Figure 2.2 shows an object of arbitrary height y and position z. The magnification of the system is determined by the single ray through the front focal point which emerges parallel to the axis. Considering the similar triangles shows that

$$m \equiv \frac{y'}{y} = \frac{f}{f-z}. \tag{2.7}$$

Reference to Figure 2.1 shows that

$$z = Z_0 - T_\varepsilon(y-Y_0). \tag{2.8}$$

Using Eqs. (2.5) and (2.6) the value of Z_1 for an undistorted object is found to be

$$Z_1 = -T_\varepsilon Y_1. \tag{2.9}$$

Next, Equation (2.6) may be used to yield the dependence of the magnification on the field parameter H_y,

$$m = \frac{f}{f - Z_0 - Z_1 H_y}, \tag{2.10}$$

which reduces to

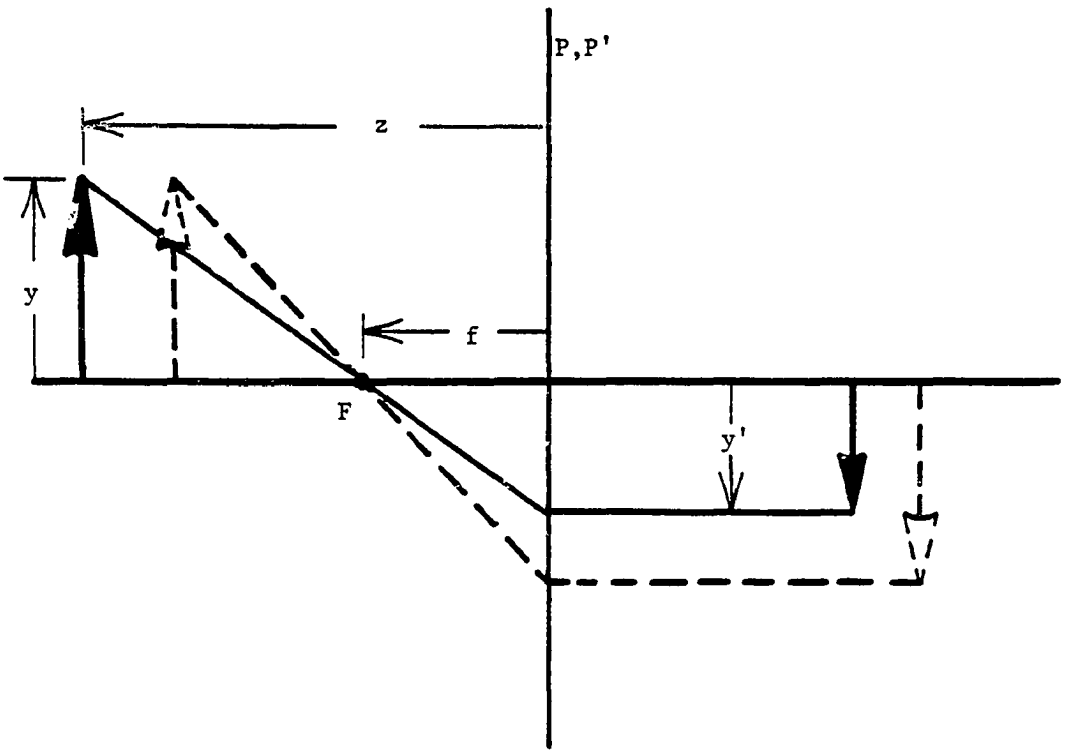

Figure 2.2. Variation of Magnification with Object Position.

$$m = \frac{m_0}{1 - \left[\frac{Z_1}{f-Z_0}\right]} H_y, \tag{2.11}$$

where

$$m_0 \equiv \frac{f}{f - Z_0} \tag{2.12}$$

may be recognized as the magnification at the center of the field. The initial keystone parameter K may now be defined as

$$K \equiv \frac{Z_1}{f - Z_0}. \tag{2.13}$$

The form of the image may be found by multiplying the object height (Equation 2.5) by the magnification (Equation 2.11) to yield

$$y' = \frac{Y_0' + Y_1'(H_y)}{1-K(H_y)}, \tag{2.14}$$

where

$$Y_0' \equiv m_0 Y_0 \tag{2.15}$$

$$Y_1' \equiv m_0 Y_1. \tag{2.16}$$

Applying the field dependent magnification to the x-coordinate (Equation

2.4) yields

$$x' = \frac{X_1'(H_y)}{1-KH_y}, \tag{2.17}$$

where

$$X_1' = m_0 X_1. \tag{2.18}$$

To find the form of z for the image, Eq. (2.14) may be inserted for y' in the image-space version of Equation (2.8), yielding

$$z' = \frac{Z_0' + Z_1' H_y}{1 - KH_y}. \tag{2.19}$$

where

$$Z_1' \equiv -K'Z_0' - T\varepsilon' (Y_1' + Y_0'K') \tag{2.20}$$

and Z_0' is the Gaussian image distance associated with the object distance Z_0. We have found the form of the image of a tilted, decentered, but undistorted object.

To find the form of the image of an object which is distorted, Equations (2.14) and (2.17) must be treated as descriptions of the object (dropping the primes) and re-apply the magnification. This exercise will also yield the general relations relating conjugate pairs of the parameters Y_0, Y_1, X_1, and K. Combining Equations (2.7) and (2.19) yields

the magnification as a function of the field variable,

$$m = \frac{f(1-KH_y)}{(f-Z_0) - (fK + Z_1)H_y}. \tag{2.21}$$

Applying this to the object yields the y-height of the image,

$$y' = \frac{f(Y_0 + Y_1 H_y)}{(f-Z_0) - (fK + Z_1)H_y}. \tag{2.22}$$

This may be put into the same form as Equation (2.14) by dividing both numerator and denominator by $(f-Z_0)$ and making the identification

$$K' \equiv m_0\left[K + \frac{Z_1}{f}\right]. \tag{2.23}$$

The x-coordinate resulting from this second imaging process is also of the same form as the object (Equation 2.17).

It has now been shown that an object whose form is given by Equations (2.14), (2.17), and (2.19) causes an image of the same mathematical form to be produced. It remains to be shown that this form is also unaltered when the coordinate axes are rotated from the local axis of one optical surface to that of the next. Consider Figure 2.3 with the distances a, b, c, and d as shown. The following facts are evident from the figure:

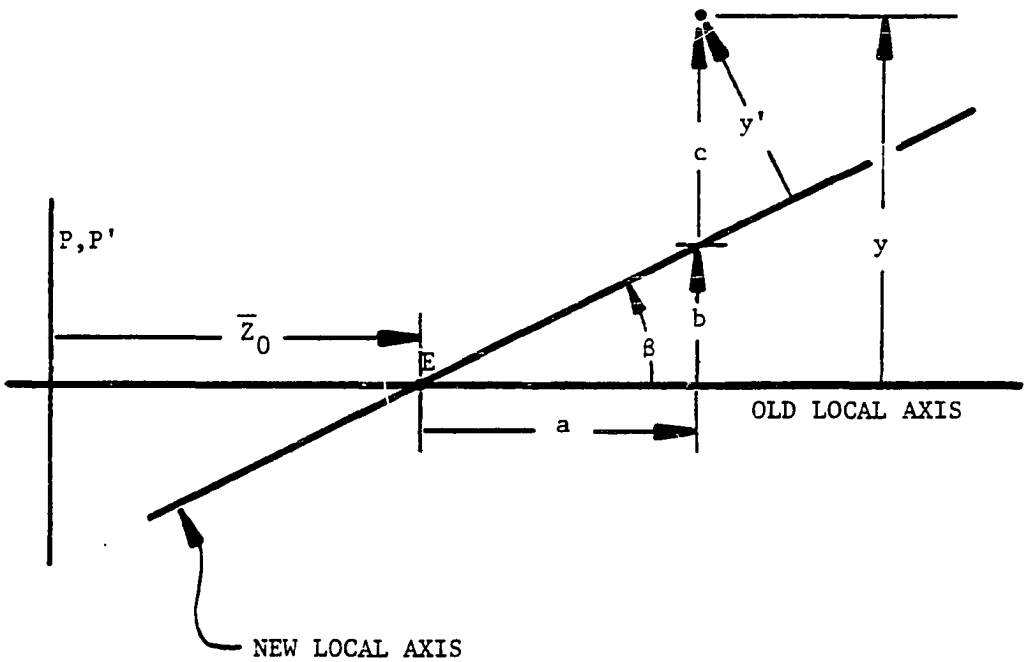

Figure 2.3. Rotation of Coordinate Axes.

$$a = z - \overline{Z}_0,$$

$$b = a(\tan\beta),$$

$$c = y - b,$$

and

$$y' = c(\cos\beta).$$

Combining these yields

$$y' = (y-(z-\overline{Z}_0)\tan\beta)\cos\beta. \tag{2.24}$$

Using Equations (2.14) and (2.19) for y and z, and simplifying, one obtains

$$y = \frac{(Y_0\cos\beta - (Z_0-\overline{Z}_0)\sin\beta) + (Y_1\cos\beta - (Z_1+\overline{Z}_0K)\sin\beta)H_y}{1 - KH_y}. \tag{2.25}$$

This is the same form as Eq. (2.14), with the constants Y_0 and Y_1 changed. It is significant that the keystone parameter K has not changed its value, for this means that the keystone parameter in the denominator of the y-expression (Equations (2.14) and (2.25) remains the same as that for the x-expression (Eq. (2.17)). (It is taken as obvious that since the value of x is unaltered by the tilt of the axes in the y-z plane, the

expression for x is unchanged.) It has now been shown that the parameters Y_0, Y_1, X_1 and K are sufficient for describing the object/image pairs, for the image always remains of the same form.

At this point, it is useful to examine the nature of the keystone distorted image. For the purposes of this discussion the decentration will be assumed to be zero. Expanding Equation (2.14) into the customary form of a power series in H_y yields

$$y' = Y_1' H_y [1 + KH_y + K^2 H_y^2 + K^3 H_y^3 + \ldots]. \tag{2.26}$$

Recognizing the first term as the traditional first-order image, the remaining terms constitute the keystone distortion, which has the form

$$\Delta y' = Y_1' [KH_y^2 + K^2 H_y^3 + \ldots]. \tag{2.27}$$

Similarly, the x-component of the distortion may be expanded to yield

$$\Delta x' = X_1 [KH_x H_y + K^2 H_x H_y^2 + \ldots]. \tag{2.28}$$

As can be seen, the keystone distortion contains terms in all powers of the field beyond the first, with each term diminishing from the previous term by a factor of K. The physical significance of the parameter K may be seen by noting that the terms in K^2 and higher powers will be small. Thus, the distortion is approximately equal to K times the image height times a second-order factor in the field variables. The parameter K is

therefore approximately equal to the fractional distortion at the edge of the field.

An unusual property of keystone distortion is that it cannot be treated as the sum of individual surface contributions, for the distortion at one surface has a strong dependence on the distortion induced by previous surfaces. This is in direct contrast to the ordinary third order aberrations of symmetrical systems which cannot depend on aberrations of that same order at earlier surfaces. The transferred component of keystone distortion may be seen in Figure 2.4, which shows a tilted object and two 1:1 relays. Rays 1 and 2 emerge from an untilted object and form an untilted image, for reference. Rays 1 and 3 locate the tilted and distorted image of the tilted version of the object. Also drawn is an undistorted but tilted image. The distortion induced by lens 1 is labeled Δy_1. Treating the three images as objects, three rays are drawn through the second lens. Ray 4 yields the height of the undistorted reference image. Ray 5 yields the height of the actual, fully distorted image, and the distortion of the combination of lenses is labeled $\Delta y_{(1+2)}$. Ray 6 is drawn from the tilted but undistorted object, yielding the distortion of the second lens, Δy_2. It may be seen at a glance that the overall distortion $\Delta y_{(1+2)}$ is not even approximately equal to the sum of the individual contributions, Δy_1 and Δy_2.

Anamorphism

The anamorphism caused by a rigid rotation of an object from a position normal to the axis to a tilted position is given simply by a cosine factor applied to the y- coordinate of the object. For the initial object, this means that $Y_1 = X_1 \cos\alpha_1$ where α is the tilt angle of

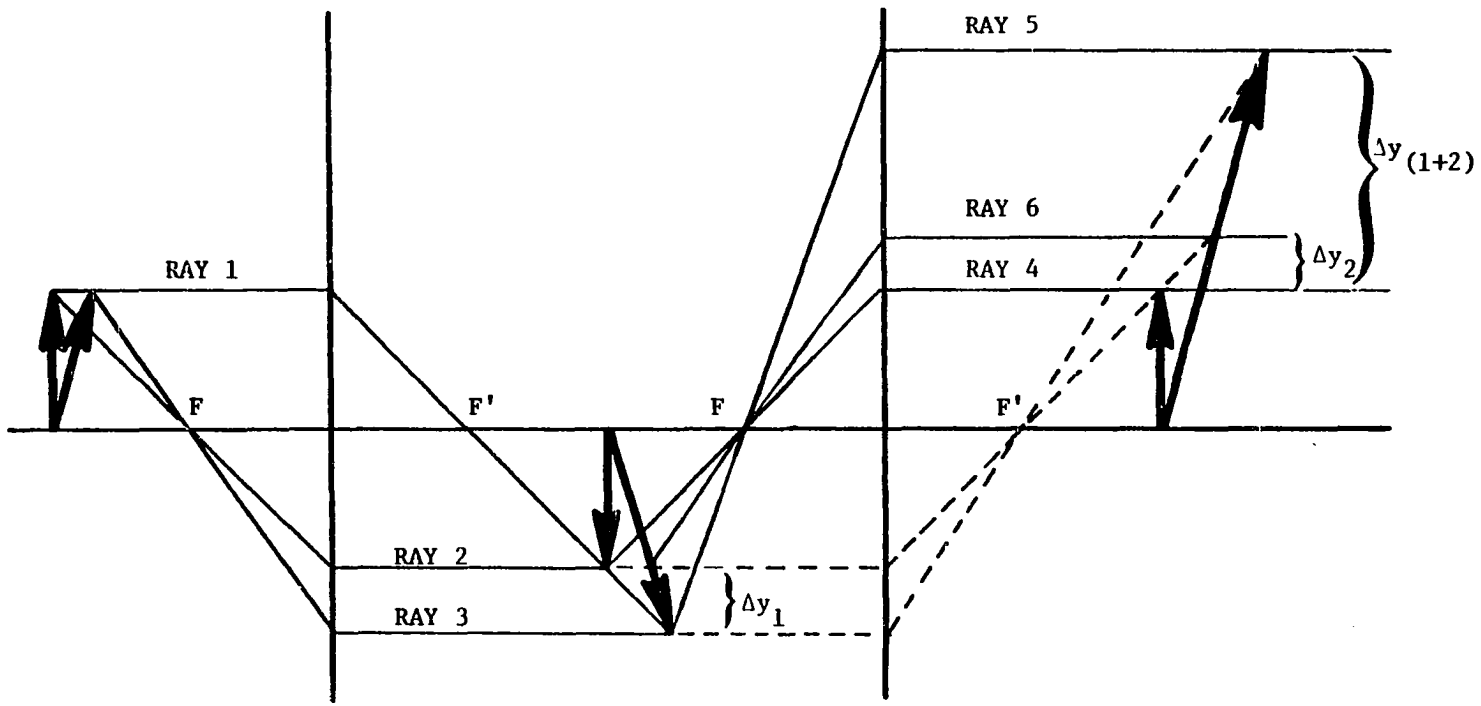

Figure 2.4. Transfer of Keystone Distortion.

the object. Equations (2.15) and (2.18) show that the ratio of Y_1 to X_1 does not change upon imaging; however, this ratio will change at the next optical surface, if its local axis is tilted with respect to this one. The transformation of the parameters from image space to the object space of the next optical surface is best treated with the canonical variables described in the next chapter.

Refraction Equations

The equations relating the object-space parameters to their image space equivalents have been derived above, and are summarized in Table 2.1 for reference.

Pupil Parameters

Although the parameters derived above are explicitly for the description of the properties of the object and image, the entrance and exit pupils will also have the same properties. An analogous set of parameters and conjugate relations is appropriate, and the inclusion of an overbar ($\bar{}$) will be used to denote pupil, rather than object coordinates. Using ρ_x and ρ_y as the fractional coordinates of an undistorted pupil, the actual pupil coordinates are of the form

$$\bar{y} = \frac{\bar{Y}_1 \rho_y}{1 - \bar{K}\rho_y}, \tag{2.29}$$

$$\bar{x} = \frac{\bar{X}_1 \rho_x}{1 - \bar{K}\rho_y}, \tag{2.30}$$

Table 2.1 Refraction Equations for the Object Parameters

$$T_\varepsilon' = \frac{T_\varepsilon Z_0'}{Z_0 + T_\varepsilon(T_0 - Y_0')} \tag{2.3}$$

$$Y_0' = m_0 Y_0 \tag{2.15}$$

$$Y_1' = m_0 Y_1 \tag{2.16}$$

$$X_1' = m_0 X_1 \tag{2.18}$$

$$K' = m_0\left[K + \frac{Z_1}{f}\right] \tag{2.23}$$

where

$$m_0 \equiv \frac{f}{f - Z_0} \tag{2.12}$$

is the magnification at the center of the object.

and

$$\bar{z} = \frac{\bar{Z}_0 + \bar{Z}_1 \rho_y}{1 - \bar{K}\rho_y}. \tag{2.31}$$

Note that $\bar{y}$ has no constant (independent of ρ_y) term, since the pupil is by definition on the local axis. The refraction equations for the pupil parameters may be derived in direct analogy with those for the object parameters, and are listed in Table 2.2.

Table 2.2 Refraction Equations for the Pupil Parameters

$$\overline{T}_\varepsilon' = \frac{\overline{T}_\varepsilon \overline{Z}_0'}{\overline{Z}_0 + \overline{T}_\varepsilon T_0} \tag{2.32}$$

$$\overline{Y}_0' = \overline{m}_0 \overline{Y}_0 \tag{2.33}$$

$$\overline{Y}_0' = \overline{m}_0 \overline{Y}_0 \tag{2.34}$$

$$\overline{X}_1' = \overline{m}_0 \overline{X}_1 \tag{2.35}$$

$$\overline{K}' = \overline{m}_0 \left[\overline{K} + \frac{\overline{Z}_1}{f} \right] \tag{2.36}$$

where

$$\overline{m}_0 \equiv \frac{f}{f - \overline{Z}_0} \tag{2.37}$$

is the magnification at the center of the pupil.

CHAPTER 3

CANONICAL PARAMETERS

The real-space parameters developed in the previous chapter suffer several drawbacks. For infinite object or pupil positions, some of the parameters will themselves become infinite; although this accurately reflects the properties of the object or pupil, calculations for subsequent optical surfaces become difficult. Additionally, these parameters must be transformed at each surface due to the inclination of the new local axis with respect to the present one.

Hopkins (1983) suggests the use of canonical variables which are the product of the image height and the angular subtent of the pupil as viewed from the object. Alternatively, they may be regarded as the product of the pupil height and the angular subtent of the object, as viewed from the image. These variables remain non-zero and finite for all object and pupil positions, for if the object becomes infinitely large, it must be located at infinity, and the pupil angle is therefore infinitely small. This chapter extends this concept to the case of tilted, decentered objects and tilted pupils. In the special case of the Schmidt system, the object and image are on-axis but tilted, and the pupils are decentered (from the local axis) and tilted. In this case the roles of the canonical variables are simply switched; the same definitions and transformations apply.

Object Parameters

The canonical parameters used here will be similar to those of Hopkins (1983) in that they will be the product of an angular measure of the object and a linear measure of the pupil. In Chapter 2 it was noted that the nonlinearities of the image shape in both the x- and y-directions may be represented by a single parameter, K. Once this parameter is known, it is possible to describe arbitrary positions on the object in terms of angles measured from the line OE joining the object and pupil, as shown in Figure 3.1.

It is now convenient to define a variable which will be used throughout this chapter. Let Z_{EO} be the distance along the local axis from the pupil to the object center, as shown in the figure. Thus,

$$Z_{EO} \equiv Z_O - \overline{Z}_O. \tag{3.1}$$

Defining now the quantity

$$T_X \equiv n\overline{X}_1 \tan\alpha_X, \tag{3.2}$$

and referring to Figure 3.1, we see that

$$T_X = \frac{n\overline{X}_1 X_1 H_X}{Z_{EO}} \cos\alpha_O. \tag{3.3}$$

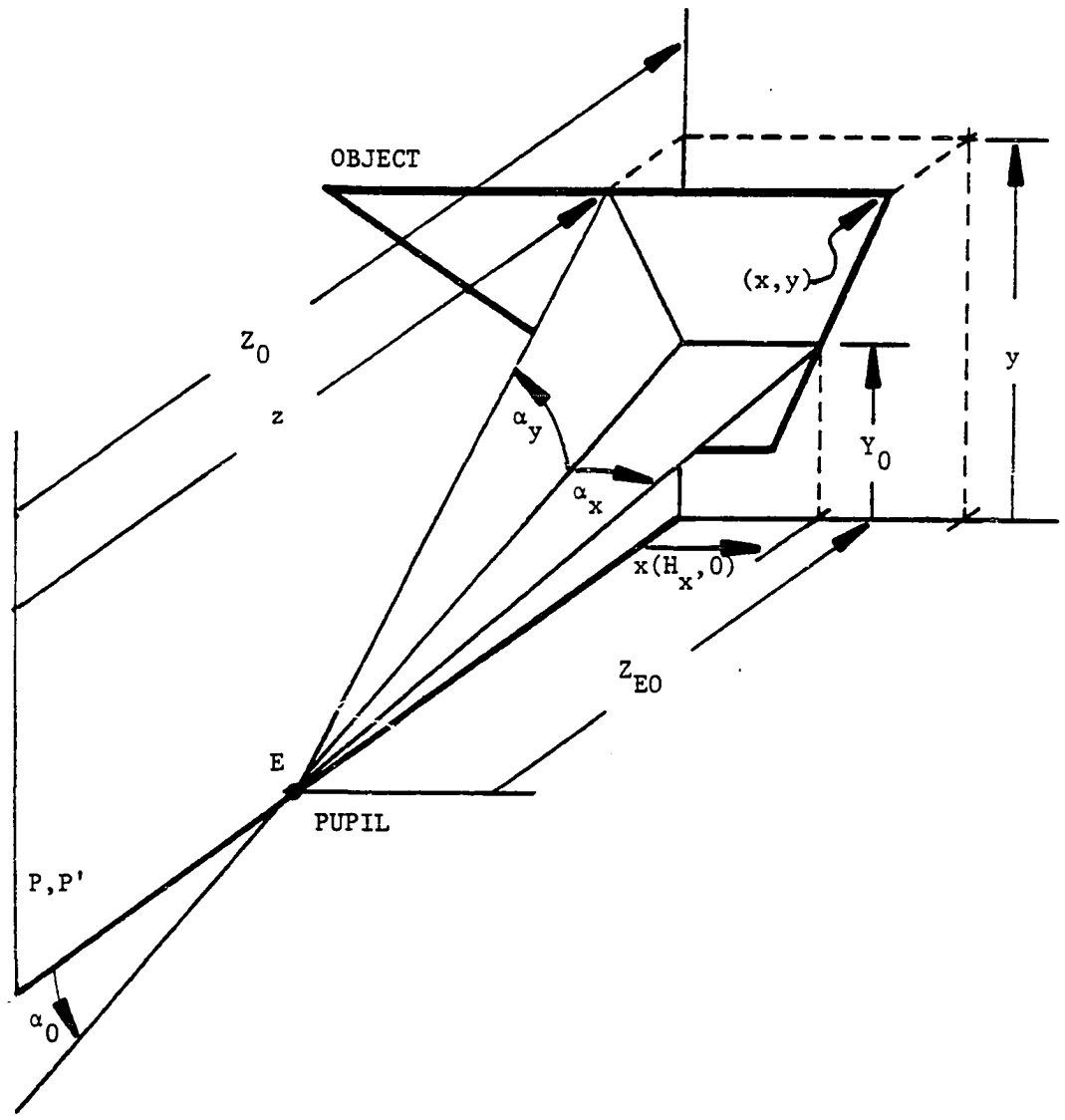

Figure 3.1. Geometry of a Tilted and Decentered Object.

Thus we define the parameter

$$T_{X1} \equiv \frac{n\bar{X}_1 X_1}{Z_{EO}} \cos\alpha_0 \tag{3.4}$$

as the linear coefficient of H_x in Eq. (3.3).

To find the canonical parameters in the y-direction, it will be necessary to refer to the trigonometric identity for the tangent of the sum of two angles,

$$\tan(\alpha + \beta) = \frac{\tan\alpha + \tan\beta}{1 - (\tan\alpha)(\tan\beta)}. \tag{3.5}$$

Since the quantity $\tan\alpha_0$ will appear frequently in what is to follow, it is convenient to define it as a formal parameter of the system. From the figure one may see that

$$T_0 \equiv \tan\alpha_0 = \frac{Y_0}{Z_{EO}}. \tag{3.6}$$

It is also clear that

$$\tan(\alpha_0 + \alpha_y) = \frac{y}{Z - \bar{Z}_0}. \tag{3.7}$$

Using the identity of Eq. (3.5), and solving for $\tan\alpha_y$, and simplifying

using Eq. (3.6), one obtains

$$\tan\alpha_y = \frac{y - T_0(z - \bar{Z}_0)}{(z - \bar{Z}_0) + yT_0}. \tag{3.8}$$

Using Eqs. (2.8) and (2.14) to replace z and y, and simplifying using Eq. (3.1) yields

$$\tan\alpha_y = \frac{(y_1 + KY_0)(1 + T_0T_\varepsilon)H_y}{(Z_{E0} + Y_0T_0) - [Z_{E0}K(1 + T_0T_\varepsilon) + Y_1(T_\varepsilon - T_0)]H_y}. \tag{3.9}$$

This may be further simplified using the trigonometric identity

$$\cos\theta = \frac{1}{\sqrt{1 + \tan^2\theta}}. \tag{3.10}$$

Factoring Z_{E0} out of the denominator of Eq. (3.9) and applying this identity, one obtains

$$\tan\alpha_y = \frac{(Y_1 + KY_0)(1 + T_0T_\varepsilon)H_y}{(Z_{E0}/\cos^2\alpha_0) - [Z_{E0}\,K(1 + T_0T_\varepsilon) + Y_1(T_\varepsilon - T_0)]H_y}. \tag{3.11}$$

Defining the quantity

$$T_y \equiv n\bar{X}_1\tan\alpha_y, \tag{3.12}$$

one may see that T_y is of the form:

$$T_y = \frac{T_{Y1} H_y}{(1 - K_T H_y)}, \tag{3.13}$$

where

$$T_{Y1} \equiv \frac{n\bar{X}_1(Y_1 + KY_0)(1 + T_0 T_\varepsilon)\cos^2\alpha_0}{Z_{E0}} \tag{3.14}$$

and

$$K_T \equiv \left[K(1 + T_0 T_\varepsilon) + \frac{Y_1(T_\varepsilon - T_0)}{Z_{E0}}\right] \cos^2\alpha_0. \tag{3.15}$$

Pupil Parameters

The canonical pupil parameters will be defined (in direct analogy with the object parameters) as the product of a linear measure of the object (taken, for convenience in the x-direction) and an angular measure of the pupil. Referring to Figure 3.2 we see that

$$\tan\bar{\alpha}_x = \frac{-\bar{x}}{Z_{E0}} \cos\alpha_0. \tag{3.16}$$

Repeating the steps which lead from Eq. (3.2) to Eq. (3.4), but switching

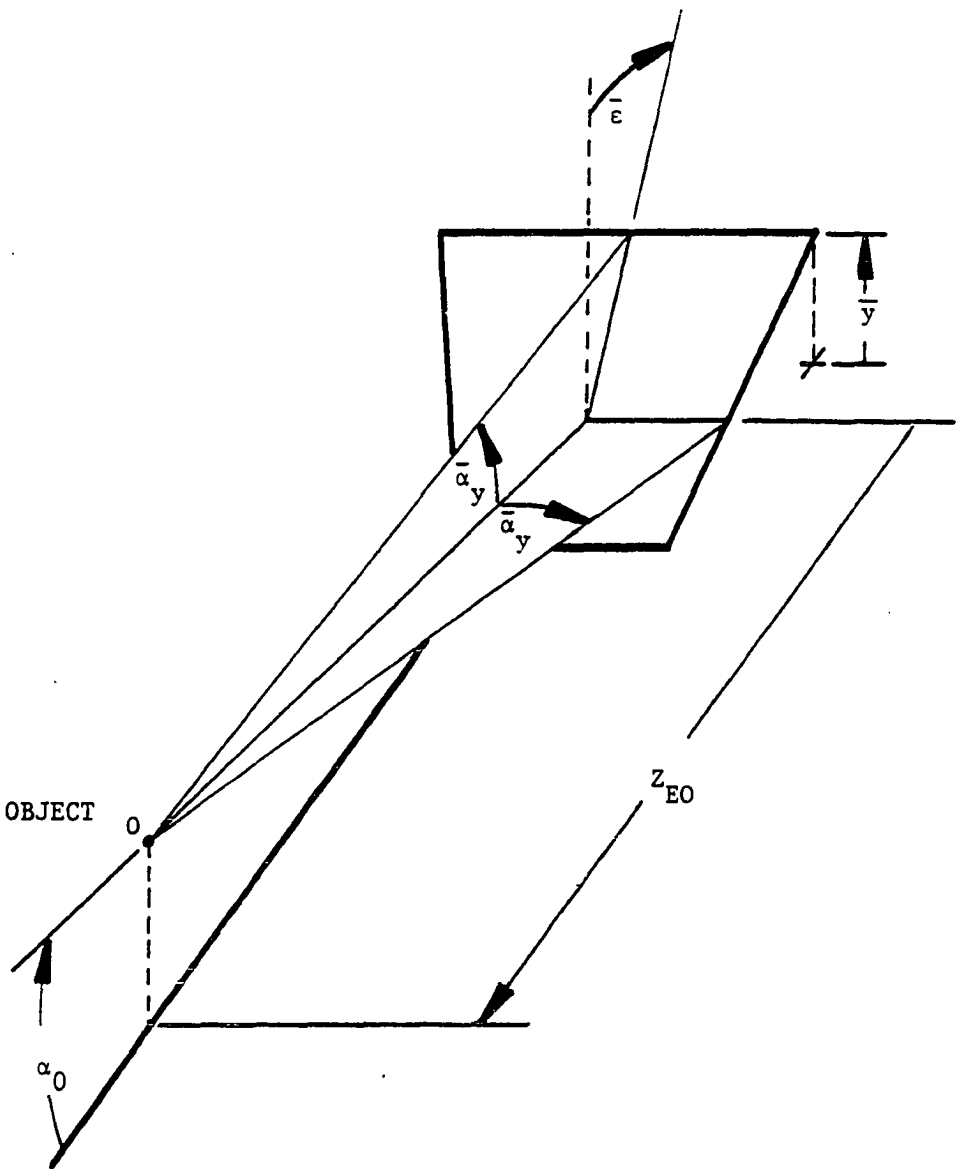

Figure 3.2. Geometry of a Tilted Pupil.

the roles of the object and pupil quantities, we obtain:

$$\bar{T}_x \equiv nX_1 \tan\bar{\alpha}_x \tag{3.17}$$

$$\bar{T}_x = \bar{T}_{X1}\rho_x, \tag{3.18}$$

where,

$$\bar{T}_{X1} \equiv \frac{-n\bar{X}_1 X_1}{Z_{EO}} \cos\alpha_O. \tag{3.19}$$

Comparing Eqs. (3.4) and (3.19) we see that

$$\bar{T}_{X1} = - T_{X1}. \tag{3.20}$$

The parameter $\bar{T}_{X1}$ thus represents redundant information, and need not be calculated.

Referring again to Figure 3.2, one sees that for the y-direction, the tangent of the sum of angles must be used. From the figure,

$$\tan(\alpha_O + \bar{\alpha}_y) = \frac{Y_O - \bar{y}}{Z_{EO} + \bar{y}\bar{T}_\varepsilon}. \tag{3.21}$$

Using the identity (Eq.(3.5)), solving for $\tan\bar{\alpha}_y$ and simplifying, one

obtains

$$\tan\bar{\alpha}_y = \frac{-(1+T_0\bar{T}_\varepsilon)\bar{y}}{(Z_{E0}/\cos^2\alpha_0) + (\bar{T}_\varepsilon - T_0)\bar{y}}. \tag{3.22}$$

Inserting Eq. (2.29) for $\bar{y}$, this now becomes

$$\tan\bar{\alpha}_y = \frac{-(1+T_0\bar{T}_\varepsilon)\bar{Y}_1\rho_y}{(Z_{E0}/\cos^2\alpha_0) - \left[K(Z_{E0}/\cos^2\alpha_0) - \bar{Y}_1(\bar{T}_\varepsilon - T_0)\right]\rho_y}. \tag{3.23}$$

Defining the quantity $\bar{T}_y$ to be

$$\bar{T}_y \equiv nX_1\tan\bar{\alpha}_y, \tag{3.24}$$

then

$$\bar{T}_y = \frac{\bar{T}_{Y1}\rho_y}{1 - \bar{K}_T\rho_y}, \tag{3.25}$$

where

$$\bar{T}_{Y1} \equiv \frac{-nX_1\bar{Y}_1(1 + T_0\bar{T}_\varepsilon)\cos^2\alpha_0}{Z_{E0}} \tag{3.26}$$

and

$$\overline{K}_T \equiv K - \left[\frac{\overline{Y}_1(\overline{T}_\varepsilon - T_0)\cos^2\alpha_0}{Z_{E0}}\right] \tag{3.27}$$

Table 3.2 summarizes the equations defining the canonical parameters.

Refraction Equations

Having now a canonical description of the object and entrance pupil, the next step is to find the corresponding parameters for the image and exit pupil.

Before considering the canonical parameters explicitly, Figure 3.3 will be used to establish an identity relating ray angles in object space to image space. From the figure, it is evident that for any ray through E,

$$\tan\alpha' = \frac{h_p}{\overline{Z}_0'} \tag{3.28}$$

and

$$\tan\alpha = \frac{h_p}{\overline{Z}_0}. \tag{3.29}$$

Table 3.1 Equations defining the Canonical Parameters

$$T_0 \equiv \frac{Y_0}{Z_{E0}} \tag{3.6}$$

$$T_{X1} \equiv \frac{n\bar{X}_1 X_1}{Z_{E0}} \cos\alpha_0 \tag{3.4}$$

$$T_{Y1} \equiv \frac{n\bar{X}_1(Y_1+KY_0)(1+T_\varepsilon T_0)\cos^2\alpha_0}{Z_{E0}} \tag{3.14}$$

$$K_T \equiv \left[K(1+T_\varepsilon T_0) + \frac{Y_1(T_\varepsilon-T_0)}{Z_{E0}}\right] \cos^2\alpha_0 \tag{3.15}$$

$$\bar{T}_{X1} \equiv -T_{X1} \tag{3.20}$$

$$\bar{T}_{Y1} \equiv \frac{-nX_1\bar{Y}_1(1+T_0\bar{T}_\varepsilon)\cos^2\alpha_0}{Z_{E0}} \tag{3.26}$$

$$\bar{K}_T \equiv K - \left[\frac{\bar{Y}_1(\bar{T}_\varepsilon-T_0)}{Z_{E0}}\right] \cos^2\alpha_0 \tag{3.27}$$

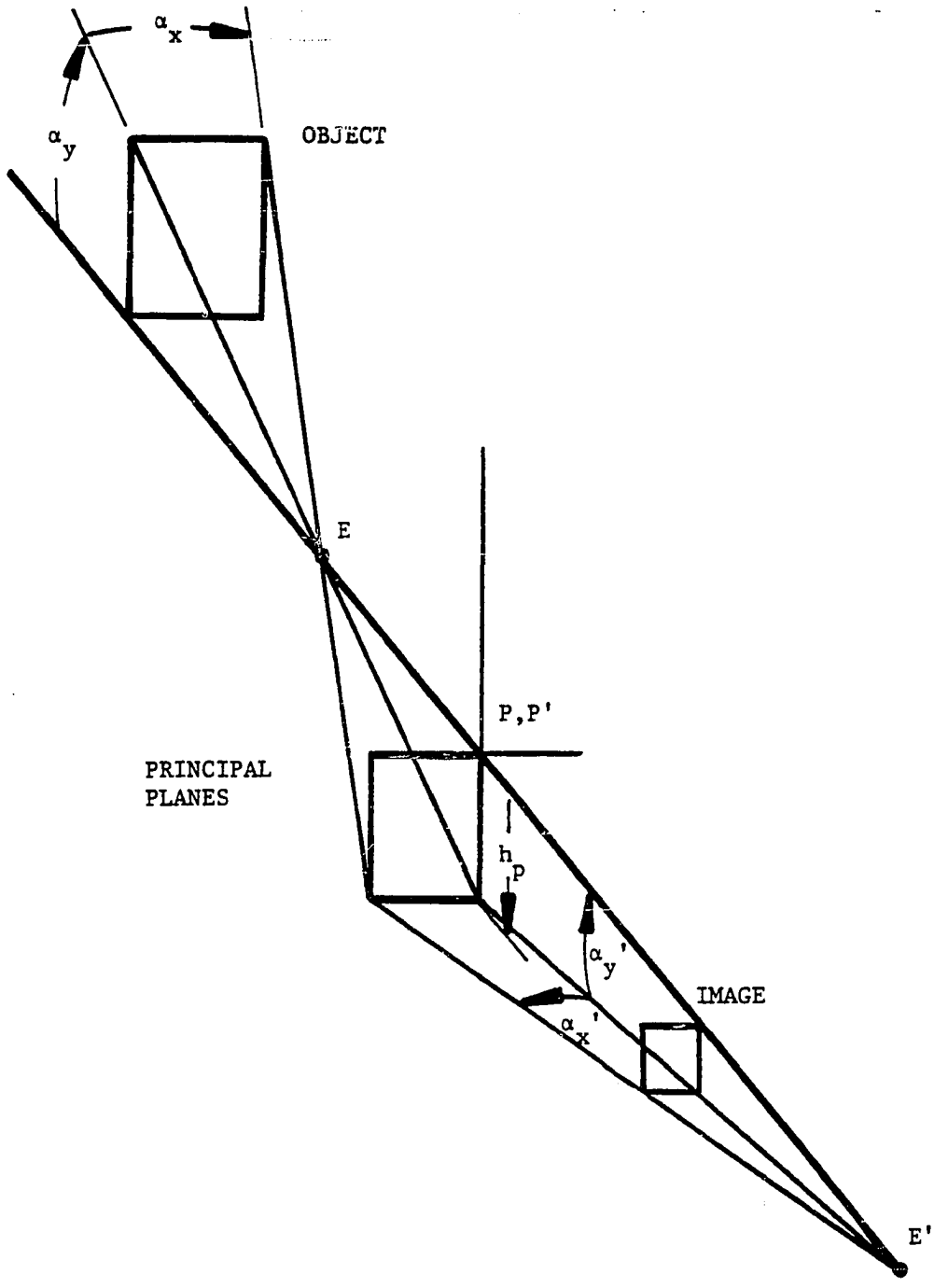

Figure 3.3. Relating Image Space and Object Space Ray Angles.

Hence,

$$\tan\alpha' = \frac{\bar{Z}_0}{\bar{Z}_0'} \tan\alpha. \tag{3.30}$$

Using the well known behavior of the (pupil) magnification

$$m \equiv \frac{\bar{X}_1'}{\bar{X}_1} = \frac{n'\bar{Z}_0'}{n\bar{Z}_0}, \tag{3.31}$$

then

$$\tan\alpha' = \bar{R} \tan\alpha \tag{3.32}$$

where

$$\bar{R} \equiv \frac{n\bar{X}_1}{n'\bar{X}_1'} = \frac{\bar{Z}_0}{\bar{Z}_0'}. \tag{3.33}$$

The objection might be raised that this construction is invalid in the event that the pupil resides at the surface, for then the right-hand side of Eq. (3.30) become indeterminate. Nevertheless, Equation (3.33) gives two definitions for $\bar{R}$, and it may be seen that as the pupil approaches the principal plane, $\bar{R}$ approaches the limiting value of (n/n'). With $\bar{R}$ defined in this way, the equations which follow remain valid.

Applying Equation (3.33) to the y-direction, and replacing the angle α with α_0 yields the conjugate relation for the decentration parameters,

$$T_0' = \bar{R}T_0' \tag{3.34}$$

Equation (3.30) may also be applied to a general field ray in the y-direction, yielding

$$\tan(\alpha_0' + \alpha_y') = \bar{R}\tan(\alpha_0 + \alpha_y). \tag{3.35}$$

Using the trigonometric identity (Equation (3.5)) on both sides, solving for $\tan \alpha_y'$ and simplifying yields

$$\tan\alpha_y' = \frac{\tan\alpha_y\ (\bar{R} + T_0T_0')}{(1+T_0'^2) - \tan\alpha_y\ (T_0-\bar{R}T_0')} \tag{3.36}$$

Using Equations (3.12) and (3.13) to replace $\tan\alpha_y$, and requiring $\tan\alpha_y'$ to have the form given by the primed versions of those same two equations yields the conjugate relationships for the y-direction,

$$T_{Y1}' = T_{Y1}\left[\frac{\cos\ \alpha_0'}{\cos\ \alpha_0}\right]^2 \tag{3.37}$$

and

$$K_T' = K_T + \frac{T_{Y1}T_0(1-\bar{R}^2)\cos^2\alpha_0'}{n\bar{X}_1}. \tag{3.38}$$

To derive the conjugate relations in the x-direction, consider again Figure 3.3. An identity similar to Eq. (3.30) exists, but the slopes of the planes containing the angles α_x and α_x' must be accounted for, and the identity becomes

$$\tan\alpha_x' = \bar{R}\tan\alpha_x \left[\frac{\cos\alpha_0'}{\cos\alpha_0}\right]. \tag{3.39}$$

Using equations (3.2) and (3.3) to replace $\tan\alpha_x$, and requiring $\tan\alpha_x'$ also to have that form, it may be seen that

$$T_{X1}' = T_{X1}\left[\frac{\cos\alpha_0'}{\cos\alpha_0}\right]. \tag{3.40}$$

Before considering the pupil parameters, note that the construction of Figure 3.3 holds equally well if the roles of the pupil and object are switched. By simply interchanging the pupil (barred) and object (unbarred) quantities in Eqs. (3.32) and (3.33) on obtains the analogous identity

$$\tan\alpha_y' = R\tan\alpha_y, \tag{3.41}$$

where

$$R \equiv \frac{nX_1}{nX_1'} = \frac{Z_0}{Z_0'}. \tag{3.42}$$

Note that as the object approaches the principal plane, R approaches the limiting value of (n/n').

Considering now the parameter $\overline{T}_x$, it may be seen from Eq. (3.41) and the discussion leading to Eq. (3.39) that

$$\tan\alpha_x' = R\left[\frac{\cos\alpha_0'}{\cos\alpha_0}\right]\tan\alpha_x. \tag{3.43}$$

Replacing tan $\bar{\alpha}_x$ with the form given by Equations (3.17) and (3.19), and requiring that tan $\bar{\alpha}_x'$ also have that form yields

$$\overline{T}_{x1}' = \overline{T}_{x1}\left[\frac{\cos\alpha_0'}{\cos\alpha_0}\right]. \tag{3.44}$$

To find $\overline{T}_{y1}'$ and $\overline{K}_{T1}'$ consider Figure 3.4, which shows the y-z meridian of a system with a tilted pupil and a decentered object. From the figure, it is evident that

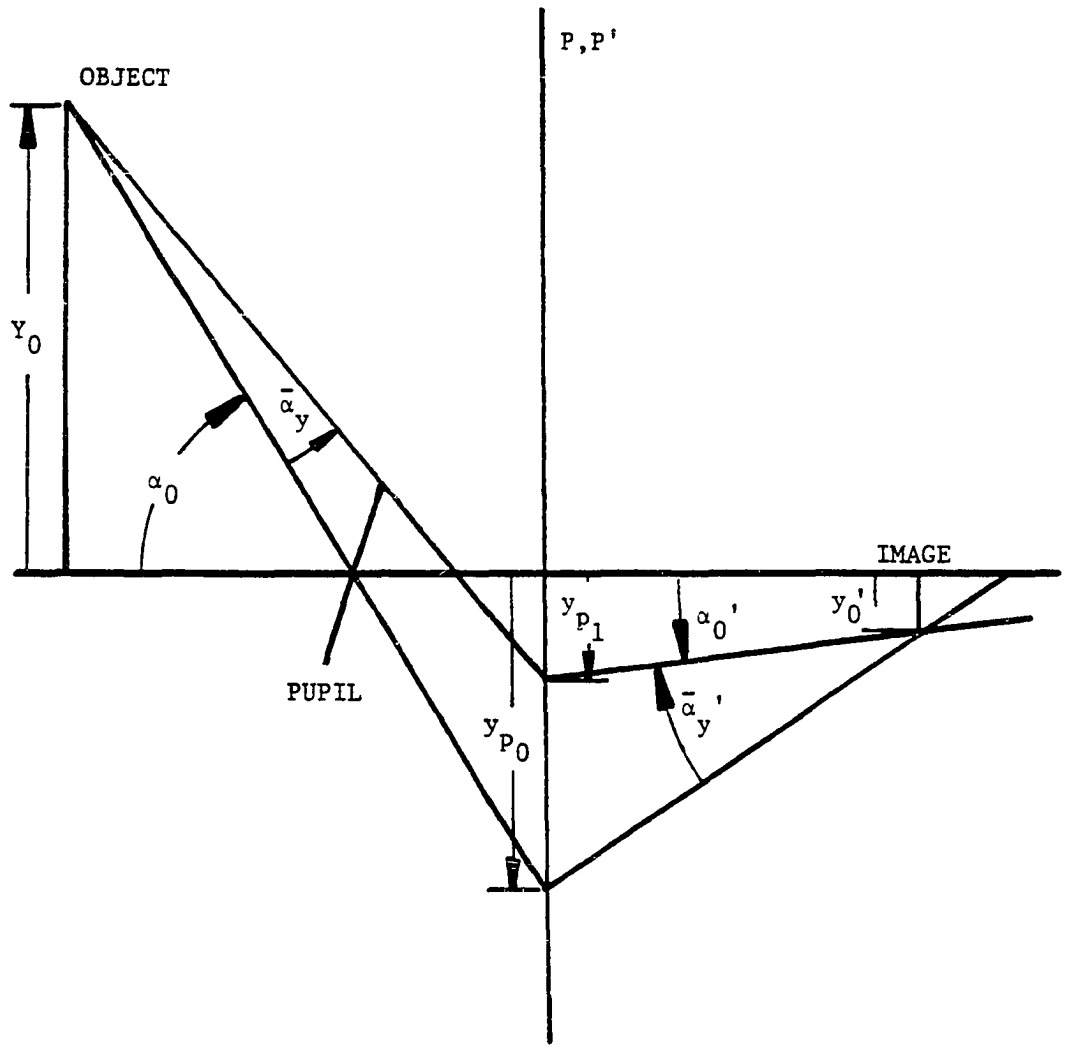

Figure 3.4. Relating Pupil Angles from Object to Image Space.

$$\tan(\bar{\alpha}_0' + \bar{\alpha}_y') = \frac{Y_0' - Y_{p_1}}{Z_0'} \tag{3.45}$$

and

$$Y_{p_1} = Y_0 - Z_0 \tan(\bar{\alpha}_0 + \bar{\alpha}_y). \tag{3.46}$$

Combining these expressions,

Using the trigonometric identity (Eq. (3.5)), and solving for $\tan\bar{\alpha}_y'$ yields

$$\tan\bar{\alpha}_y = \frac{Y_0'-Y_0-T_0'Z_0'+T_0Z_0+(T_0Y_0-T_0Y_0'+T_0T_0'Z_0'+Z_0)\tan\bar{\alpha}_y}{Z_0'+T_0'(Y_0'-Y_0+T_0Z_0)+[T_0Z_0'-T_0'(Z_0-T_0(Y_0'-Y_0))]\tan\bar{\alpha}_y} \tag{3.47}$$

By noting from the figure that

$$T_0 = \frac{Y_0-Y_{p_0}}{Z_0}, \tag{3.48}$$

Equation (3.47) may be reduced to

$$\tan\bar{\alpha}_y' = \frac{\left[\frac{Z_0(1+T_0^2)}{Z_0'(1+T_0'^2)}\right]\tan\bar{\alpha}_y}{1 - \left[\frac{T_0Z_0' - T_0'Z_0 + T_0T_0'(T_0'Z_0' - T_0Z_0)}{Z_0'(1+T_0'^2)}\right]\tan\bar{\alpha}_y} \tag{3.49}$$

Using the trigonometric identity of Eq. (3.10), and putting both $\tan\bar{\alpha}_y$ and $\tan\bar{\alpha}_y'$ into the form given by Eqs. (3.24) and (3.25) yields the canonical pupil parameters,

$$\bar{T}_{y1}' = \left[\frac{\cos\alpha_0'}{\cos\alpha_0}\right]^2 \bar{T}_{Y1} \tag{3.50}$$

$$\bar{K}_T' = \bar{K}_T + \left[\frac{\bar{T}_{Y1}T_0}{nX_1}\right](\bar{R}-K)(1 + \bar{K}T_0^2)\cos^2\alpha_0'. \tag{3.51}$$

The equations relating the canonical variables in object space to those in image space are summarized in Table 3.2.

Transfer Equations

The canonical parameters in the image space of one optical surface must be transformed into the object space for the following surface, allowing for the possibility that the local axis of this new surface is not coincident with the present local axis. The new axis must

Table 3.2 Refraction Equations for the Canonical Parameters

$$T_0' = \bar{R}T_0 \tag{3.34}$$

$$T_{X1}' = T_{X1}(\cos\alpha_0'/\cos\alpha_0) \tag{3.40}$$

$$T_{Y1}' = T_{Y1}(\cos\alpha_0'/\cos\alpha_0)^2 \tag{3.37}$$

$$K_T' = K_T + \left[\frac{T_{Y1}T_0}{n\bar{X}_1}\right](1-\bar{R}^2)\cos^2\alpha_0' \tag{3.38}$$

$$\bar{T}_{X1}' = \bar{T}_{X1}(\cos\alpha_0'/\cos\alpha_0) \tag{3.44}$$

$$\bar{T}_{Y1}' = \bar{T}_{Y1}(\cos\alpha_0'/\cos\alpha_0)^2 \tag{3.50}$$

$$\bar{K}_T' = \bar{K}_T + \left[\frac{\bar{T}_{Y1}\,T_0}{n\,\bar{X}_1}\right](\bar{R}-R)(1+\bar{R}T_0^2)\cos^2\alpha_0' \tag{3.51}$$

where $\bar{R} \equiv (n\bar{X}_1/n'\bar{X}_1') = (\bar{Z}_0/Z_0')$ (3.33)

and $R \equiv (nX_1/n'X_1') = (Z_0/Z_0')$ (3.42)

by definition pass through the entrance pupil for the new surface, (which is the exit pupil for the old surface), and may be tilted in the y-z meridian by some angle, β. Since the canonical quantities T_x, T_y, $\overline{T}_x$ and $\overline{T}_y$ consist only of linear distances in the x-direction and angles measured from the object center (not from the local axis itself), these quantities will remain invariant under such a rotation of the local axis. The quantities T_0, T_ε, and $\overline{T}_\varepsilon$, which reference the local axis, will change during a coordinate axis rotation. If α_0 is the angular "decentration" of the object from the local axis and α_0' is the same, but measured from the new local axis, then

$$\alpha_0' = \alpha_0 - \beta. \tag{3.52}$$

Using the identity of Eq. (3.5), then

$$T_0' = \frac{T_0 - \tan\beta}{1 + T_0\tan\beta}. \tag{3.53}$$

The tangent parameters T_ε and $\overline{T}_\varepsilon$ will transform in an identical fashion. Table 3.3 lists the transfer equations for the object and pupil parameters.

Conversion from Canonical to Real-Space Parameters

Given a set of real-space parameters for a system, one may find their canonical counterparts using Table 3.1. One may then find the canonical image space parameters using Table 3.2. Table 3.3 allows one

Table 3.3 Transfer Equations for the Canonical Parameters

$$T_0' = \frac{T_0 - \tan\beta}{1 + T_0\tan\beta} \tag{3.53}$$

$$T_\varepsilon' = \frac{T_\varepsilon - \tan\beta}{1 + T_\varepsilon\tan\beta} \tag{3.54}$$

$$\overline{T}_\varepsilon' = \frac{\overline{T}_\varepsilon - \tan\beta}{1 + \overline{T}_\varepsilon\tan\beta} \tag{3.55}$$

where β is the angle between the old and new local axes.

The following parameters are unchanged:

$$T_{X1},\ T_{Y1},\ K_T,\ \overline{T}_{Y1},\ \overline{K}_{TY}.$$

to transform the image of one surface into the object of the next, so that one may again image the object. All that remains is to convert the final image parameters from canonical to real-space parameters.

Consider first the parameter X_1. Solving Equation (3.4) for X_1 yields immediately,

$$X_1 = \frac{Z_{EO}T_{x1}}{n\bar{X}_1\cos\alpha_0} \tag{3.56}$$

This same equation may also be solved for $\bar{X}_1$ yielding

$$\bar{X}_1 = \frac{Z_{EO}T_{X1}}{nX_1\cos\alpha_0} \tag{3.57}$$

To obtain the y-direction parameters it is necessary to again resort to the tangents of sums of angles. The procedure for the object/image parameters is as follows: Equation (2.8) is inserted for z in Eq. (3.7), which is then solved for y. Eq. (3.5) is used to replace the quantity $\tan(\alpha_0 + \alpha_y)$ in the resulting equation. The quantity $\tan\alpha_y$ is then replaced with an expression in terms of the parameters T_{Y1} and K_T, which is derived from Eqs. (3.12) and (3.13). Finally, the parameters Y_0, Y_1 and K are identified by requiring the final expression for y to have the form of Eq. (2.14), yielding

$$Y_0 = Z_{EO}T_0, \tag{3.58}$$

$$Y_1 = Z_{EO}\left[\frac{T_{Y1}}{n\bar{X}_1} - K_T Y_0\right], \tag{3.59}$$

and

$$K = K_T - \frac{T_{Y1}(T_\varepsilon - T_0)}{n\bar{X}_1(1+T_0 T_\varepsilon)}. \tag{3.60}$$

The pupil parameters in the $\bar{y}$ direction are found in an analogous manner, using Equations (3.21), (3.24), and (3.25) yielding

$$\bar{Y}_1 = -\frac{\bar{T}_{Y1}}{nX_1}\left[\frac{Z_{EO} + T_0 Y_0}{1 + T_0\,\bar{T}_\varepsilon}\right] \tag{3.61}$$

and

$$\bar{K} = \bar{K}_T - \frac{\bar{T}_{Y1}}{nX_1}\left[\frac{\bar{T}_\varepsilon - T_0}{1 + T_0\,\bar{T}_\varepsilon}\right]. \tag{3.62}$$

Table 3.4 summarizes the results of this section.

It may be noted that the object and pupil parameters have been defined in terms of one another; for instance, to compute X_1 from Eq.

Table 3.4 Conversion from Canonical to Real Space Parameters

$$X_1 = \frac{Z_{E0}T_{X1}}{n\bar{X}_1\cos\alpha_0} \tag{3.56}$$

$$Y_0 = Z_{E0}T_0 \tag{3.58}$$

$$Y_1 = Z_{E0}\left[\frac{T_{Y1}}{n\bar{X}_1} - K_T T_0\right] \tag{3.59}$$

$$K = K_T - \frac{T_{Y1}(T_\varepsilon - T_0)}{n\bar{X}_1(1+T_0T_\varepsilon)} \tag{3.60}$$

$$\bar{X}_1 = \frac{Z_{E0}T_{X1}}{nX_1\cos\alpha} \tag{3.57}$$

$$\bar{Y}_1 = -\frac{\bar{T}_{Y1}}{nX_1}\left[\frac{Z_{E0} + T_0Y_0}{1 + T_0\bar{T}_\varepsilon}\right] \tag{3.61}$$

$$\bar{K} = \bar{K}_T - \frac{\bar{T}_{Y1}}{nX_1}\left[\frac{\bar{T}_\varepsilon - T_0}{1 + T_0\bar{T}_\varepsilon}\right] \tag{3.62}$$

(3.56) it is necessary to know not only the canonical parameter T_{X1} but also the real-space parameter $\overline{X}_1$. Similarly, Eq. (3.57) shows that X_1 must be known for $\overline{X}_1$ to be computed. Thus, in order to compute the real-space parameters one must know all the canonical parameters and one or the other (not both) of the quantities X_1 and $\overline{X}_1$. Fortunately it will always be possible to compute one of theses two quantities using the appropriate paraxial magnification m_0 or $\overline{m}_0$. Once that has been done, the remaining parameters may be computed using Table 3.4.

CHAPTER 4

SEIDEL ABERRATIONS

This chapter is an extension of the work by Thompson (1980) who developed a vector aberration theory applicable to perturbed optical systems. Although the computational method employed by him breaks down when large tilts are decentrations are encountered, the underlying principle of the theory is still applicable, with minor modifications. The following section summarizes the appropriate portions of that work; the reader is referred to it for details not supplied herein.

Theoretical Background

The basis of the vector theory of aberrations is that each optical surface introduces aberration contributions of the same form as for a rotationally symmetric system, but that the centers of the contributions are not necessarily located at the center of the image. Furthermore, two independent sets of aberrations are introduced by each surface: one induced by the base sphere of the surface and the other introduced by the aspheric departure of the surface. These two sets of aberration terms, along with those introduced by other optical surfaces, may be combined vectorially to yield the final behavior of the system.

Base Sphere Contributions

The Local Axis defined in Chapter 2 was chosen as the line joining the center of the entrance pupil and the center of curvature for that surface. It may be noted that except for the possibility of a tilted or distorted pupil, the optical system consisting of the base sphere and the pupil is rotationally symmetric about this axis. Thus, this optical system contributes aberrations of the ordinary type, centered along this axis. (The effects of tilts and distortions of the pupil are considered in Chapters 5).

Aspheric Contributions

Treating the aberrations introduced by the asphericity of the surface separately from those of the base sphere enables one to visualize an optical system comprised of the entrance pupil and the thin aspheric plate which remains after the base sphere has been removed from the system. This optical system is now approximately rotationally symmetric about the line joining the pupil and the aspheric vertex. This axis will be referred to as the Aspheric Axis.

Special Cases

It was noted in Chapter 2 that if the pupil and center of curvature of the base sphere are nearly coincident, the Local Axis joining those two points may be so oblique to the actual ray bundle as to be inappropriate for the calculation of aberrations. Similarly, if the pupil and aspheric vertex are nearly coincident, the Aspheric Axis as

defined above may be also inappropriate.

Considering the latter case of a (possibly decentered) aspheric located at the pupil, it may be seen that every chief ray pierces the aspheric plate at the same place, and therefore experiences the same wavefront retardation in traversing the plate, so that no variation in aberration with field is experienced, to third order. The resulting wavefront deformation is rotationally symmetric about the aspheric vertex, but the "shearing" of the pupil from this vertex center introduces asymmetric terms in the pupil variable, ρ.

The case of a base sphere centered at or near the pupil is similar. Using the theory of Burch (1942), the aberrations of the base sphere may be regarded as originating from an aspheric plate located at the center of curvature of the base sphere. Once this replacement has been made, the situation is identical to that of an aspheric plate at the pupil plane.

The dependence of the aberrations on the decentration of the pupil will be given explicitly in the section on computational technique.

Vector Form of Aberrations

The familiar scalar form of the wave aberration function for the third order aberrations is

$$W = W_{040}\rho^4 + W_{131}H\rho^3\cos\phi + W_{222}H^2\rho^2\cos^2\phi + W_{220}H^2\rho^2 + W_{311}H^3\rho\cos\phi. \qquad (4.1)$$

The terms in this equation represent the aberrations spherical

aberration, coma, astigmatism, field curvature, and distortion, respectively. By replacing H and ρ with the vector form given in Figure 4.1, one obtains the vector form of the wave aberration function,

$$W = W_{040}(\boldsymbol{\rho}\cdot\boldsymbol{\rho})^2 + W_{131}(\mathbf{H}\cdot\boldsymbol{\rho})(\boldsymbol{\rho}\cdot\boldsymbol{\rho}) + W_{222}(\mathbf{H}\cdot\boldsymbol{\rho})^2 + W_{220}(\mathbf{H}\cdot\mathbf{H})(\boldsymbol{\rho}\cdot\boldsymbol{\rho}) + W_{311}(\mathbf{H}\cdot\mathbf{H})(\mathbf{H}\cdot\boldsymbol{\rho}). \quad (4.2)$$

Summation of Aberration Fields

As was previously stated, the aberration field in the final image plane is the sum of the individual fields (due to both the base sphere and the aspheric terms) of the optical surfaces comprising the system. These fields will not coincide, in general, with each other or with the field center. If the aberration field associated with the i^{th} surface component is centered at $\mathbf{H} = \boldsymbol{\sigma}_i$ rather than at the center of the image field, then the wave aberration field may be obtained simply by replacing $\mathbf{H}$ with $(\mathbf{H} - \boldsymbol{\sigma}_i)$ in Equation (4.2). The total aberration function is the sum of all of these contributions. Rather than write out the entire wave aberration function for the system, consider the aberration terms individually.

Spherical Aberration. The vector form of the spherical aberration term for the entire system is

$$W_{SA} = \sum_i W_{040_i}(\boldsymbol{\rho}\cdot\boldsymbol{\rho})^2. \quad (4.3)$$

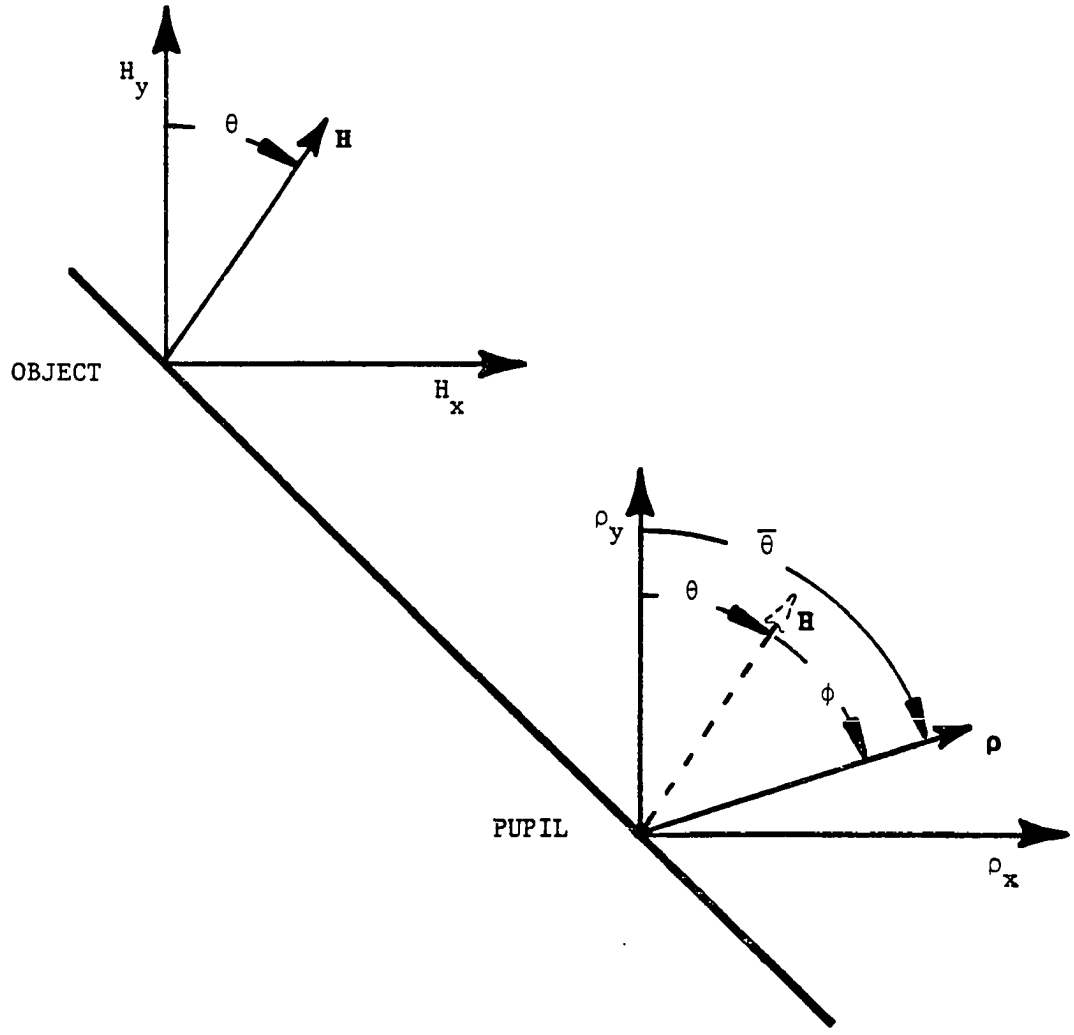

Figure 4.1. Vectoral Coordinates of the Object and Pupil.

where the summation includes both the spherical and aspheric contributions from all surfaces. Since each contribution is independent of **H** (and therefore independent of σ_i), the resulting aberration field is independent of **H**, and is insensitive to the tilts and decentrations of the elements of the system. It is worth noting that this result was obtained without regard to the change of conjugate position with field that would accompany a tilt object of finite size. Buchroeder (1976) considered this effect and determined that the variation in spherical aberration with field induced by it is small, although he points out that it might become considerable in a wide field system with large tilts. This effect will be neglected in this work also.

Coma. Referring to Eq. (4.2), the wave aberration term for coma resulting from the sum of several displaced coma fields is

$$W_c = \sum_i W_{131_i}[(\mathbf{H} - \sigma_i)\cdot\rho](\rho\cdot\rho). \tag{4.4}$$

This may be manipulated into the form

$$W_c = W_{131}[(\mathbf{H} - \mathbf{a}_{131})\cdot\rho](\rho\cdot\rho) \tag{4.5}$$

where

$$W_{131} \equiv \sum_i W_{131_i} \tag{4.6}$$

and

$$a_{131} \equiv \frac{\sum_i W_{131_i} \sigma_i}{W_{131}}. \tag{4.7}$$

Scrutiny of Eq. (4.5) shows that the aberration field resulting from the sum is of the same form as ordinary coma, but centered at the point a_{131}. The magnitude, or strength of the coma field about this node is given by the coefficient W_{131}.

Medial Field Curvature. The curvature of the image field in the presence of astigmatism is best described from the viewpoint of the medial field, midway between the sagittal and tangential focal surfaces. The coefficient of medial field curvature is defined as in an ordinary centered system,

$$W_{220M} = W_{220} + \frac{1}{2} W_{222}. \tag{4.8}$$

Returning temporarily to the scalar form (Equation (4.1)), by considering both the field curvature and astigmatism terms and using the trigonometric identity

$$\cos^2\phi = \frac{1}{2} + \frac{1}{2} \cos 2\phi, \tag{4.9}$$

one obtains

$$W_{FC+A} = W_{220M}\, H^2\rho^2 + \frac{1}{2}\, W_{222}H^2\rho^2\cos 2\phi. \tag{4.10}$$

Rewriting the first term in vector notation and summing the (displaced) contributions, the field curvature term is found to be

$$W_{FC} = \sum_i W_{220M_i}[(\mathbf{H} - \boldsymbol{\sigma}_i)\cdot(\mathbf{H} - \boldsymbol{\sigma}_i)](\boldsymbol{\rho}\cdot\boldsymbol{\rho}). \tag{4.11}$$

This may be manipulated into the form

$$W_{FC} = W_{220M}[(\mathbf{H} - \boldsymbol{\alpha}_{220M})\cdot(\mathbf{H} - \boldsymbol{\alpha}_{220M}) + b_{220M}](\boldsymbol{\rho}\cdot\boldsymbol{\rho}), \tag{4.12}$$

where

$$W_{220M} \equiv \sum_i W_{220M_i}, \tag{4.13}$$

$$\mathbf{a}_{220M} \equiv \frac{\sum_i W_{220M_i}\boldsymbol{\sigma}_i}{W_{220M}}, \tag{4.14}$$

and

$$b_{220M} \equiv \frac{\sum_i W_{220M_i}(\boldsymbol{\sigma}_i\cdot\boldsymbol{\sigma}_i)}{W_{220M}} - (\mathbf{a}_{220M}\cdot\mathbf{a}_{220M}). \tag{4.15}$$

Considering Eq. (4.12), one sees that it is similar in form to ordinary

field curvature (Equation (4.11) shows the sum of several such terms, for comparison), except that the field is decentered by the vector $\mathbf{a}_{220_M}$, and has a constant additive term of b_{220_M}. This last term introduces a constant focal shift of

$$\Delta Z_{220M} = -8(\bar{f}^{\#})^2 W_{220M} b_{220M}. \tag{4.16}$$

The term involving **H** is quadratic in the field, decentered by $\mathbf{a}_{220M}$, and gives rise to a focal surface with radius

$$R_M = \frac{-\mathcal{H}^2}{4 W_{220M}}, \tag{4.17}$$

where $\mathcal{H}$ is the Lagrange or optical invariant.

Astigmatism. From Equation (4.10) it is evident that the astigmatism measured relative to the medial surface is

$$W_A = \frac{1}{2} W_{222} H^2 \rho^2 \cos 2\phi. \tag{4.18}$$

The double angle in the argument of the cosine requires the use of vector multiplication, introduced by Thompson (1980). By writing the vectors **H** and $\boldsymbol{\rho}$ in exponential, or polar form, recalling that ϕ is the angle between the two vectors, one obtains

$$\mathbf{H} = H\, e^{i\theta} \tag{4.19}$$

and

$$\boldsymbol{\rho} = \rho\, e^{i(\theta+\phi)}. \tag{4.20}$$

Squaring these two expressions using ordinary complex arithmetic on the right hand side yields

$$\mathbf{H}^2 = H^2\, e^{i2\theta} \tag{4.21}$$

and

$$\boldsymbol{\rho}^2 = \rho^2\, e^{i(2\theta+2\phi)}. \tag{4.22}$$

Noting that the angle between these two squared vectors is 2ϕ enables one to find their dot product:

$$\mathbf{H}^2 \cdot \boldsymbol{\rho}^2 = H^2\rho^2\cos 2\phi. \tag{4.23}$$

Comparing this with Eq. (4.18) shows that the wave function for astigmatism may be rewritten in vector form as

$$W_A = \frac{1}{2}\, W_{222}\, \mathbf{H}^2 \cdot \boldsymbol{\rho}^2. \tag{4.24}$$

Now summing the individual (displaced) field contributions, the resultant field is obtained,

$$W_A = \frac{1}{2} \sum_i W_{222_i} (H - \sigma_i)^2 \cdot \rho^2.$$

This may be put into the form

$$W_A = \frac{1}{2} W_{222} [(H - a_{222})^2 + b_{222}^2] \cdot \rho^2, \tag{4.26}$$

where

$$W_{222} \equiv \sum_i W_{222_i}, \tag{4.27}$$

$$a_{222} \equiv \frac{\sum_i W_{222_i} \sigma_i}{W_{222}}, \tag{4.28}$$

and

$$b_{222}^2 \equiv \frac{\sum_i W_{222_i} \sigma_i^2}{W_{222}} - a_{222}^2. \tag{4.29}$$

To locate the nodes of the astigmatism, one must find the roots of the equation

$$0 = (H - a_{222})^2 + b_{222}^2. \tag{4.30}$$

Treating the vectors as complex numbers again, this yields

$$H = a_{222} \pm i\, b_{222}, \tag{4.31}$$

where b_{222} is the complex square root of b_{222}^2, and the factor of i multiplying introduces a rotation of 90° to the vector.

The magnitude of the astigmatism at any point in the field is given by the product of the distances to the two nodes. Far from the nodes, where their separation may be considered negligible, this reduces to ordinary quadratic astigmatism. Close to one node, where the distance to the other node is essentially constant, the astigmatism varies only with the distance to the nearby node, giving linear astigmatism. Midway between the two nodes, the astigmatism is essentially constant.

Distortion. The vector algebra involved in locating the nodes of Seidel distortion is complicated, and will not be repeated here. The final wave aberration function is computed by Thompson (1980) to be

$$W_D = W_{311}[((H - a_{311})^2 + b_{311}^2)H_{311}^*] + 2W_{311}d_{311}(H - a_{111})]\cdot\rho, \tag{4.32}$$

where

$$W_{311} \equiv \sum_i W_{311_i}, \tag{4.33}$$

$$a_{311} \equiv \frac{\sum_i W_{311_i}\ \sigma_i}{W_{311}}, \tag{4.34}$$

$$b_{311}^2 \equiv \frac{\Sigma\, W_{311_i}\, \sigma_i^2}{W_{311}} - a_{311}^2,$$

$$d_{311} \equiv \frac{\sum_i W_{311_i}(\sigma_i \cdot \sigma_i)}{W_{311}} - (a_{311} \cdot a_{311}), \tag{4.36}$$

$$a_{111} \equiv \frac{[c_{311} - b_{311}^2\, a^*_{311}]}{2d_{311}}, \tag{4.37}$$

$$c_{311} \equiv \frac{\sum_i W_{311_i}(\sigma_i \cdot \sigma_i)\sigma_i}{W_{311}} - (a_{311} \cdot a_{311})a_{311}, \tag{4.38}$$

and the symbol (*) denotes complex conjugation. The interpretation of Eq. (4.32) is that a first order distortion node appears at a_{111} with magnitude $2W_{311}\, d_{311}$, and three third order nodes, each with magnitude W_{311}, appear at the points a_{311}, $a_{311} \pm ib_{311}$.

Computational Technique

In order to apply the theory of the last section, the vector σ_i and the wavefront aberration coefficients W_{040_i}, W_{131_i}, $W_{220_{M_i}}$, W_{222_i}, and W_{311_i} for each surface contribution (both spherical and aspheric) must be obtained. The author made use of the lens design program ACCOSV to perform most of the computational task, and then converted the output of ACCOSV into a form suitable for use by the theory. The details of the computation are given below.

In the previous section, the vector σ_i was defined as the relative location in the object/image field of the center of the i^{th} aberration field. Mathematically, this is expressed as the ratio of the decentration of the aberration center to the field size. Recalling that the object field is in general, anamorphically and keystone distorted, one realizes that the "size" of the field may not be characterized by any single number. However, in order to apply the theory, some single length characteristic must be chosen; the quantity chosen for the purposes of this work is X_1, which is equal to $x(H_x=1,H_y=0)$. Thus, the aberration field displacement vector is

$$\sigma \equiv \frac{Y_0}{X_1} = \frac{\sin\alpha_0}{\tan\alpha_x|_{H_x=1}}. \tag{4.39}$$

This then is a measure of the aberration displacement relative to the object/image field, disregarding the effects of keystone and anamorphic distortion. These effects will be considered in the next chapter.

Using Equations (3.4) and (3.10), referring to Fig. 3.1, Equation (4.39) may be put into canonical form,

$$\sigma = \frac{n\bar{X}_1 T_0}{T_{X1}\sqrt{1+T_0^2}}. \tag{4.40}$$

Although this is a suitable form for the computation of σ, it neglects the effects of distortions on the ray angles α_0 and α_x. The Gaussian

distortions of the field shape will be considered in a later chapter, and the seidel distortion of the field might well be neglected, as its effect on the aberration field is a higher-order effect in the ordinary sense. However, in an unobscured all-reflecting system, the object field for any surface may be expected to be decentered by much more than the field size ($\sigma >> 1$). With this comparatively large angle separating the field and the aberration centers, it is reasonable to expect a significant shift of the object field due to the seidel distortion introduced at previous surfaces. Thus, the tangent of the angle of the ray joining the object and pupil centers (which will be referred to as the Optical Axis Ray), may vary significantly from the Gaussian prediction, T_0. This effect may be accounted for simply by using a real ray angle in place of α_0. Accordingly, a real Optical Axis Ray (OAR) is traced through the system using ACCOSV, and the ray angles and surface intersections are input to the Vector Aberration Theory program. Since ACCOSV gives the ray angles referenced to the mechanical axis each surface, the angle β of the Local Axis must be subtracted from α_{ACCOS} to yield $\alpha_{0_{real}}$, as shown in Figure 4.2. (In computing σ for the aspheric contribution, the Aspheric Axis rather than the Local Axis is used.) The vector σ may now be computed as

$$\sigma = \frac{(\sin\alpha_{0_{real}})\ n\bar{X}_1}{T_{X1}}. \tag{4.41}$$

With σ defined in this way, the component of fifth (and higher) order

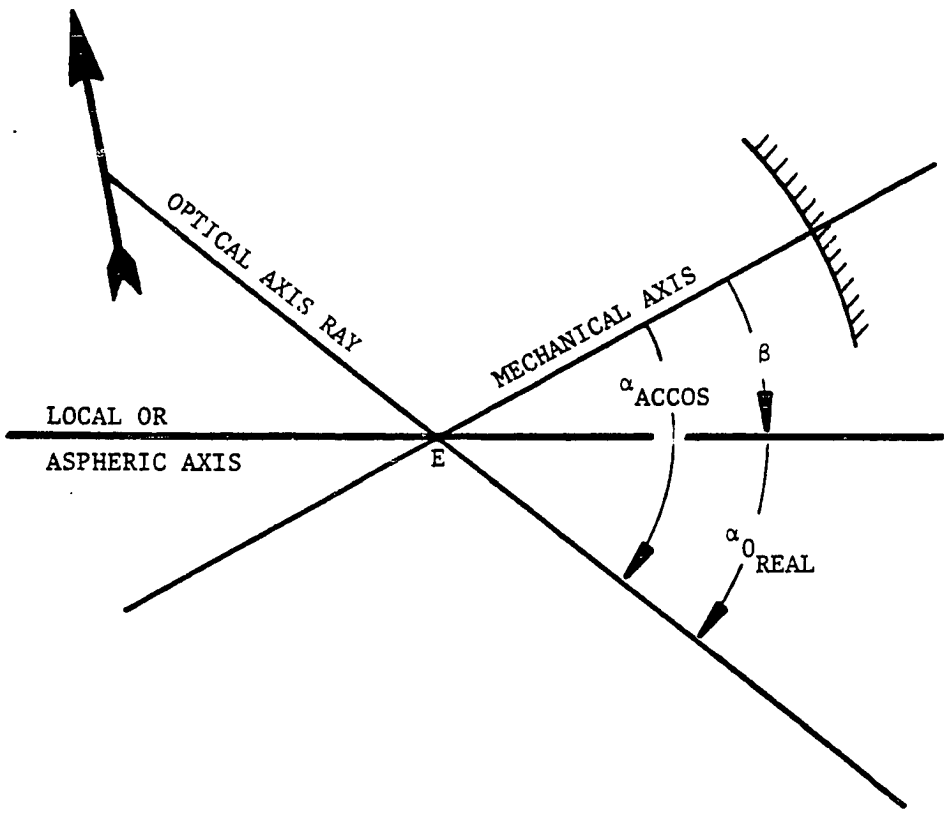

Figure 4.2. Computation of Real Object Decentration Angle.

distortion due to distortion of earlier surfaces has been accounted for at the center of the field.

Special Cases

As previously stated, the cases of a base sphere concentric with the pupil or an aspheric at the pupil may be dealt with by expanding the spherical aberration introduced by the surface about the center of the pupil, which may be sheared with respect to the center of the aberration function. The vector form of the wave aberration function for the i^{th} surface contribution is

$$W_i = W_{040_i} (\rho' \cdot \rho')^2, \tag{4.42}$$

Where ρ' is measured from the Local Axis (or Aspheric Axis, as appropriate). Denoting the relative decentration of the pupil from this axis by $\Delta\rho$, as in Figure 4.3, then

$$\rho' = \rho + \Delta\rho. \tag{4.43}$$

Substituting this into Eq. (4.42), expanding and collecting terms yields

$$\begin{aligned} W_i = W_{040_i}[&(\rho \cdot \rho)^2 + 4(\rho \cdot \rho)(\rho \cdot \Delta\rho) + 4(\rho \cdot \Delta\rho)^2 \\ &+ 4(\rho \cdot \rho)(\Delta\rho \cdot \Delta\rho) + 4(\rho \cdot \Delta\rho)(\Delta\rho \cdot \Delta\rho) \\ &+ (\Delta\rho \cdot \Delta\rho)^2]. \end{aligned} \tag{4.44}$$

The last term in this expression has no pupil dependence, and is

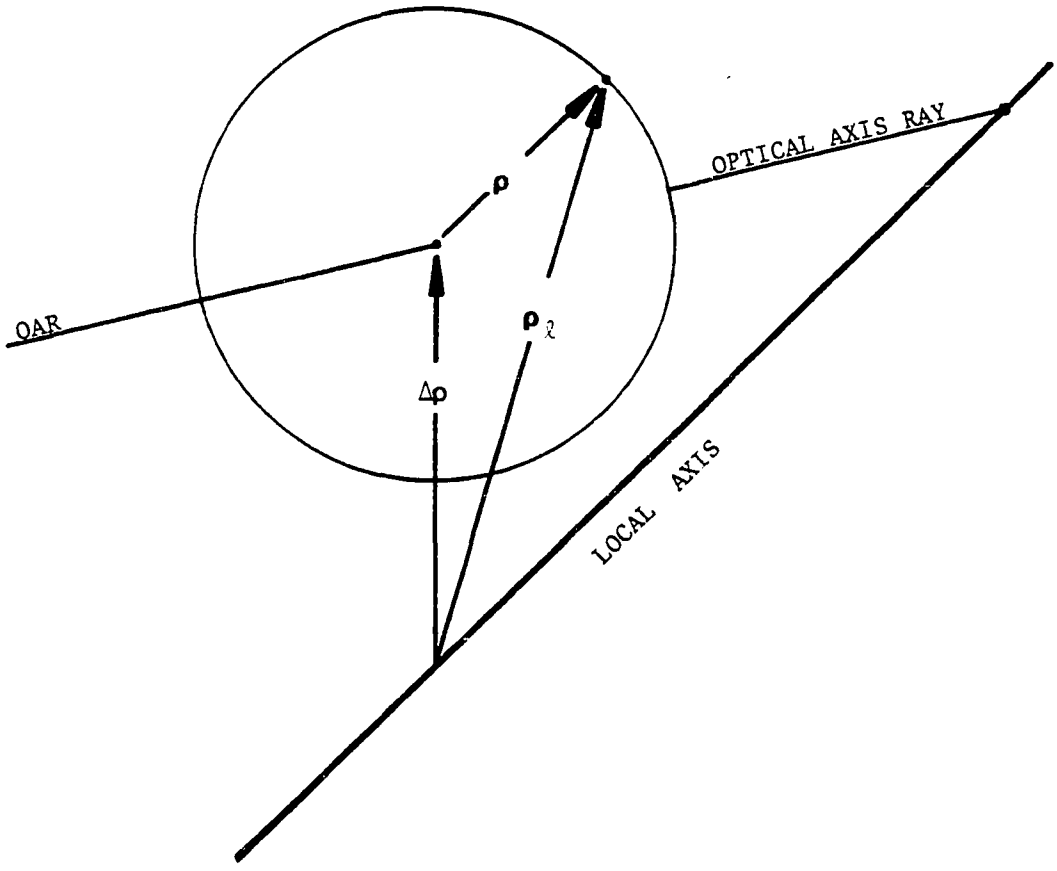

Figure 4.3. Geometry for Pupil Expansion.

identified as piston error, which causes no image degradation, and is therefore ignored. Comparing the remaining terms to those of Eq. (4.2), it is seen that, as far as the pupil dependence is concerned, there is a one-to-one correspondence between the terms of the two equations. The field variable **H** has been replaced with $\Delta\rho$, meaning that in this case there is no field dependence, but the relative amounts of the various aberrations are governed by the decentration of the pupil. By repeating the derivations outlined in the previous section, and including these field independent terms, one may see that this set of field constant aberrations will introduce the following changes in the aberrational parameters of the system:

$$\Delta W_{040} = W_{040_i} \tag{4.45}$$

$$\Delta W_{131} = \Delta W_{220M} = \Delta W_{222} = \Delta W_{311} = 0 \tag{4.46}$$

$$\Delta\alpha_{311} = -4W_{040_i}\Delta\rho_i/W_{131} \tag{4.47}$$

$$\Delta b_{220M} = 4W_{040_i}(\Delta\rho_i\cdot\Delta\rho_i)/W_{220} \tag{4.48}$$

$$\Delta b_{222}{}^2 = 2W_{040_i}\Delta\rho^2/W_{222} \tag{4.49}$$

$$\Delta c_{311} = -4W_{040_i}(\Delta\rho\cdot\Delta\rho)\Delta\rho \tag{4.50}$$

$$\Delta a_{220M} = \Delta a_{222} = \Delta a_{311} = \Delta b_{311}{}^2 = \Delta d_{311} = \Delta a_{111} = 0. \tag{4.60}$$

Once these numerical changes have been made, the interpretation of the vectors is the same. It is interesting to note that the introduction of the field constant aberrations only relocates the nodes of the field aberrations and introduces no change in their coefficients, as indicated by Eq. (4.46).

To find the vector $\Delta\rho$ associated with a surface, it suffices to notice that $\Delta\rho$ is to the pupil coordinates what σ is to the field coordinates. With this in mind, one might expect that interchanging the pupil (barred) and object (unbarred) quantities in Equation (4.41) would yield the correct result. Actually, this is not required, since the roles of all the object and pupil parameters are interchanged whenever a surface of this type is encountered. Interchanging them again for the purpose of obtaining $\Delta\rho$ rather than σ restores the right-hand side of Equation (4.41) to its original form, giving

$$\Delta\rho = \frac{(\sin\alpha_{U_{real}})\, n\bar{X}_1}{T_{X1}} \tag{4.61}$$

(with the pupil and object parameters interchanged).

Calculation of the Wave Aberration Coefficients

In order to obtain the wave aberration coefficients for any particular surface of a system, the optical subsystem consisting of that surface, its object and its pupil is modeled on ACCOSV, using the Local Axis of the surface as the axis of the system. The field angle is taken as $\tan\alpha_x$, or in canonical terms,

$$\text{FANG} \equiv \frac{T_{x1}}{n\bar{X}_1}. \tag{4.62}$$

The pupil radius is simply taken as $\overline{X}_1$, and the object distance is taken as $-Z_0$. With the system defined in this way, the command MAB3 ALL is executed, producing the list of coefficients, SA3, CMA3, AST3, DIS3, and PTZ3. These are coefficients which, when multiplied by the system f/number, will give the transverse ray errors in the Gaussian image plane due to spherical aberration, coma, astigmatism relative to the Petzval surface, distortion, and Petzval curvature, respectively. Using the relation connecting transverse ray error (ϵ) and wave aberration coefficients,

$$\epsilon = -2(f\#)\nabla W, \tag{4.63}$$

it is possible to convert the transverse error coefficients (from ACCOSV) into "pseudo-wave aberration" coefficients.

Here, an important point must be made, concerning the physical significance of the ACCOSV coefficients. They are coefficients of the transverse ray errors as a function of ρ measured in a flat pupil plane oriented normally to the axis of the system, as shown in Figure 4.4. As a result, the coefficients generated by the use of Equation (4.63) do not actually represent the classical wave aberration function, but rather represent a mathematical transformation of the transverse ray error coefficients. Nevertheless, they are coefficients which characterize the behavior of the optical system, and no further distinction will be made between these "pseudo-wave aberration" coefficients and those of classical geometrical optics.

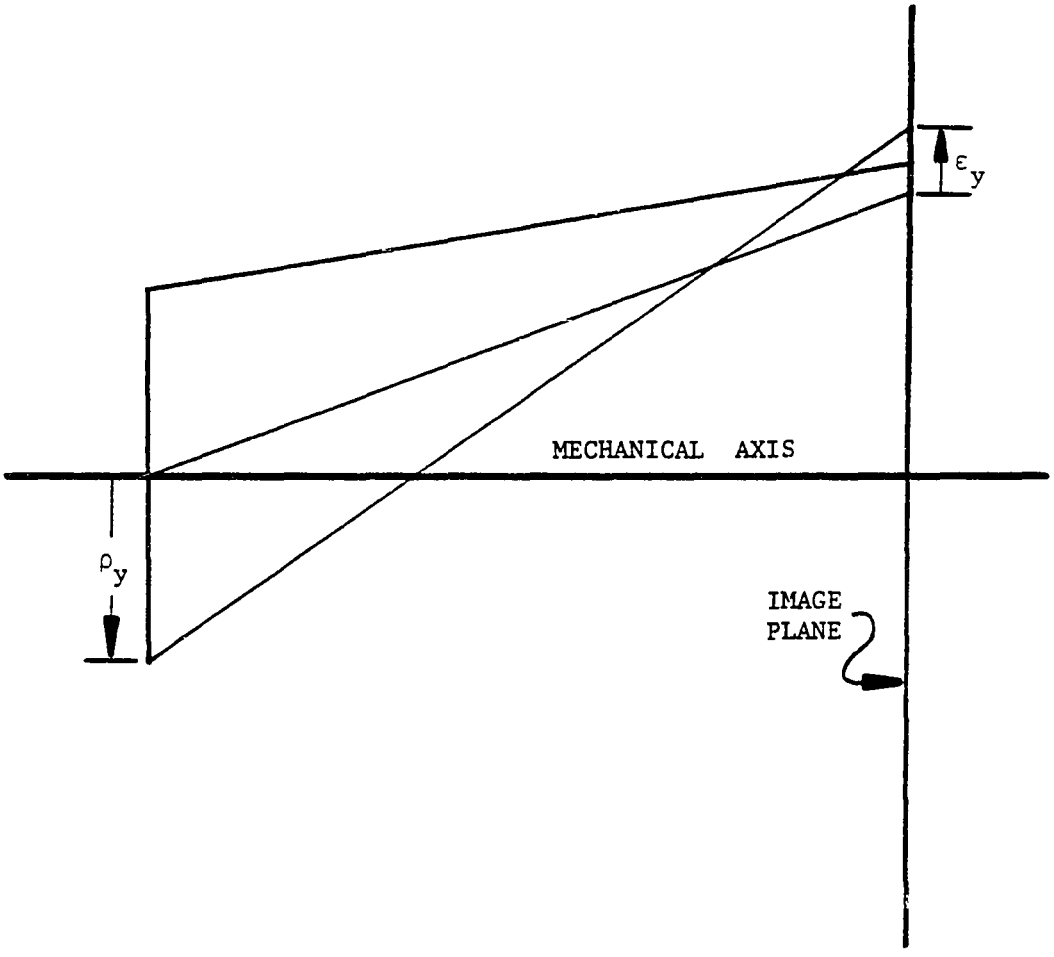

Figure 4.4. Pupil Coordinates used by ACCOSV.

Returning to the aberration coefficients obtained using Eq. (4.63), the astigmatism and Petzval coefficients may be combined to yield coefficients for astigmatism relative to the medial surface and medial field curvature, respectively. The equations converting the transverse ray error coefficients into wave aberration coefficients are given in Table 4.1. Once the coefficients are found for the surface, the aspheric terms for the surface are removed, and the process repeated, yielding the wave aberration coefficients for the base sphere. Taking the difference between the coefficients for the actual surface and those for the base sphere gives the coefficients for the aspheric contribution only.

Correction for Obliquity. Because the aberration coefficients derived above are computed for each surface individually, each set of aberration coefficients corresponding to the aberration contributions of a particular surface is implicitly refers to a pupil variable, ρ_ℓ, measured transversally to the Local Axis of that particular surface. Clearly, before the aberration coefficients can be combined in a meaningful way, they must be put in terms of a single pupil variable, the logical choice for which is ρ, measured in the aperture stop. The primary difference between ρ and ρ_ℓ is an anamorphism due to the obliquity of the ray bundle relative to the Local Axis, but there are also the Gaussian distortions for the pupil introduced by previous surfaces. For this reason, the effect of the pupil obliquity will be considered along with the pupil distortion, in the next chapter.

Table 4.1 Conversion from ACCOSV to Wave Aberration Coefficients

$$W_{040_i} = - SA3_i /8$$

$$W_{131_i} = -CMA3_i /6$$

$$W_{222_i} = -AST3_i /2$$

$$W_{2220M_i} = W_{222_i} - PTZ3_i /4$$

$$W_{311_i} = -DIS3_i /2$$

CHAPTER 5

EFFECTS OF GAUSSIAN DISTORTIONS ON THE ABERRATIONS

The theory described in the previous chapter considered the locations and sizes of the entrance pupils for the various surfaces, but neglected the fact that each pupil is likely to be tilted, anamorphic and keystone distorted. Likewise, the Gaussian distortions of the object field were also not considered. (The effect of a tilted object field upon the aberrations was mentioned only to state that it would be neglected.)

From a physical point of view, the pupil for any particular surface represents only the boundary of the pencil of light which passes through the surface. If this were the only optical surface in the system, the aberrations could be measured against an undistorted pupil coordinate system, and the non-circularity of the pupil treated in the same fashion as vignetting. However, in a tilted and decentered system, the pupil is expected to change its shape as it passes through the system, due to the oblique intersections of the ray bundle with the principal planes. With this fact in mind, it is necessary to retain a map of the pupil shape, so that at any particular surface, the amount of aberration associated with each ray is appropriate to the position of that ray in the local pupil of the surface.

At this point it is necessary to call attention to the fact that the ordinary Seidel aberrations depend on the cosine of the angle φ between the field vector and the pupil vector (see Figure 4.1). A complete treatment of the interactions of the Gaussian distortions of the object and pupil with the aberrations would yield aberrations depending on the cosine (and sine) of the angles θ and $\bar{\theta}$, instead. The reason for this is that the Gaussian distortions are necessarily aligned with the y-z plane, which contains all the tilts and decentrations.

In this chapter, the assumption will be made that H_x is small enough that the angle θ may be neglected, and that $\bar{\theta}$ represents the same angle as ϕ. This is actually a much less severe restriction than might be expected. Recalling from Chapter 4 that the vector forms of the aberrations vary with the vector $(\mathbf{H} - \mathbf{a})$, where $\mathbf{a}$ represents the node of the appropriate aberration or surface contribution, then the angle θ in the approximation is given by the expression $\theta \equiv \text{Arctan}(\frac{Hx}{Hy - a})$. When dealing with the individual surface contributions, which are generally large, it must be remembered that in an unobscured system, the tilt angle of each surface must exceed the field angle. For wide aperture, narrow field applications, the required tilt angle is many times the field angle, and the approximation is valid over the entire field of view. For wide field systems, the theory will at least be accurate near the Hy axis. In Chapter 8 it will be seen that an understanding of the behavior of the surface contributions along this axis leads to a powerful design technique.

It will be seen in this chapter that the aberrational effects of the Gaussian distortions are proportional to the Seidel aberrations. Consequently, when analyzing the imagery near the final resultant aberration nodes, where the above approximation breaks down, the Seidel aberrations are expected to be small, and the effects discussed in this chapter are expected to be negligible.

Effects of Pupil Distortions

As mentioned at the end of the last chapter, the wave aberration coefficients describe the wave aberration function in terms of the normalized radius from the Local Axis of the surface. In this chapter, it will be necessary to make this fact explicit by writing this variable as ρ_ℓ, the subscript indicating that this it is a variable of the local coordinate system. The mathematical definition of ρ_ℓ is given by the pair of equations

$$\rho_{\ell y} \equiv \frac{\bar{y}_\ell}{\bar{X}_1}, \tag{5.1}$$

$$\rho_{\ell x} \equiv \frac{\bar{x}_\ell}{\bar{X}_1}. \tag{5.2}$$

Given a wave aberration function in terms of ρ_ℓ, one may convert it into terms of ρ by inserting, in place of ρ_ℓ, the expression relating it to ρ.

To find this expression, consider first the y-direction. Figure 5.1 shows a cone of rays converging from a pupil to an object point on the OAR. The absolute pupil coordinates $\bar{y}_{\ell}$ and $\bar{y}_{OAR}$ as measured perpendicular to the Local Axis and the OAR, respectively, are shown. Applying the law of sines to the shaded triangle, and simplifying, one obtains

$$\bar{y}_{\ell} = \frac{\bar{y}_{OAR} \cos\bar{\alpha}_y}{\cos(\alpha_0 + \bar{\alpha}_y)}. \tag{5.3}$$

Using the identity for the cosine of the sum of angles, and dividing numerator and denominator by $\cos\bar{\alpha}_y \cos\alpha_0$, this becomes

$$\bar{y}_{\ell} = \frac{\bar{y}_{OAR}/\cos\alpha_0}{1 - T_0 \tan\bar{\alpha}_y}. \tag{5.4}$$

The quantity $\bar{y}_{OAR}$ may be written as

$$\bar{y}_{OAR} = -Z_{EO} \tan\bar{\alpha}_y/\cos\alpha_0. \tag{5.5}$$

Expressing $\tan\bar{\alpha}_y$ in terms of canonical quantities, this becomes

$$\bar{y}_{OAR} = \frac{-Z_{EO}\, \bar{T}_{y1}\, \rho_y}{nX_1(1-\bar{K}_T\rho_y)\cos\alpha_0}. \tag{5.6}$$

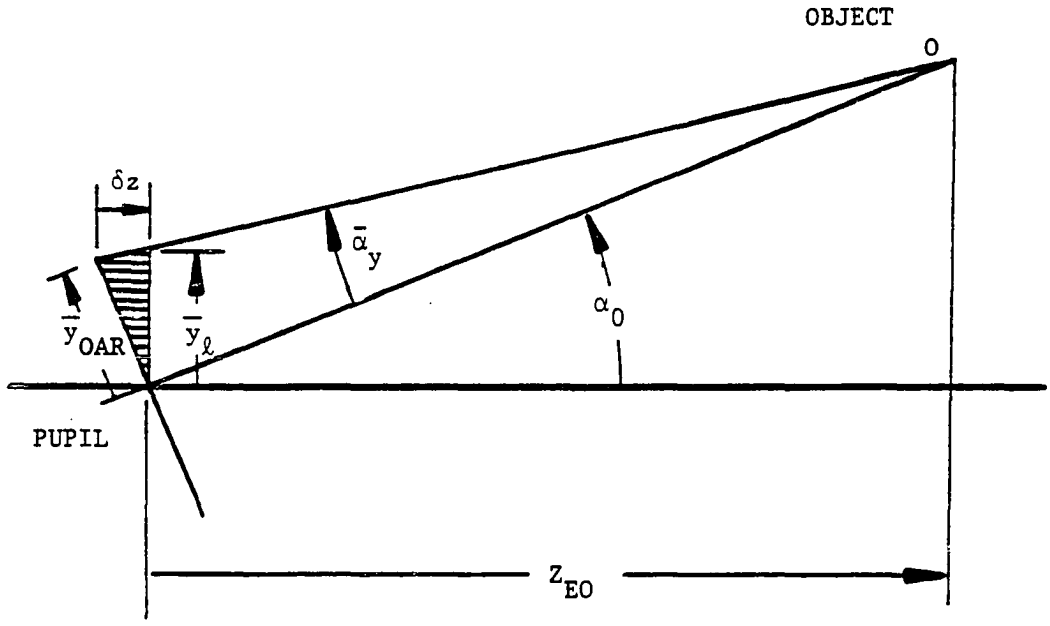

Figure 5.1. Relating Local and OAR Pupil Coordinates.

Doing the same for $\tan\bar{\alpha}$ in Eq. (5.4) and using Eq. (5.6) for $\bar{y}_{OAR}$ gives

$$\bar{y}_{\ell} = \frac{\rho_Y \left[-Z_{EO}\ \bar{T}_{Y1}/(n\bar{X}_1 \cos^2\alpha_0)\right]}{1 - \left[\bar{K}_T + (T_0\bar{T}_{y1}/n\bar{X}_1)\right]\rho_y} \tag{5.7}.$$

Dividing both sides of this equation by $\bar{X}_1$, and simplifying using Eq. (3.4) gives an expression for ρ_{ℓ_y},

$$\rho_{\ell_y} = \frac{(1-\bar{A}_{\ell})\rho_y}{1 - \bar{K}_{\ell}\rho_y} \tag{5.8}$$

where the pupil anamorphism parameter, $\bar{A}_{\ell}$, is defined as

$$\bar{A}_{\ell} \equiv 1 + \left[\bar{T}_{Y1}/(T_{X1}\cos\alpha_0)\right], \tag{5.9}$$

and the local pupil keystone parameter, $\bar{K}_{\rho}$, is defined as

$$\bar{K}_{\ell} \equiv \bar{K}_T + \left[T_0\bar{T}_{Y1}/(nX_1)\right]. \tag{5.10}$$

Finding ρ_{ℓ_x} is somewhat more complicated, because the angle $\bar{\alpha}_x$ only represents the angular separation of the point $(\bar{x},\bar{y})$ from the $\bar{y}$-$\bar{z}$ plane if $\bar{y}$=0. However, referring to Figure 5.2, it may be seen that

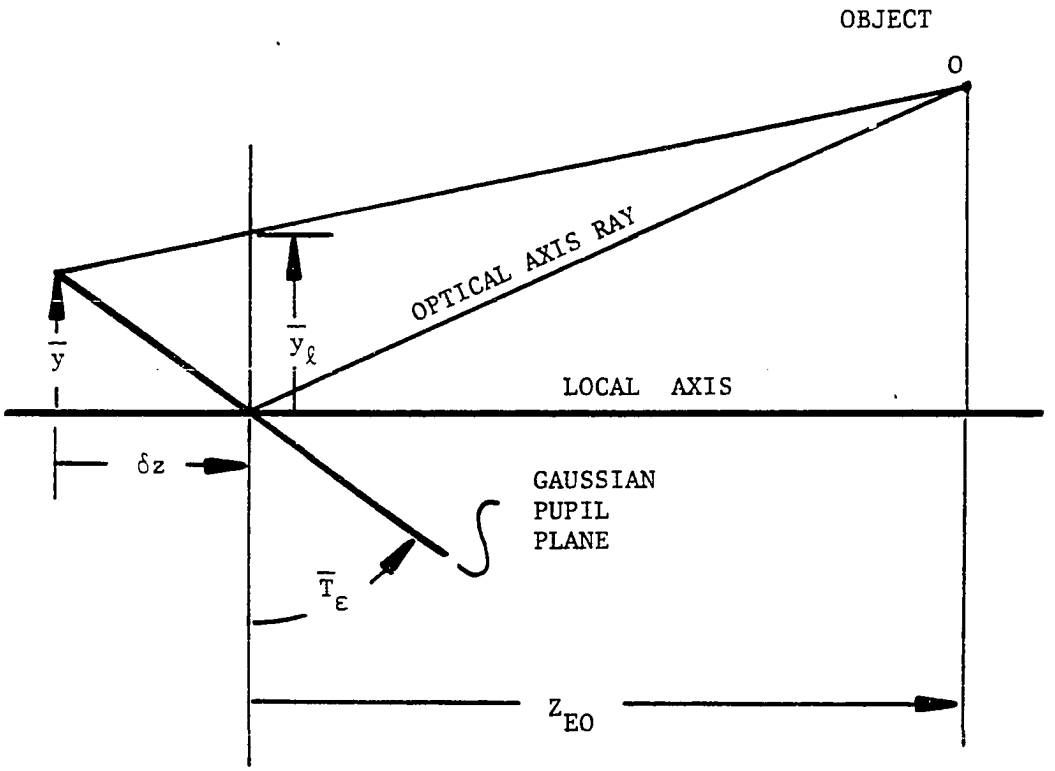

Figure 5.2. Relating Gaussian and Local Pupil Coordinates.

$$\overline{x}_{\ell} = \frac{\overline{x}\, Z_{EO}}{Z_{EO} + \overline{yT}_{\varepsilon}} \tag{5.11}$$

Using Eqs. (2.29) and (2.30) for $\overline{y}$ and $\overline{x}$, this expression becomes (after simplification),

$$\overline{x}_{\ell} = \frac{\overline{X}_1 \rho_x}{1 - \left[\overline{K} - \dfrac{\overline{T}_{\varepsilon}\overline{Y}_1}{Z_{EO}}\right]\rho_y}. \tag{5.12}$$

Dividing by $\overline{X}_1$ to obtain ρ_{ℓ_x}, and using Eqs. (3.61) and (3.62) to replace $\overline{K}$ and $\overline{Y}_1$, one obtains

$$\rho_{\ell_x} = \frac{\rho_x}{1 - \overline{K}_{\ell}\rho_y} \tag{5.13}$$

where $\overline{K}_{\ell}$ is defined as in Eq. (5.10).

In order to study the aberrations in their traditional (power series) form, it is necessary to expand the denominators of Eqs. (5.8) and (5.13). Because both $\overline{A}_{\ell}$ and $\overline{K}_{\ell}$ are small, only the first order terms need to be retained, giving the following (approximate) equations

relating the pupil coordinates used in the local wave aberration expansion to the ray coordinates in the aperture stop of the system:

$$\rho_{\ell y} = (1-\overline{A}_\ell)\rho_y + \overline{K}_\ell \rho_y{}^2 \tag{5.14}$$

$$\rho_{\ell x} = \rho_x + \overline{K}_\ell \rho_x \rho_y. \tag{5.15}$$

Since the surface contributions are implicitly a function of ρ_ℓ, these last two equations may be used to transform the aberration function into an expansion in ρ, instead. The aberration terms will be considered individually, with a subscript of ℓ indicating the coefficient computed with respect to the local pupil variable ρ_ℓ.

Spherical Aberration

The wave aberration function for spherical aberration may be written in terms of $\rho_{\ell x}$ and $\rho_{\ell y}$ as

$$W_{SA} = W_{040\ell}(\rho_{\ell x}{}^2 + \rho_{\ell y}{}^2)^2 \tag{5.16}$$

At this point it is useful to compute the quantities $\rho_{\ell x}{}^2$ and $\rho_{\ell y}{}^2$. Squaring Eqs. (5.14) and (5.15), and keeping only terms of first-order in $\overline{A}_\ell$ and $\overline{K}p$, one finds

$$\rho_{\ell y}{}^2 = (1 - 2\overline{A}_\ell)\rho_y{}^2 + 2\overline{K}_\ell \rho_y{}^3 \tag{5.17}$$

$$\rho_{\ell x}{}^2 = \rho_x{}^2 + 2\overline{K}_\ell \rho_x{}^2 \rho_y. \tag{5.18}$$

Inserting these expressions into Eq. (5.16) and collecting terms yields

$$W_{SA} = W_{040_\ell}(\rho^2 + 2\bar{K}_\ell \rho^2 \rho_y - 2\bar{A}_\ell \rho_y{}^2)^2. \tag{5.19}$$

Performing the square in this expression, keeping only first order terms, one finds

$$W_{SA} = W_{040_\ell}(\rho^4 + 4\bar{K}_\ell \rho^4 \rho_y - 4\bar{A}_\ell \rho^2 \rho_y{}^2). \tag{5.20}$$

Using the fact that $\rho_y = \rho\cos\phi$, this may be rewritten as

$$W_{SA} = W_{040_\ell}\rho^4 + 4\bar{K}_\ell \rho^5 \cos\phi - 4\bar{A}_\ell \rho^4 \cos^2\phi. \tag{5.21}$$

Thus, the coefficient of ρ^4 remains the same, but two new aberrations have been found. Using the convention that the subscripts of W represent (in order) the powers of H, ρ, and $\cos\phi$, the coefficients of the system aberration function induced by spherical aberration at this surface are

$$W_{040} = W_{040_\ell} \tag{5.22}$$

$$W_{051} = 4\bar{K}_\ell \, W_{040_\ell} \tag{5.23}$$

$$W_{042} = -4\bar{A}_\ell \, W_{040_\ell}. \tag{5.24}$$

Coma

The aberration function for coma may be written as

$$W_C = W_{131_\ell} H(\rho_{\ell_x}{}^2 + \rho_{\ell_y}{}^2)\rho_{\ell_y}. \tag{5.25}$$

Inserting Eqs. (5.14), (5.17), and (5.18), multiplying, and eliminating the higher order terms yields

$$W_C = W_{131_\ell} H\left[(1-\bar{A}_\ell)\rho^2\rho_y + 3\bar{K}_\ell\rho^2\rho_y{}^2 - 2\bar{A}_\ell\rho_y{}^3\right]. \tag{5.26}$$

From this, the coefficients of the expansion in terms of ρ may be identified:

$$W_{131} = (1-\bar{A}_\ell)W_{131_\ell} \tag{5.27}$$

$$W_{142} = 3\bar{K}_\ell W_{131_\ell} \tag{5.28}$$

and

$$W_{133} = -2\bar{A}_\ell W_{131_\ell}. \tag{5.29}$$

Astigmatism and Field Curvature

For the purpose of this section, it will be easiest to return to the sagittal image field and the astigmatism with respect to that

surface. Solving Eq. (4.8) for W_{220} yields

$$W_{220} = W_{220M} - \frac{1}{2} W_{222}. \tag{5.30}$$

The aberration function for (sagittal) field curvature may be written as

$$W_{SFC} = W_{220_\ell} H^2(\rho_{\ell x}^2 + \rho_{\ell y}^2) \tag{5.31}$$

Replacing the local axis parameters with those of the stop and simplifying yields

$$W_{SFC} = W_{220_\ell} H^2\left[\rho^2 + 2\bar{K}_\ell \rho^2 \rho_y - 2\bar{A}_\ell \rho_y^2\right]. \tag{5.32}$$

Using Eq. (5.30) to express W_{220}, the new coefficients are:

$$W_{220} = W_{220M_\ell} - \frac{1}{2} W_{222_\ell} \tag{5.33}$$

$$W_{231} = 2\bar{K}_\ell(W_{220M_\ell} - \frac{1}{2} W_{222_\ell}) \tag{5.34}$$

and

$$W_{222} = -2\bar{A}_\ell(W_{220M_\ell} - \frac{1}{2} W_{222_\ell}). \tag{5.35}$$

Turning next to astigmatism, one may write

$$W_A = W_{222_\ell} H^2 \rho_{\ell y}{}^2. \tag{5.36}$$

Using Eq. (5.17) yields immediately,

$$W_A = W_{222_\ell} H^2 \left[(1-2\bar{A}_\ell)\rho_y{}^2 + 2\bar{K}_\ell \rho_y{}^3 \right]. \tag{5.37}$$

From this, one may identify the terms

$$W_{222} = (1-2\bar{A}_\ell)\, W_{222_\ell} \tag{5.38}$$

and

$$W_{233} = 2\bar{K}_\ell\, W_{222_\ell}. \tag{5.39}$$

Since the astigmatism term in Eq. (5.38) arises independently of that of Eq. (5.35), the total astigmatism is the sum of the two. After simplifying, the total astigmatism coefficient is

$$W_{222} = (1-\bar{A}_\ell)\, W_{222_\ell} - 2\bar{A}_\ell\, W_{220M_\ell}. \tag{5.40}$$

The field curvature may now be expressed again using the medial focal surface. Using (a primed version of) Eq. (4.8) and substituting Eq. (5.40)

for W_{222}, one finds

$$W_{220M} = (1-\bar{A}_\ell)\, W_{220M_\ell} - \frac{1}{2}\,\bar{A}_\ell W_{222_\ell}. \tag{5.41}$$

Distortion

The aberration function for distortion may be written as

$$W_D = W_{311_\ell} H^3 \rho_{\ell_y}. \tag{5.42}$$

Using Eq. (5.14) immediately yields

$$W_D = W_{311_\ell} H^3 \left[(1-\bar{A}_\ell)\rho_y + \bar{K}_\ell \rho_y{}^2\right] \tag{5.43}$$

The new aberration coefficients are:

$$W_{311} = (1-\bar{A}_\ell)\, W_{311_\ell} \tag{5.44}$$

and

$$W_{322} = \bar{K}_\ell\, W_{311_\ell}. \tag{5.45}$$

It has been seen that the presence of anamorphic and keystone distortions of the pupil alters some of the Seidel aberration

coefficients and introduces some entirely new aberration terms. These effects are summarized in Table 5.1.

Effects of Object Distortions

The consequences of having an object field which is anamorphically and keystone distorted should at this point be obvious. Just as ρ_ℓ needed to be replaced with ρ, in the case of the pupil aberrations, a similar change of variables must take place in the field coordinates. Because the aberrations for each surface are computed using an object field which is described in angular terms (see Eq. (4.62)), the obliquity of the object plane need not be considered; however, the anamorphic and keystone distortions of the field angle will be of importance.

Considering first the y-direction, define H_{ℓ_y} as the tangent of the (distorted) field angle in the y-direction normalized by the quantity $\tan\alpha_x|_{H_x=1;H_y=0}$. Using Eqs. (3.12), (3.13) and (3.17), then

$$H_{\ell_y} = \frac{(T_{Y1}/T_{X1})H_y}{1 - K_T H_y}. \tag{5.46}$$

The x-direction is more complicated, because of the way in which $\tan\alpha_x$ was defined. However, using a technique similar to that used to derive Eq. (5.13), it can be shown that

$$H_{\ell_x} = \frac{H_x}{1 - K_T H_y}. \tag{5.47}$$

Table 5.1. Aberrational Consequences of Gaussian Distortions of the Pupil

Modified Coefficients:

$$W_{040} = W_{040_\ell} \tag{5.22}$$

$$W_{131} = (1-\bar{A}_\ell)\, W_{131_\ell} \tag{5.27}$$

$$W_{220M} = (1-\bar{A}_\ell)\, W_{220M_\ell} - \frac{1}{2}\,\bar{A}\, W_{222_\ell} \tag{5.41}$$

$$W_{222} = (1-\bar{A}_\ell)\, W_{222_\ell} - 2\bar{A}\, W_{220M_\ell} \tag{5.40}$$

$$W_{311} = (1-\bar{A}_\ell)\, W_{311_\ell} \tag{5.44}$$

New Coefficients:

$$W_{051} = 4\bar{K}_\ell\, W_{040_\ell} \tag{5.23}$$

$$W_{042} = -4\bar{A}_\ell\, W_{040_\ell} \tag{5.24}$$

$$W_{142} = 3\bar{K}_\ell\, W_{131_\ell} \tag{5.28}$$

$$W_{133} = -2\bar{A}_\ell\, W_{131_\ell} \tag{5.29}$$

$$W_{231} = 2\bar{K}_\ell\, (W_{220M_\ell} - \frac{1}{2}\, W_{222_\ell}) \tag{5.34}$$

$$W_{233} = 2\bar{K}_\ell\, W_{222_\ell} \tag{5.39}$$

$$W_{322} = \bar{K}_\ell\, W_{311_\ell} \tag{5.45}$$

The above expressions may now be used to put the wave aberration function from each surface contribution in terms of the system parameter, **H**, rather than the local parameter $\mathbf{H}_\ell$. In order to retain the power series form of the aberration expansion, the expressions are expanded, keeping only the linear terms, yielding

$$H_{\ell_y} = (1-A_\ell)H_y + K_T H_y{}^2 \tag{5.48}$$

$$H_{\ell_x} = H_x + K_T H_x H_y \tag{5.49}$$

Where the anamorphism parameter A is defined as

$$A_\ell \equiv 1 - (T_l/T_{Xl}) \tag{5.50}$$

Proceeding in exactly the same manner as for the pupil distortions (except that $\cos\phi$ is now associated with H, so that $H\rho^3\cos\phi = H_y\rho^3$, etc.), the changes in the Seidel coefficients and the new aberration coefficients induced by the presence of object distortion may be computed. The resulting coefficients are quite similar in form to those induced by the pupil distortions, and are listed in Table 5.2.

Discussion

Many of the new aberration forms which appear in Tables 5.1 and 5.2 bear similarities to the ordinary fifth-order aberrations, both in mathematical form and in origin. For instance, the term $W_{042}\ \rho^4\cos^2\phi$ is a consequence of the interaction of spherical aberration and pupil

Table 5.2. Aberrational Consequences of Gaussian Distortions of the Object

Modified Coefficients:

$$W_{040} = W_{040_\ell} \tag{5.51}$$

$$W_{131} = (1-A_\ell)\, W_{131_\ell} \tag{5.52}$$

$$W_{220M} = (1-2A_\ell)\, W_{220M_\ell} \tag{5.53}$$

$$W_{222} = (1-2A_\ell)\, W_{222_\ell} \tag{5.54}$$

$$W_{311} = (1-3A_\ell)\, W_{311_\ell} \tag{5.55}$$

New Coefficients

$$W_{411} = 3K_T\, W_{311_\ell} \tag{5.56}$$

$$W_{320} = 2K_T\, (W_{220M_\ell} - \tfrac{1}{2}\, W_{222_\ell}) \tag{5.57}$$

$$W_{322} = 2K_T\, W_{222_\ell} \tag{5.58}$$

$$W_{231} = K_T\, W_{131_\ell} \tag{5.59}$$

anamorphism. In a symmetric system, the obliquity of the pupil causes an anamorphism varying as the cosine of the field angle, which interacts with spherical aberration to produce the term $W_{242}\ H^2\rho^4\cos^2\phi$. This is one component of the aberration known as oblique spherical aberration. It may seem at first glance that the introduction of the coefficient W_{042} simply amounts to the realization that due to the decentration of the object field from the Local Axis, there is a non-zero contribution of ordinary oblique spherical aberration at the center of the field. This is incorrect, for in a tilted and decentered system, the pupil may not only be oblique, but may also be actually anamorphic, so that it does not appear circular from any point of view in the y-z plane. This fact is reflected in Equation (5.9), which shows that the pupil anamorphism parameter has a component due to the cosine of the object decentration angle α_0 (which accounts for the "ordinary" part of the oblique spherical aberration), and another component due to the anamorphic properties of the tangent parameters T_{Y1} and T_{X1}.

It is also important to realize that the pupil distortions considered in this chapter are considered constant in the field; no attempt has been made to model the changes in $\overline{A}$ and $\overline{K}_\ell$ with field angle.

The field dependent aberrations should properly be treated in the same manner as the Seidel aberrations in Chapter 3; however, the addition of ten more field aberrations would complicate matters beyond the point of usefulness. From the equations in the tables, it may be seen that unless the Gaussian distortions of the object or pupil become enormous, these higher order aberrations should remain small, although

not necessarily insignificant. In calculating the aberrations of the systems discussed in Chapter 7, the Seidel coefficients were modified according to the tables, and the coefficients W_{042} and W_{051} were computed, but the ten new field dependent terms were neglected altogether.

CHAPTER 6

PROJECTION OF THE IMAGE ONTO THE DETECTOR PLANE

In a rotationally symmetric optical system, the detector plane is expected to lie close to the Gaussian image plane. A consequence of this is that except for a small change in focus, the Gaussian and aberrational properties of the system are essentially unchanged by the shift of the detector plane from the Gaussian image plane.

As Figure 6.1 demonstrates, one may expect the detector to be located relatively far from the Gaussian image when the system contains tilted and decentered elements. Not surprisingly, both the Gaussian and the aberrational properties will be affected by the projection of the rays from the Gaussian image surface onto the detector plane.

Gaussian Properties

There are two logical coordinate systems for reporting the Gaussian image properties, both of which have their x- and y- axes contained in the plane of the detector. The first coordinate system is centered on the intersection of the OAR with the detector. The logic used in this choice of coordinates is that in any real system, it is the location of the detector that defines the object/image field of the system, so the origin of the detector coordinates should by definition, coincide with the center of the image field. Unfortunately, most optical design programs trace rays from a "real" object, whose position

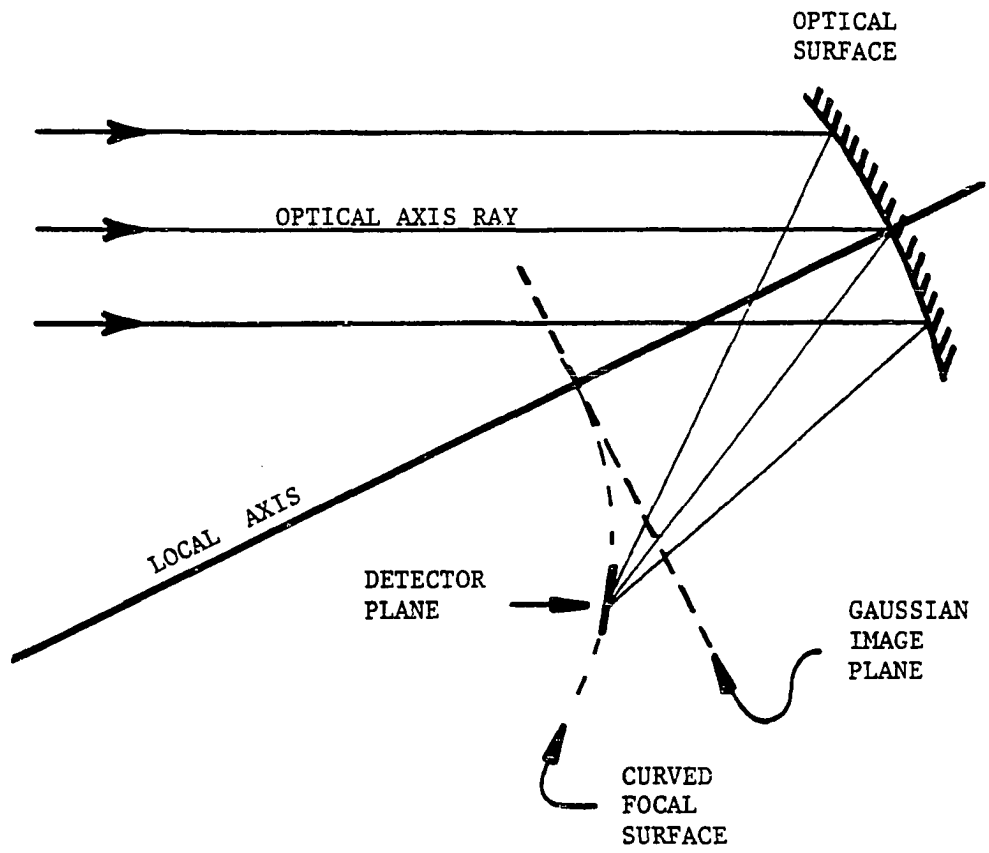

Figure 6.1. Separation of Gaussian Image and Detector Plane.

determines the locations of the ray intersections with the final surface of the system, assumed to be the detector. The coordinate system used in this work has its origin at the mechanical center of the detector plane. Using these coordinates admits the possibility that the detector might not be located in the proper position to receive the rays from the "real" object used by the design program. It is convenient to define the Detector Axis to be normal to the detector plane at the origin of the detector coordinates, which are labeled X_D and Y_D. This axis coincides with the local mechanical axis used by most design programs to define the location of the surface.

Since the detector is one of the optical surfaces of the system, its local axis is normal to it, and since it is assumed here to be planar, then the Local Axis is parallel to the Detector Axis, as shown in Figure 6.2. The separation of these two axes is y_{E_D}, the y-coordinate of the pupil in the detector coordinate system, and may be found by a coordinate transformation. From the figure, it is clear that

$$y_D = Y_{E_D} - \overline{Z}_0 \tan(\alpha_0 + \alpha_y). \tag{6.1}$$

Using the identity for the tangent of the sum of angles, expressing $\tan\alpha_y$ in terms of canonical parameters, and simplifying yields

$$Y_D = \frac{Y_{D_0} + Y_{D_1} H_y}{1 - K_D H_y}, \tag{6.2}$$

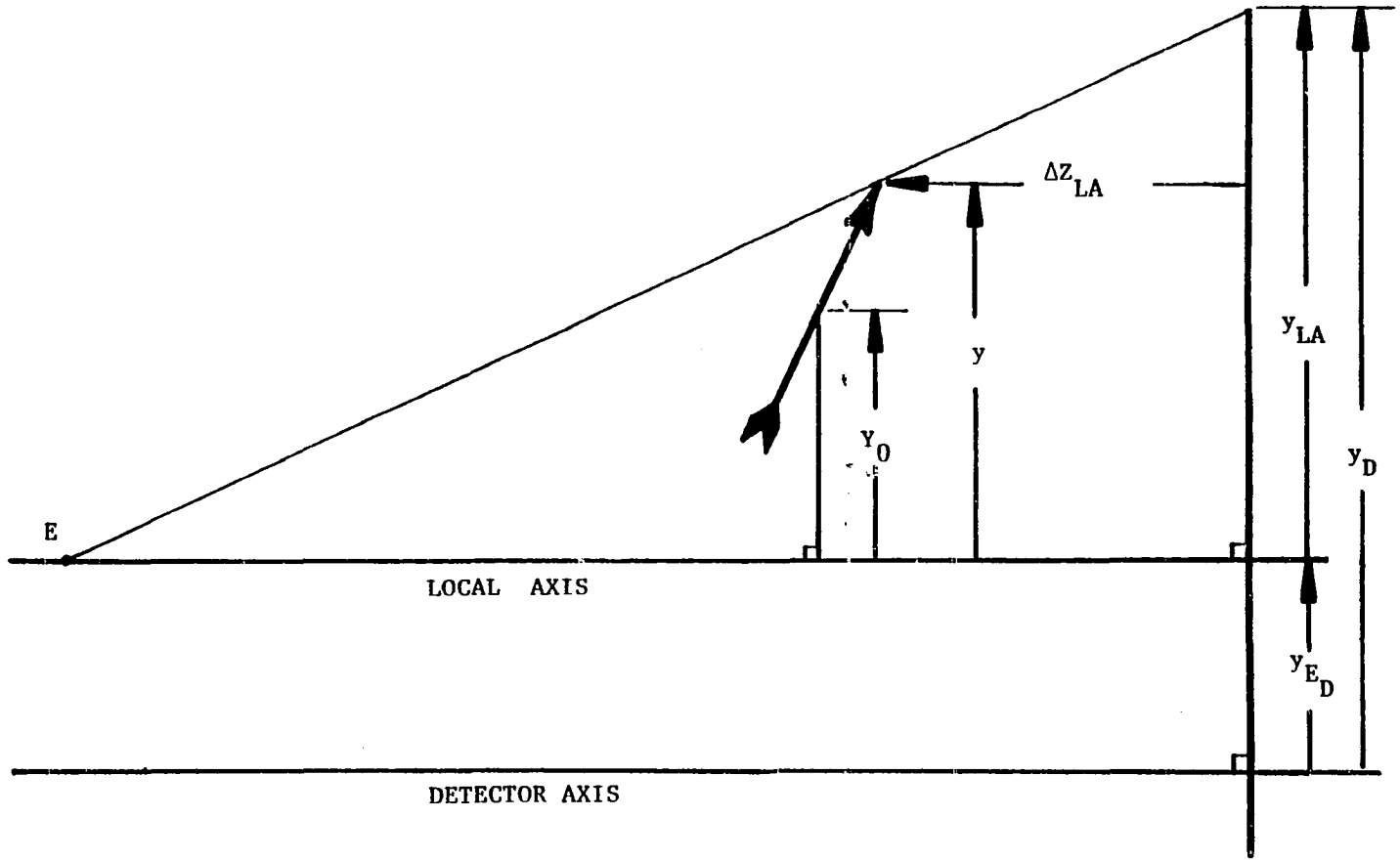

Figure 6.2. Projecting the Gaussian Image onto the Detector Plane.

where

$$Y_{D_0} \equiv -\bar{Z}_0 T_0 + y_{E_D}, \tag{6.3}$$

$$Y_{D_1} \equiv \left[\frac{T_{Y1}}{n\bar{X}_1}\right](\bar{Z}_0 - T_0 y_{E_D}) - K(\bar{Z}_0 T_0 + Y_{E_D}), \tag{6.4}$$

and

$$K_D \equiv K + T_0 T_{Y1}/(n\bar{X}_1). \tag{6.5}$$

A similar procedure for the x-direction yields

$$X_D = \frac{X_{D_1} H_x}{1 - K_D H_y}, \tag{6.6}$$

where

$$X_{D_1} \equiv \left[\frac{T_{X1}}{n\bar{X}_1}\right](\bar{Z}_0 \cos\alpha_0). \tag{6.7}$$

The defocus, Δz_{LA} may be computed simply by noting that

$$\Delta z_{LA} = Z_0 - T_\varepsilon (y - Y_0). \tag{6.8}$$

Substituting the canonical expression for y and simplifying yields

$$\Delta z_{LA} = \frac{DZ_0 + DZ_1 H_y}{1 - KH_y}, \tag{6.9}$$

where

$$DZ_0 = Z_0, \tag{6.10}$$

and

$$DZ_1 = -Z_0K - T_\epsilon(Y_1 + Y_0K). \tag{6.11}$$

The simplest way to relate the defocus to the transverse ray error at the detector plane is to convert the parameter ΔZ into a wave aberration coefficient W_{20} so that it may be treated in the same manner as the Seidel aberrations of the next section. Given a field position in terms of **H**, the value of ΔZ_{LA} may be found, from which the focal shift ΔZ_{OAR} measured parallel the OAR is computed,

$$\Delta Z_{OAR} = \Delta Z_{LA}/\cos\alpha_0. \tag{6.12}$$

Knowing this, the coefficient W_{20} is then computed using the well known relation between focal shift and aberration coefficient,

$$W_{20_{OAR}} = \frac{-n(r_p)^2 \Delta Z_{OAR}}{2R^2}, \tag{6.12}$$

where R is the radius of curvature of the reference sphere and r_p is the radial extent of the pupil. For the calculations in this work, R is taken as the distance $Z_{EO/\cos\alpha 0}$, and r_p is taken to be the x-extent of the pupil $\overline{X}_1$. (The first subscript of the coefficient, which gives the power of H in the term, has been omitted in this notation, since $W_{20_{OAR}}$ will be evaluated for every particular value of H independently.)

Aberrational Properties

The equation relating the wave aberration function to transverse ray errors in the Gaussian image plane for rotationally symmetric optical systems is

$$\epsilon = \frac{-R}{nr_p} \nabla_\rho W. \tag{6.18}$$

Provided that it is still a good approximation that the longitudinal aberration (including defocus) is much less than R, this relation holds for an asymmetric system as well, but it is important to note that the planes containing ρ and ϵ must be parallel. Since the vector ϵ is desired in the detector plane (perpendicular to the LA), it is necessary to convert the aberration function into a function of ρ_ℓ.

Conversion of the wave aberration function into terms of ρ_ℓ is simply the inverse process of that of Chapter 5. Solving Equations (5.8)

and (5.13) for ρ_y and ρ_x, the following relations are obtained:

$$\rho_y = \frac{\rho_{\ell y}/(1 - \bar{A}_\ell)}{1 - \left[\frac{-\bar{K}_\ell}{1 - \bar{A}_\ell}\right]\rho_{\ell y}} \tag{6.19}$$

$$\rho_x = \frac{\rho_{\ell x}}{1 - \left[\frac{-\bar{K}_\ell}{1 - \bar{A}_\ell}\right]\rho_{\ell y}}. \tag{6.20}$$

From these equations, one may identify the parameters

$$\bar{A}_{eff} = 1/(1 - \bar{A}_\ell) \tag{6.21}$$

and

$$\bar{K}_{eff} = -\bar{K}_\ell/(1 - \bar{A}_\ell). \tag{6.22}$$

These parameters may now be used (in place of $\bar{A}_\ell$ and $\bar{K}_\ell$) in the transformations given in Table 5.1, to produce the wave aberration function in terms of ρ measured parallel to the detector plane, to the same degree of approximation as in Chapter 5. Application of Eq. (6.18) to this wave aberration function (ignoring temporarily the defocus), would yield the transverse error ε_{LA} in the plane parallel to the

detector, containing the point 0. However, one may see from the similar triangles in Figure 6.3 that the quantity ϵ_{ab} in the detector plane is given by

$$\epsilon_{ab} = \epsilon_{LA} (-\bar{Z}_0/Z_{EO}). \tag{6.23}$$

The remaining component of the transverse error, ϵ_{20} is due to defocus. However, the defocus coefficient W_{20} was not included in the theory of Chapter 5, and the effects of anamorphic and keystone distortion of the pupil on defocus must now be considered.

Writing the defocus aberration function as

$$W = W_{20_{OAR}} (\rho_x^2 + \rho_y^2), \tag{6.24}$$

and substituting Equations (5.17) and (5.18) for ρ_x^2 and ρ_y^2 (using $\bar{A}_{eff}$ and $\bar{K}_{eff}$ in place of $\bar{A}_\ell$ and $\bar{K}_\ell$), one obtains

$$W = W_{20_{OAR}} (\rho_\ell^2 - 2\bar{A}_{eff}\rho_y^2 + 2\bar{K}_{eff}\rho^2\rho_y). \tag{6.25}$$

Using the same approximations as in Chapter 5, the following wavefront coefficients may be identified:

$$W_{20_\ell} = W_{20_{OAR}} \tag{6.26}$$

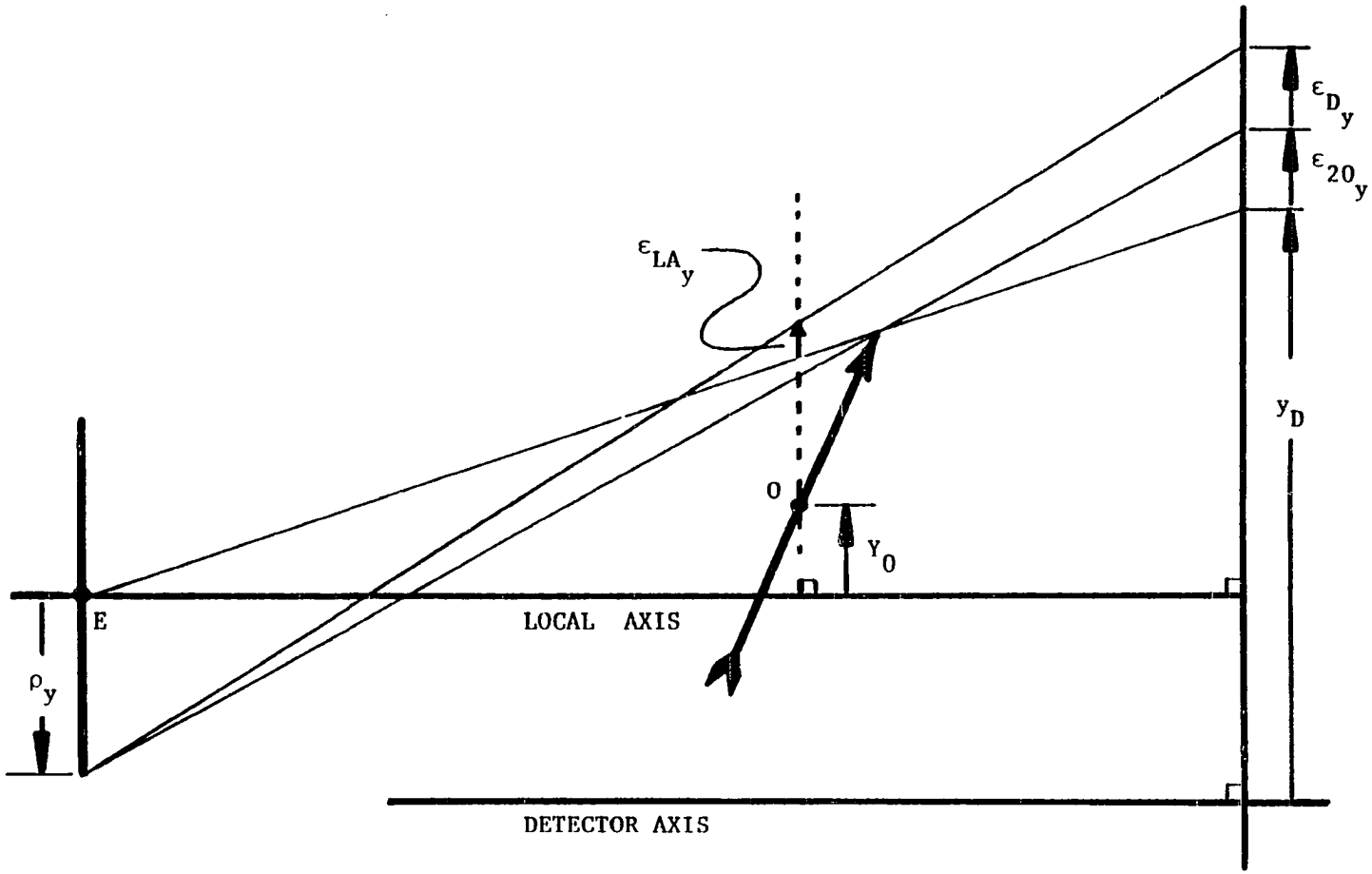

Figure 6.3. Projecting the Aberrations onto the Detector Plane.

$$W_{22_\ell} = -2\bar{A}_{eff} W_{20_{OAR}}$$

$$W_{31_\ell} = 2\bar{K}_{eff} W_{20_{OAR}}. \qquad (6.28)$$

Equation (6.18) may now be applied to the above three terms (without the correction factor of Eq. (6.23)) and the resulting ray error ε_{20} added to ε_{ab}, yielding the total ray error in the detector plane.

CHAPTER 7

ANALYSIS OF UNOBSCURED REFLECTIVE SYSTEMS

In order to verify the validity of the vector theory, as applied to systems with tilts and decentrations large enough to permit the unobscured use of reflective surfaces, the computer program described in Chapter 4 was used to analyze several optical systems, and the predictions of the theory compared to raytrace results.

Gaussian Properties and Distortion

The Gaussian properties will be tested using a single reflecting surface with a tilted object placed at the center of curvature. System 1, shown in Figure 7.1, consists of a mirror of radius -660mm, and an object which would subtend a paraxial semi-field angle of 7.5°, if untilted. The tilt of the actual object plane is 10°. Figure 7.2 shows the form of the image of a square grid with the anamorphic and keystone parameters A and K increased by a factor of 10, to make the distortion more apparent. It is interesting to note that although keystone distortion is entirely nonlinear (see Equations (2.27) and (2.28)), the x- and y- components of the distortion conspire to map the sides of a square to straight lines. It is easily seen, however, that the lines are nonlinearly distorted along their own length.

Only the theoretical results and not the raytrace data are shown in the figure. The reason for this is that there is no way to enhance

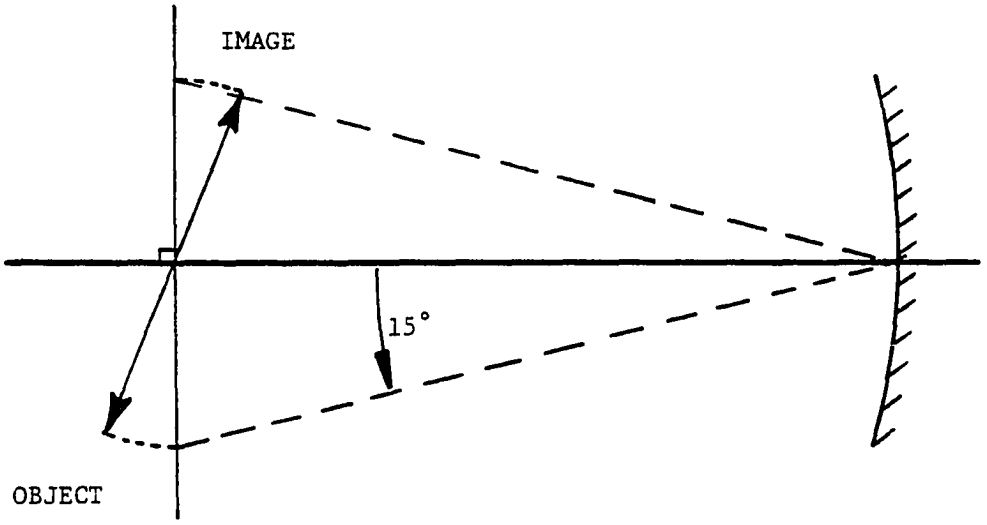

Figure 7.1. Layout of System 1.

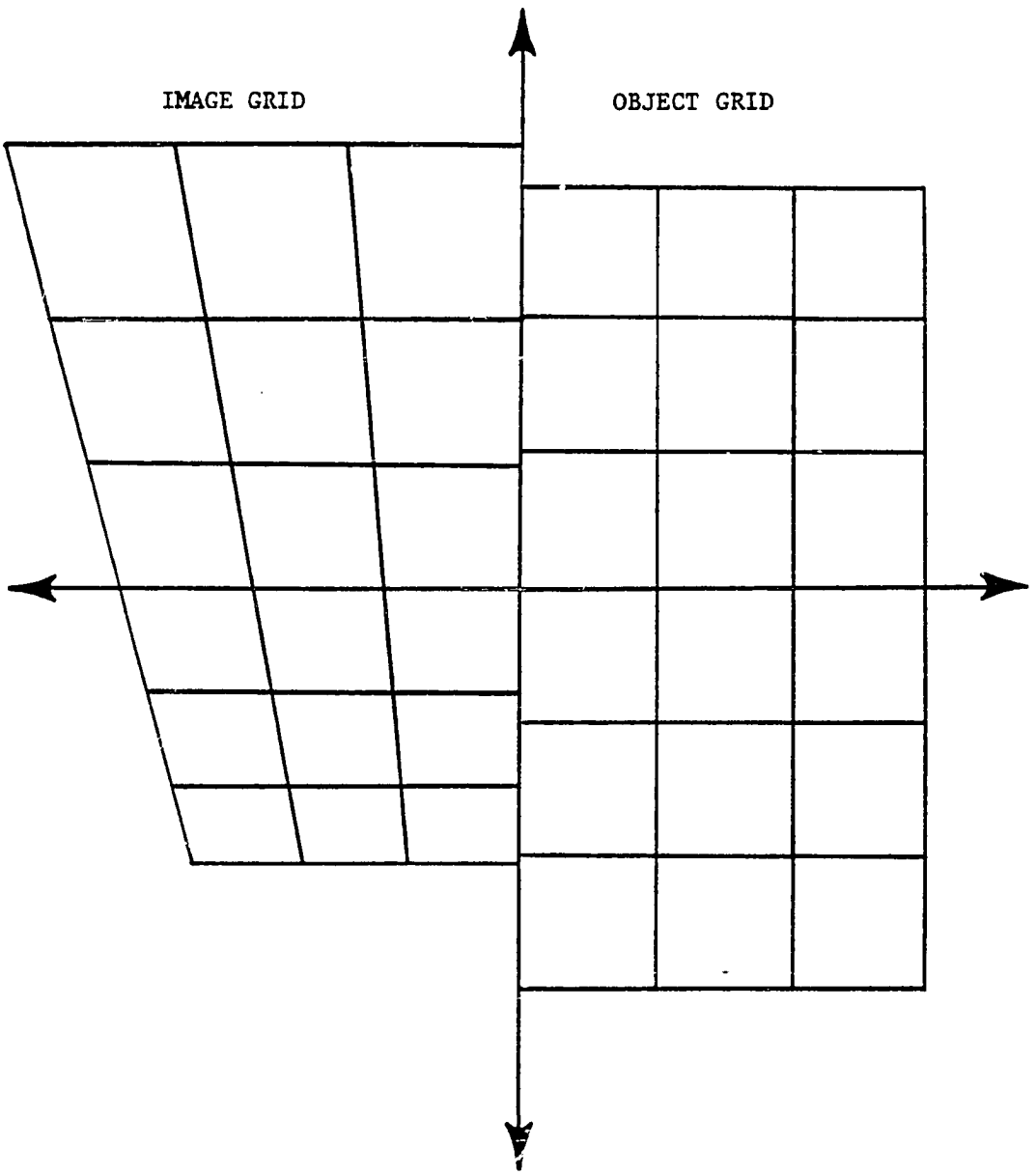

Figure 7.2. Anamorphic and Keystone Distortion of a Regular Grid.

the visibility of the raytrace data without altering the form of the distortion. One common method for displaying distortion is to numerically reduce each datum into an undistorted part and a distortion term, then plot the data with different scales for the two terms. Unfortunately, due to the inherent nonlinearity of the distortion, the resulting plot will no longer have straight grid lines, giving the viewer an incorrect representation of the distortion.

A more useful way of examining the distortion of such systems is by plotting the distortion as a function of the field variable, for two orthogonally oriented strips in the object field. In the distortion plots shown in this chapter, δy is plotted for the "fan" of rays in the H_y-direction, and δx is plotted for the "fan" of rays in the H_x-direction. These fans may be considered as the field equivalent to the "ray fan" plots of transverse ray error versus pupil coordinate.

Figure 7.3 shows a distortion plot for system 1. No difference may be seen between the plots of the theoretical and raytrace data, for they agree to five decimal places. For small field angles, the primary difference between the δx- and δy- curves is the difference in their slopes. This may be regarded as a difference in the linear scaling factor in the two directions, and therefore represents anamorphism. At larger field angles, the δy curve becomes quadratic in H_y, indicating the presence of keystone distortion. The fact that the cubic term of keystone distortion is small may also be seen. System 1 is free from Seidel distortion, because the aperture stop is placed at the mirror. To investigate the form of an image in the presence of Seidel distortion,

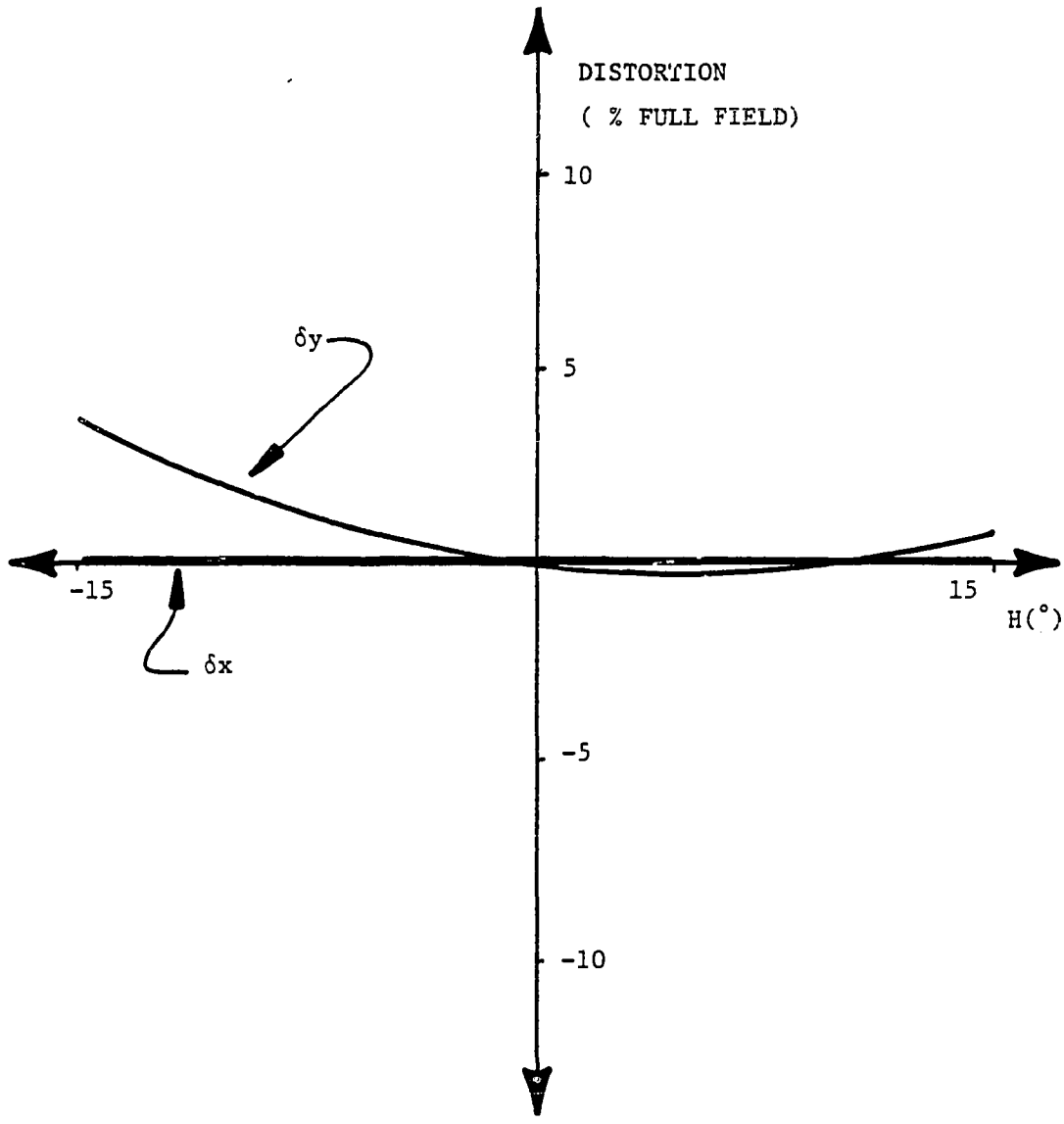

Figure 7.3. Distortion Plot for System 1.

the stop was moved to the front focal point of the lens, creating System 2.

Figure 7.4 shows the distortion plot for System 2, with the theoretical data shown as solid lines and the raytrace data shown dotted. The cubic Seidel distortion is clearly visible in the δx curve, which was previously undistorted. One may see from the relative amounts of quadratic and cubic behavior in the δ curve that the Seidel distortion at the edge of the field is approximately equal to the keystone distortion. At small field angles the curves are like those of Figure 7.3.

Aberrational Properties

To examine the theory's ability to predict the aberrations which reduce image quality, a more complicated system was analyzed. System 3 consists of a two spherical mirror unobscured Cassegrain configuration, as shown in Figure 7.5. The paraxial focal length of the system is 100mm, the paraxial f/number is 11.11, and the field angle is 0.3°. The decentration of the primary is equivalent to a tilt angle of approximately -8°, and the secondary is used about 4° "off axis". The aberrations at the center of the field for this system are shown in the ray fan plot of Figure 7.6. The dotted lines in the figure show the raytrace data, for comparison. In Chapter 5 it was stated that although the vector theory is not strictly correct for field points off the H_y-axis, it will be a good approximation if the aberration nodes are displaced in the H_y- direction, so that the angle θ remains small. This is verified by Figure 7.7, which shows ray fan plots for the system at

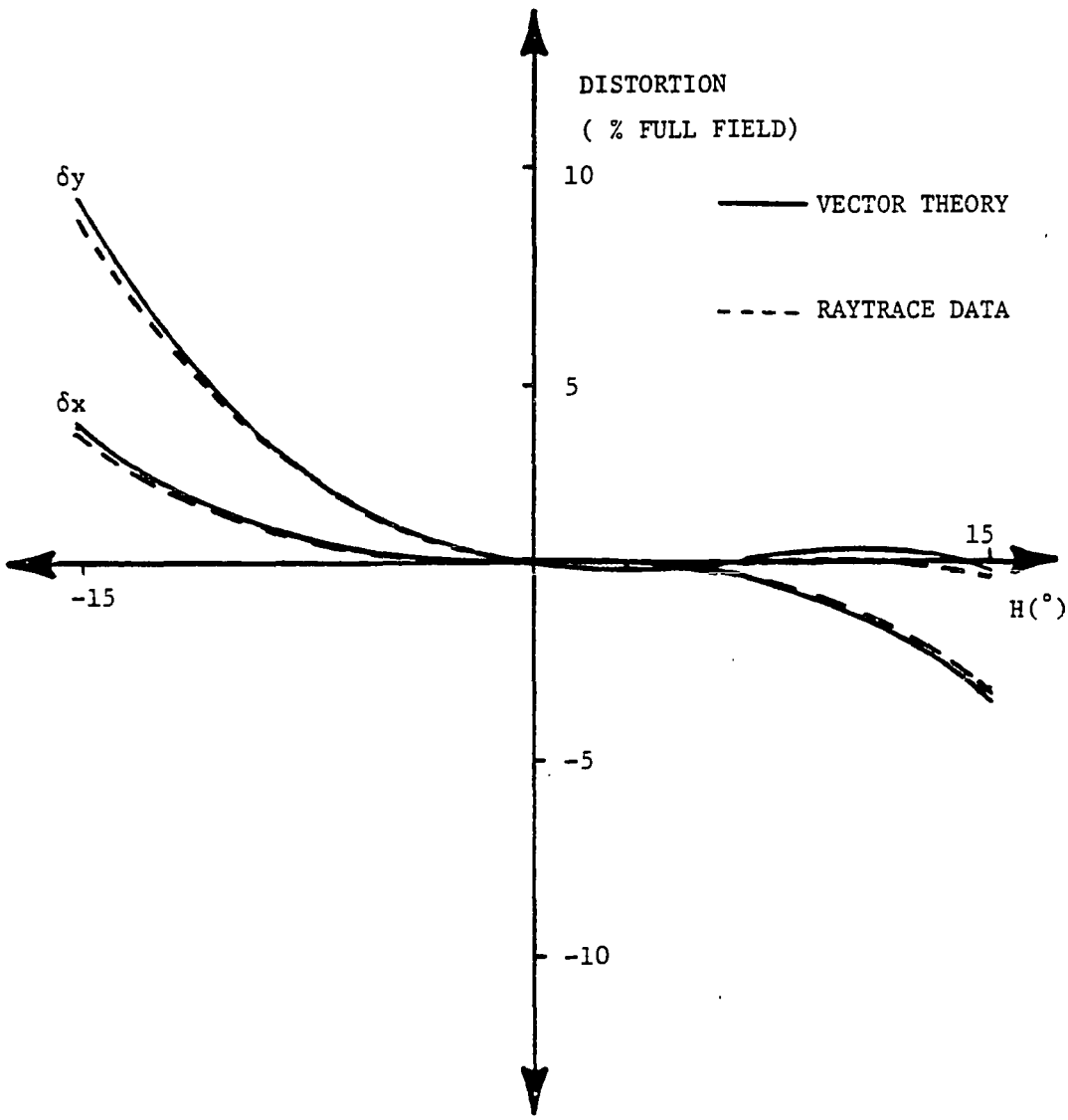

Figure 7.4. Distortion Plot for System 2.

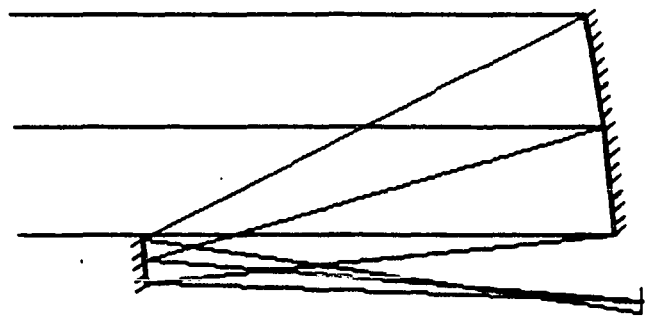

Figure 7.5. Layout of System 3.

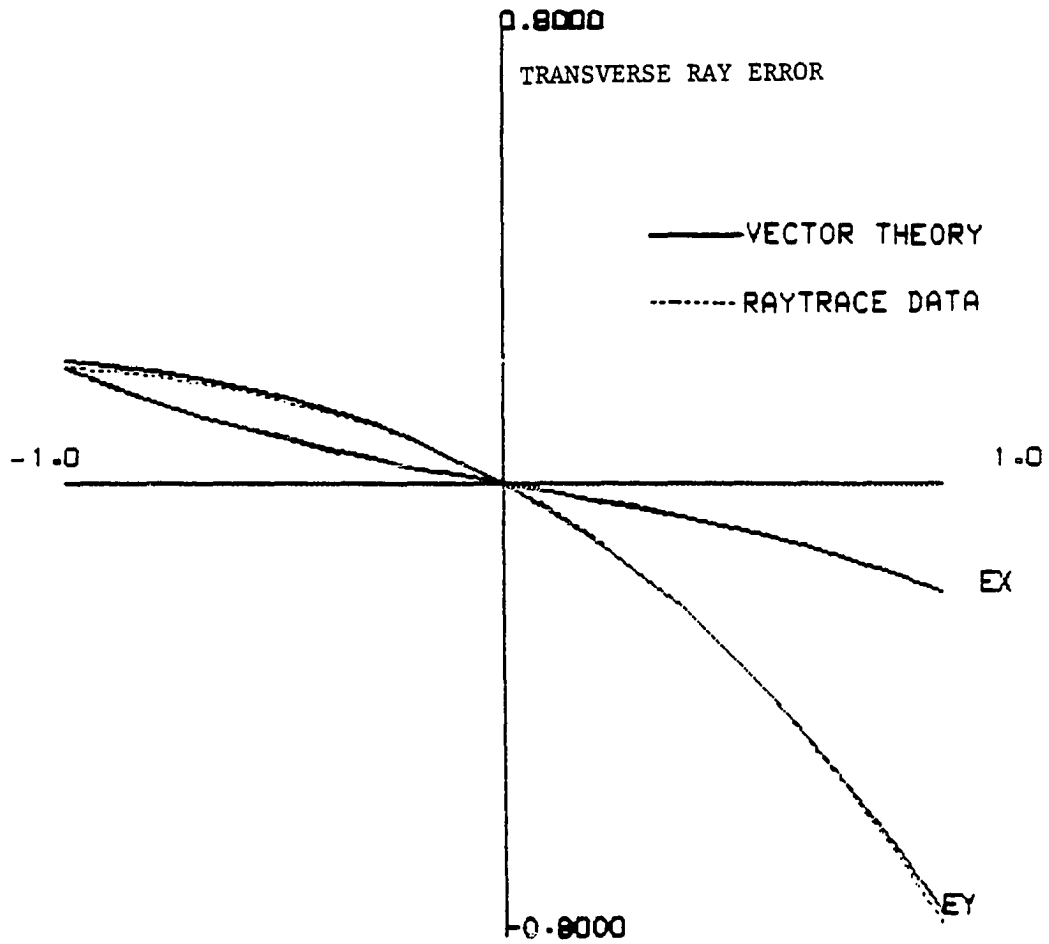

Figure 7.6. Ray Fans for System 3 at H_y=0, H_x=0.

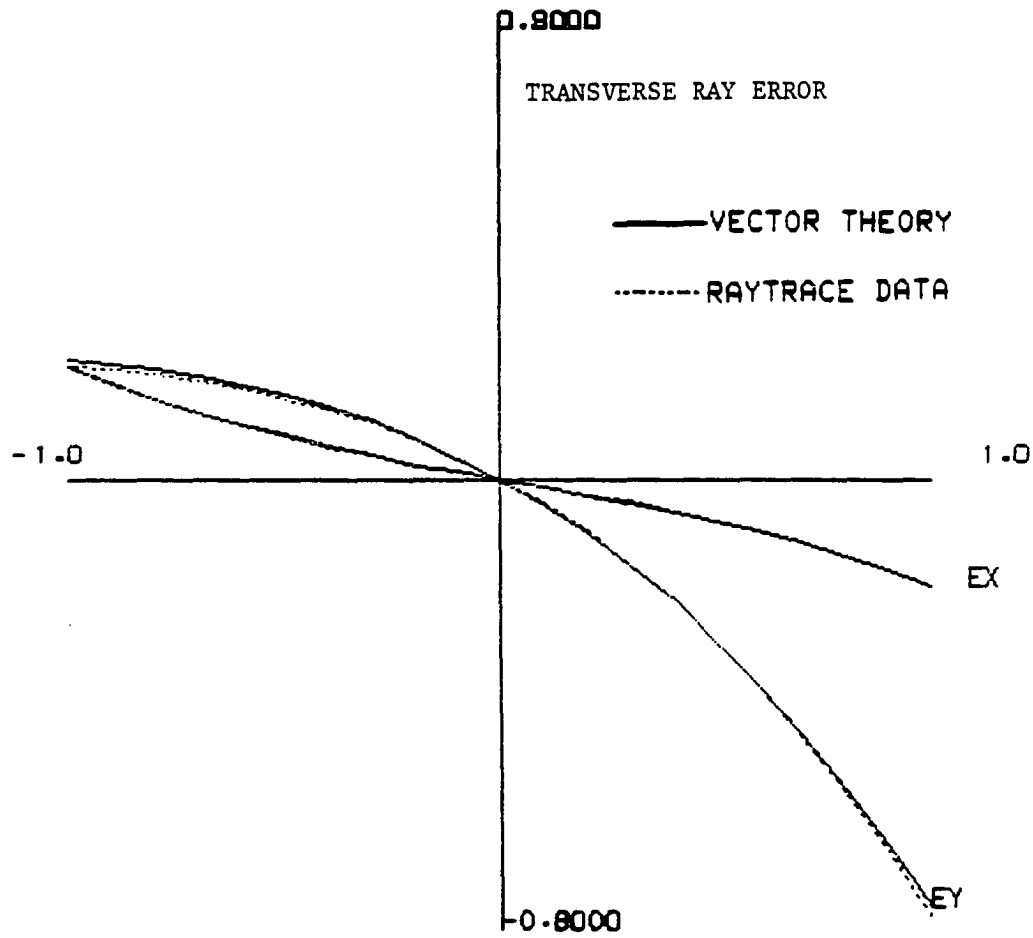

Figure 7.7. Ray Fans for System 3 at H_y=0, H_x=1.

the field point, (H_y = 0, H_x = 1.) At this scale, the difference between the fans for the two field points is difficult to see. This points out one of the useful features of an analytic aberration theory, for the aberrations at the two field points may be easily subtracted, yielding a fan showing the variation in the aberrations between the two field points, shown in Figure 7.8. From the figure, one may see that coma is changing far more readily than is astigmatism, even though the latter is the dominant aberration.

Just as the pupil dependent aberrations have nonzero values at the center of the field, so will the Seidel distortion. The distortion at the center of the field may be regarded as a shift of the entire field. Since the program has the raytrace data for the ray defining the center of the field (the OAR) available to it, it is a simple matter to correct the predicted field shift to match the actual field shift. This procedure ensures that the distortion is exactly correct at the center of the field. Figure 7.9 shows a distortion plot for System 3. The δy curve appears to be a shifted section of an ordinary cubic distortion term, indicating the presence of Seidel distortion centered far from the image field. The nonzero value of the vertical scale at the center of the plot indicates the field shift, while the slope and curvature of the δy curve indicate that this section of the field appears to be anamorphically and keystone distorted. (The origin of these last two distortions is actually in the shifted Seidel distortion.)

The excellent agreement of the theoretical predictions with the ray trace data in Figures 7.6, 7.7 and 7.9 is possible because of the fact

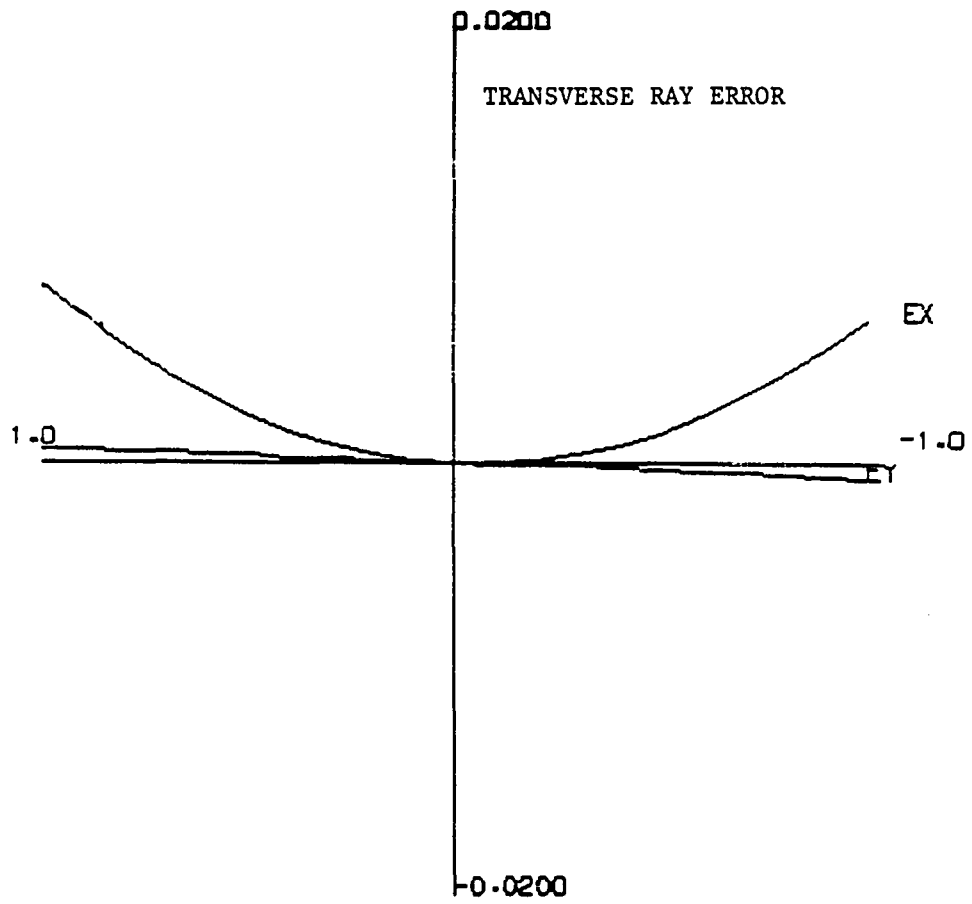

DIFFERENCE OF

(HY,HX) = (0.0,1.0) AND (0.0,0.0)

Figure 7.8. Field- Difference Fans for System 3.

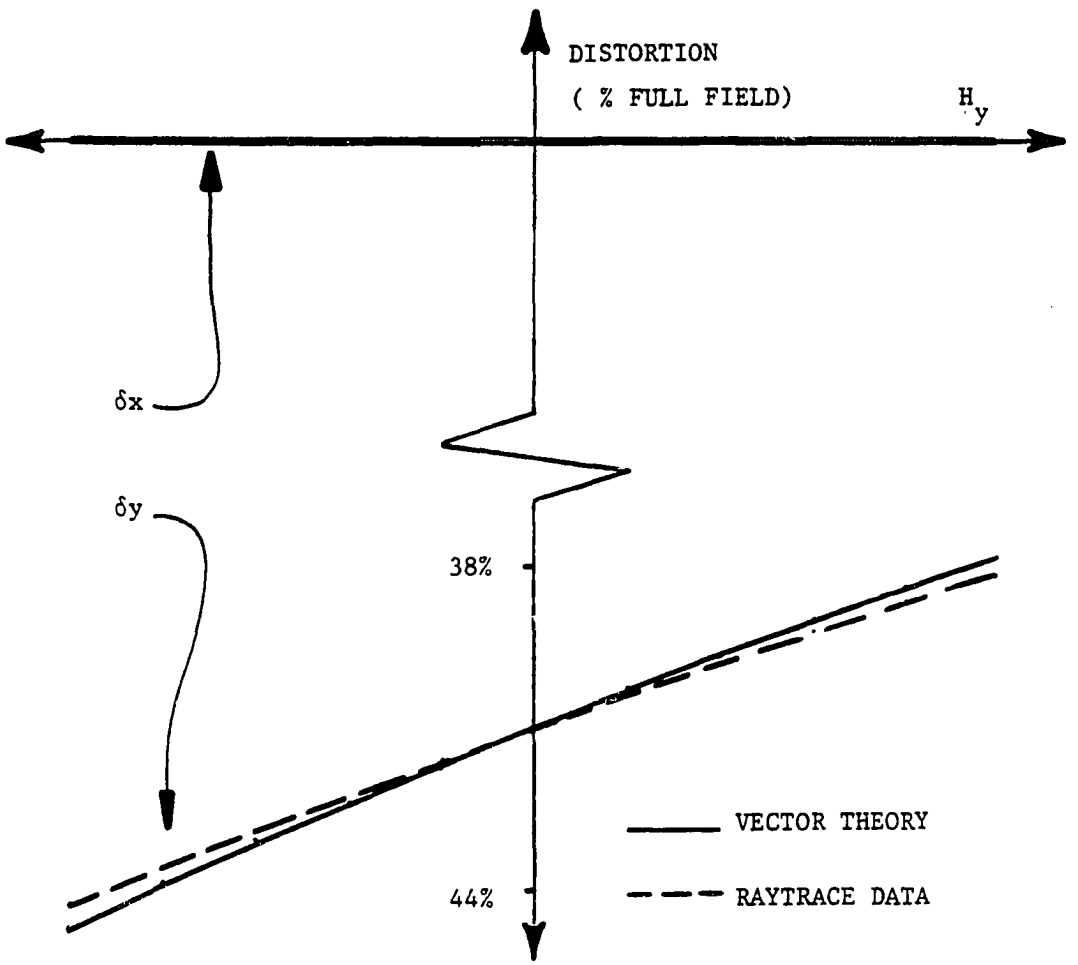

Figure 7.9. Distortion Plot for System 3.

that the third-order aberrations are dominant in this system. An attempt was made to optimize System 3 using real ray definitions of the aberrations on ACCOSV, and the system of Figure 7.10 was the result. This system, System 4, has a secondary magnification of about 2, and a large tilt angle of the secondary. Although coma and astigmatism have not been eliminated, they have been greatly reduced, as shown in Figure 7.11. The raytrace data no longer agree with the predictions of the vector theory; however, the theoretical results still give the behavior of the system in a general sense. The primary error in the theoretically predicted ray fans is in the amount of astigmatism present. This is due to a small amount of fifth order astigmatism introduced by the secondary and augmented by the fourth power of the relatively large tilt angle of that element. The fact that this optimized system still had coma and astigmatism at the center of the field will be discussed further in the next chapter.

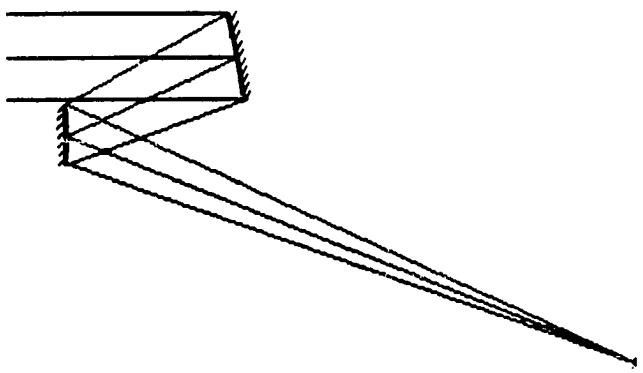

Figure 7.10. Layout of System 4.

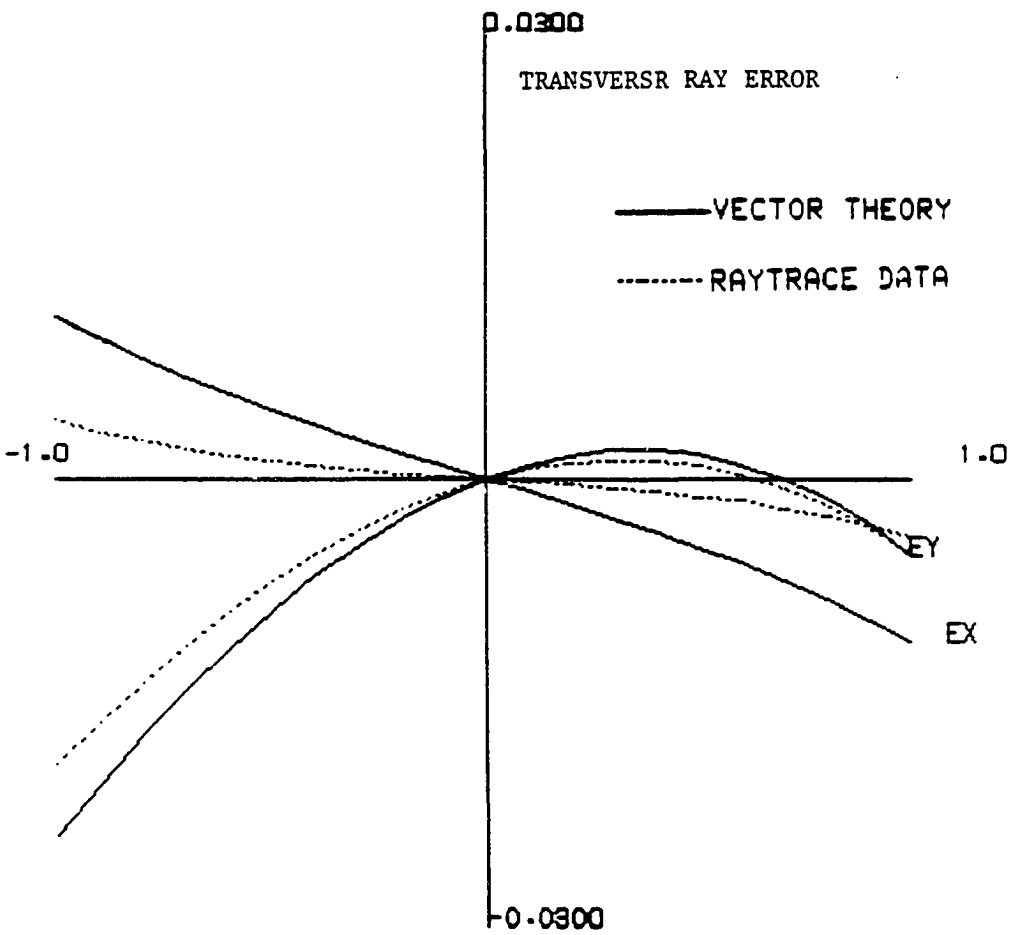

Figure 7.11. Ray Fans for System 4 at H_y=0, H_x=0.

CHAPTER 8

OPTIMIZATION OF UNOBSCURED REFLECTIVE OPTICAL SYSTEMS

The purpose of this chapter is to demonstrate the usefulness of the vector aberration theory, from the standpoint of design. A methodology of design will be developed from the theory, and applied to the design of an unobscured reflective system. The residual aberrations will be discussed, and the selection of starting points which might result in lower residual aberrations will be considered from the point of view of the theory.

The design goal is an unobscured reflective telescope having no "off axis" aspherics. By this it is meant that the aspheric vertices of all elements must lie at the mechanical centers of their respective apertures. The design specifications for the telescope are as for System 3: the telescope is to have a semiaperture of 4.5 units, operate over a 0.3° field angle, and have an f/number no higher than f/12. (If the focal length shortens, producing a faster system, it will be easy to rescale the system and stop it down so that it has the desired focal length and f/number.) It is hoped that using the vector theory, all "axial" aberration, and much of the aberration varying with field can be eliminated.

Initial Optimization Attempts

In optimizing System 3, the design philosophy initially adopted by the author was to tilt the secondary until the coma node was coincident with one of the two astigmatism nodes, then tilt the entire telescope until the field of view coincides with this common node of astigmatism and coma. This would yield a system suffering spherical aberration, ordinary coma, and astigmatism varying approximately linearly with the field. Since the stop is at the primary, aspherizing the primary (with the aspheric vertex located in the center of the stop) will only affect the spherical aberration. If the secondary is also aspherized about the center of the beam "footprint", only ordinary (field centered) aberration terms are generated, since in this case the Aspheric Axis coincides with the Optical Axis Ray. Thus the asphericity of the secondary may be used to eliminate coma, or to introduce enough quadratic astigmatism to partially balance the linear astigmatism, whichever is more desirable.

Unfortunately, the author was unable to make the coma node coincident with one of the astigmatism nodes, except in the obvious but undesired solution of an obscured, rotationally symmetric system. The author then allowed the magnification of the secondary to vary, producing System 4, which still has coma and astigmatism at the center of the field.

The author was initially puzzled by the apparent impossibility of aligning the coma node and one of the two astigmatism nodes, without

also aligning the entire system (and the two astigmatism nodes) at the same time. However, this difficulty may be understood through the geometrical view of the vector aberration theory given below. Furthermore, this geometrical point of view may be used to form the basis of an extremely useful methodology of design.

Geometrical Interpretation of the Theory

In Chapter 4, equations were given which allow the aberration contributions from several surfaces to be combined using vector algebra, to give the locations of the nodes of the various aberrations. Although this algebraic treatment is useful in analyzing a system, little insight is gained from the point of view of design. However, looking at the combination of aberration fields in a graphical way helps the designer understand qualitatively the interactions among the surface contributions. The aberrations coma and astigmatism will be discussed below, as examples.

Coma.

Consider the summation of two displaced coma fields. In order for a node to result at a given field point, two conditions must be met: 1) The absolute magnitudes of the two fields at that point must be equal, and 2) Their orientations must be opposite, so that cancellation occurs. (Because coma has an associated direction, one may not simply require that the wavefront coefficients be equal in magnitude and opposite in sign.) Because coma varies linearly with field, one may imagine the magnitude of the aberration to describe a cone centered on

the node, with the steepness of the cone determined by the absolute value of the coefficient for that surface contribution. Figure 8.1 depicts the magnitudes of two displaced coma fields, labeled P and S for primary and secondary, respectively. It is easily seen that the intersection of the two cones, which is the locus of points at which the two surface contributions are equal, forms a closed path enclosing the surface contribution having the greater coefficient. Thus is is seen that any node which may result from this combination must lie on this closed path. The orientation of the two coma fields must now be considered, which will be done by imagining a view normal to the field plane, with the orientations of the two fields indicated schematically as in Figure 8.2. Because of the radial symmetry of the coma fields, the orientations may be opposite at either point a or point b. In the figure, both coma fields are of the same sign, and the point a becomes the resultant node. If the coma introduced by the secondary were of the opposite sign, the two fields would add at point a, and the node would appear at b, instead. Having located the resultant node, one may then note that the magnitude of the aberration at neighboring points on the H_y axis is simply the difference between the magnitudes of the two contributions at that point. Referring again to Figure 7.12, it may be seen that this linear function is steeper if the node is at the crossing point between P and S, rather than at the crossing point to the left of P.

In summary, it is evident that two possible node locations exist for coma; one between the nodes of the two constituent fields, the other

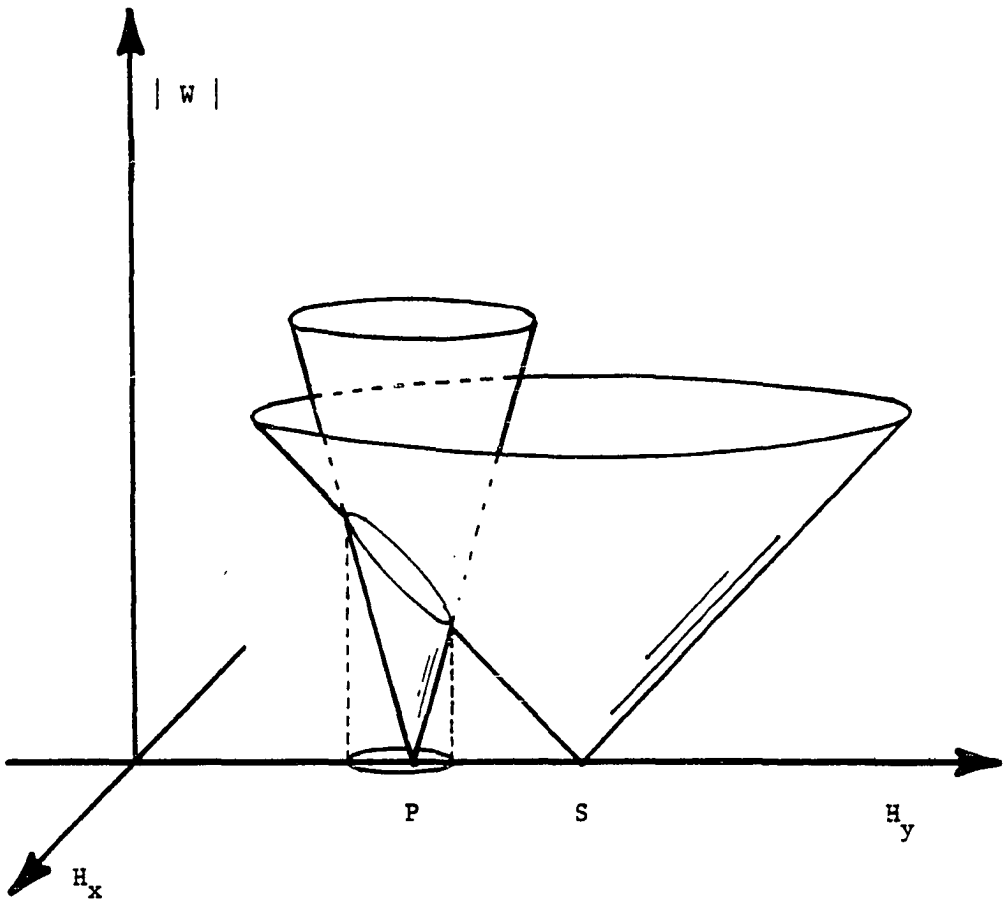

Figure 8.1. Magnitudes of Two Coma Fields.

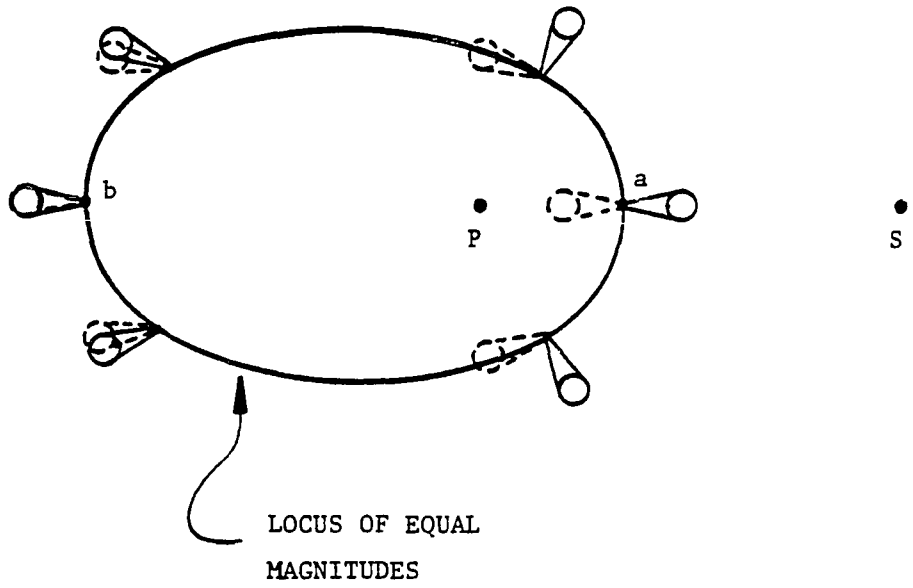

Figure 8.2. Locating the Resultant Coma Node.

outside the two, on the side of the node with the greater coefficient. The inner solution results if the two fields are of the same sign, and has a relatively large coefficient. The outer solution occurs if the two fields are of the opposite sign, and results in a smaller coefficient.

Astigmatism.

The absolute magnitude of astigmatism is a paraboloid centered on the node of the contribution. Replacing the cones of Figure 8.1 with paraboloids, as in Figure 8.3, one may easily see that the locus of possible nodes resulting from the addition of two such astigmatism fields is again a closed path enclosing the node of the stronger surface contribution. Here, the similarity with the case of coma ends, for although astigmatism has an orientation, it is bidirectional in nature. The orientation of quadratic astigmatism may be adequately described by the orientation of the tangential line focus, as shown in Figure 8.4. Clearly, the two field contributions will have the same orientations and absolute magnitudes at <u>both</u> points a and b. If the contributions are of opposite sign, nodes result at both these locations; if they are the same sign, the fields add at these points. In this case, consider the points c and d, which indicate the positions on the locus of equal magnitudes where the orientations are orthogonal. If the contributions are of the same sign, then the astigmatism combines at these points to yield the simple defocus, and astigmatism nodes result.

Once the astigmatism nodes have been found, the variation of the astigmatism in the field about the nodes is proportional to the product of the distances to the nodes. As mentioned in Chapter 4, this is

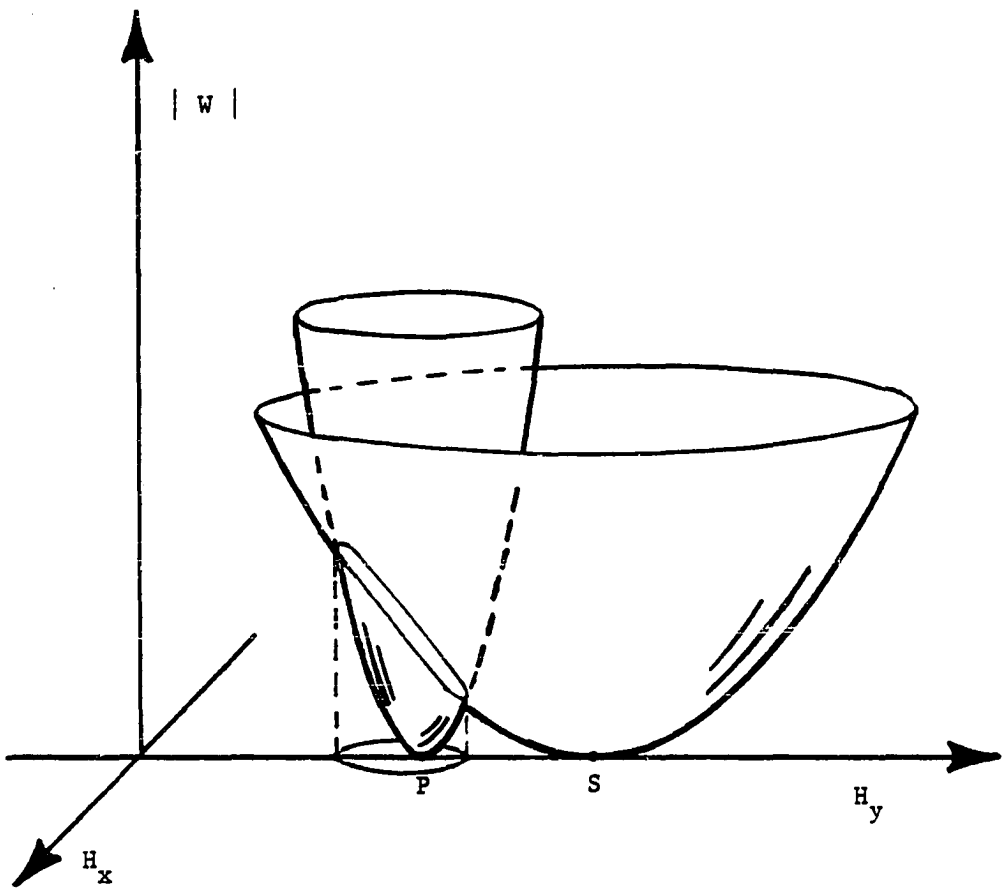

Figure 8.3. Magnitudes of Two Quadratic Astigmatism Fields.

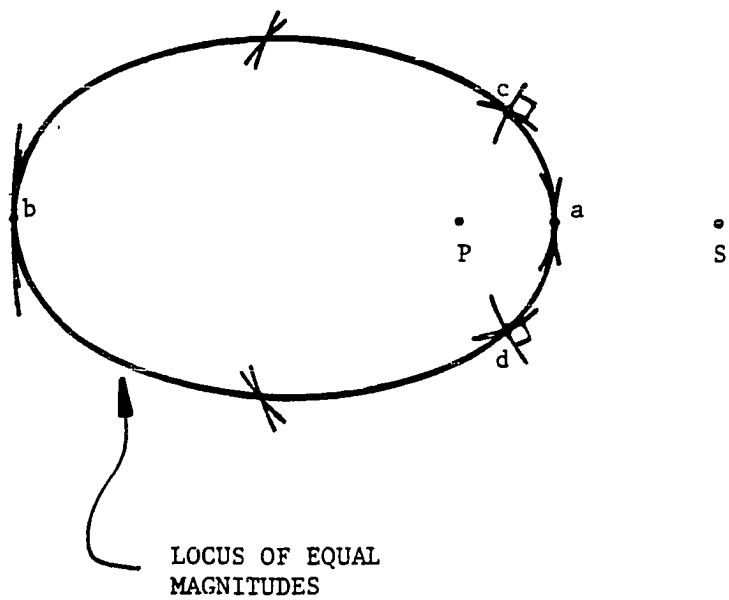

Figure 8.4. Locating the Resultant Astigmatism Node.

quadratic far from the nodes, linear near the nodes, and constant midway in between. the magnitude of binodal astigmatism thus takes on the rather complex shape suggested by Figure 8.5. In the H_y direction, the resultant astigmatism is the difference between the magnitudes of the two constituent fields.

The above treatment of astigmatism must now be extended to include the case of the addition of a quadratic astigmatism contribution to a system already possessing binodal astigmatism. Here, only the case of binodal astigmatism with the nodes on the H_y axis will be discussed. The case in which the nodes are displaced in the H_x direction follows analogously. Referring to Figure 8.5, one may see that a weak quadratic contribution placed on the H_y axis near one of the two nodes A_1 and A_2 could possibly intersect the binodal surface in <u>two</u> closed paths, each enclosing one of the two nodes. This would seem to indicate that four nodes might then result - two nodes from each of the two closed paths. That this is not the case may bee seen by considering the orientation of binodal astigmatism. Thompson (1980) shows that the line foci for the focal surface which is termed the <u>tangential</u> focal surface in a centered system are no longer tangent to circles surrounding the node(s), but are now tangent to ellipses drawn with the two nodes as foci. Figure 8.6 demonstrates why the term <u>tangential</u> is no longer appropriate. If one were to draw a closed path containing either but not both of the two nodes, the orientation of the astigmatism may be considered "tangential" on one side of the path, but not on the other, where it would more appropriately be termed "sagittal". In general, there is a 90° difference

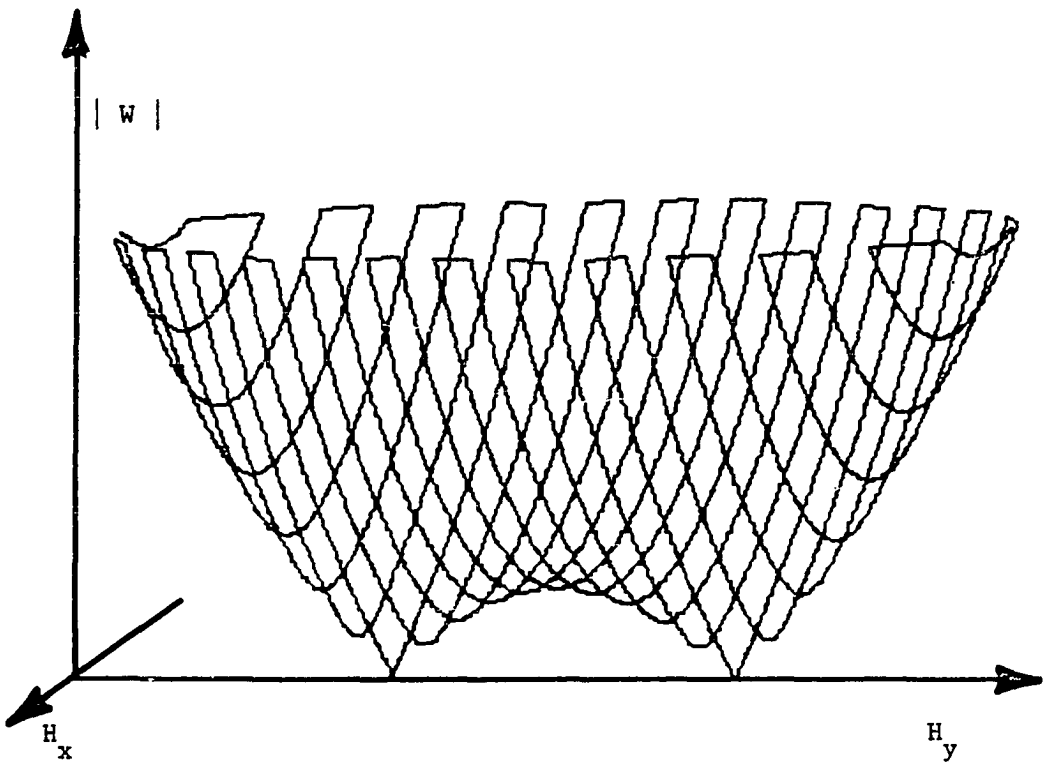

Figure 8.5. Magnitude of Binodal Astigmatism

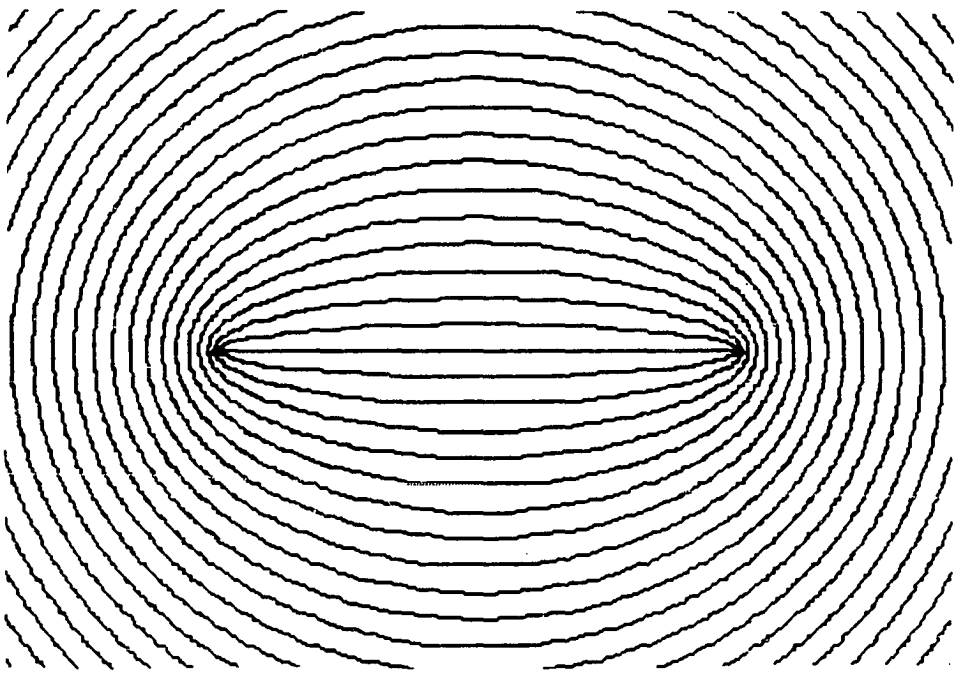

Figure 8.6. Orienation Plot for Binodal Astigmatism.

in orientation on opposite sides of the node. For this reason, the orientation of binodal astigmatism is appropriate for cancellation with quadratic astigmatism at only one point on each of the two closed curves giving the loci of equal magnitude. Thus, only two nodes are possible.

Summarizing for astigmatism, when combining two quadratic astigmatism fields of opposite sign, two nodes appear, one on each side of the surface contribution with the greater magnitude. If the two fields are of the same sign, the two resulting nodes move out in the H_x direction. When combining binodal astigmatism with a nearby term of quadratic astigmatism of the same sign, two nodes result between the two original nodes. If the quadratic term is of the opposite sign instead, the nodes will appear outside of the two original nodes. If the quadratic astigmatism is located sufficient far away that the two magnitude surfaces intersect in a single closed path, the binodal contribution may be considered as quadratic.

Application to a Two Mirror System

The above concepts may be applied to the two mirror Cassegrain type system of System 3, to investigate why no solution was found.

Table 8.1 lists the aberrations of the elements of System 3. As can be seen, the astigmatism coefficients are very nearly equal in magnitude and opposite in sign. This means that the two paraboloids representing the absolute magnitudes of the aberration fields are very nearly identical. This means that the inner resultant node is located midway between the two surface contribution nodes, and the outer resultant node is located far from the two surface contribution nodes.

Table 8.1. Aberration Coefficients for System 3.

SURFACE	W_{040}	W_{131}	W_{222}	W_{311}	W_{220M}
PRIMARY	1.39572	-.331168	.019644	-.000022	.010011
SECONDARY	-.321050	.149501	-.017404	-.006098	.017490
TOTALS	1.07467	-.181667	.002240	-.006120	.027501

Another way of saying this is that the closed path at the intersection of the two paraboloids become highly eccentric as the paraboloids begin to have the same shape.

The practical result of this is that the outer node is so far removed in the field that it is no use to the designer and only the inner node is available for use.

Referring again to Table 8.1, one sees that the coma coefficients are of opposite sign. This means that the resulting coma node will lie outside the two surface contribution nodes.

Since the resultant coma nodes is constrained to lie outside the two original nodes, and the only useful resultant astigmatism node must lie between them, the only way in which the resultant coma and astigmatism nodes may be aligned is to align the two surface contribution nodes, forcing the system into a rotationally symmetric configuration. Thus it is seen that no solution exists for a Cassegrain type system in which the magnification of the secondary has a value near four.

This conclusion is based on the fact that the outer astigmatism node is too distant in the field to be of any practical use, due to the fact that the astigmatism contributions of the primary and secondary are very nearly balanced. This balance may be changed by changing the magnification of the secondary. The author tried several starting points, and failed to find a useful solution. The best near-solution was found in System 4, which has a secondary magnification of about two.

The recognition of the nature of the problem led the author to investigate the addition of a tertiary mirror to the system.

Application to a Three Mirror System

Once the decision has been made to introduce a tertiary mirror, the following decision must be made:

1) On which side of the two mirror focus should the tertiary be placed? ("Cassegrain" or "Gregorian" type?)
2) If it is a Cassegrain type, should it be concave or convex?
3) If it is concave ("Cassegrain" or "Gregorian"), on which side of the pupil centered condition should it lie?
4) If it is a Gregorian type, on which side of the image centered condition should it lie?
5) Should it be tilted in the positive or negative direction?

The answers to these questions are found quite easily using the graphical view of the vector aberration theory, for any given two mirror starting system. This then yields a starting point for a three mirror system which may be optimized quickly to a useful solution.

As an example of this design process, the author took System 4 as a two mirror staring point. Figure 8.7 shows the computer output giving the magnitudes and locations of the aberration nodes for System 4. Because the Astigmatism nodes for this system are on the H_y axis, only the $|W|$-H_y cross section of the magnitude surfaces need be considered. These are plotted in Figure 8.8. The goal is to insert a tertiary mirror at some (unobscured) tilt angle with sufficient aberrations of the appropriate sign to obtain a common node of both coma and astigmatism at

```
VALUES AND NODES OF ABERRATION FIELDS (WAVES AT .5876UM)

COMA.  -0.310572E-01 WAVES AT HY=    11.7499     HX=   0.00

MEDIAL SURFACE.   0.388740E-02 WAVES AT HY= 37.3959 HX= 0.00
 FOCAL SHIFT =   0.132196 RADIUS OF MEDIAL SURFACE= -60.7616

ASTIGMATISM   0.519717E-02 WAVES

 FIRST  NODE AT HY=   -2.94007     HX=   0.000000
 SECOND NODE AT HY=    49.4428     HX=   0.000000

DISTORTION (FIRST-ORDER) -0.303487E-13  AT HY= 0.00 HX= 0.00

 THIRD-ORDER  -0.260693E-03 WAVES. THREE NODE LOCATIONS-
 FIRST  NODE AT HY=    65.9149     HX=   0.000000
 SECOND NODE AT HY=    65.9149     HX=   0.000000
 THIRD  NODE AT HY=    65.9149     HX=   0.000000
```

Figure 8.7. Node Locations and Magnitudes for System 4.

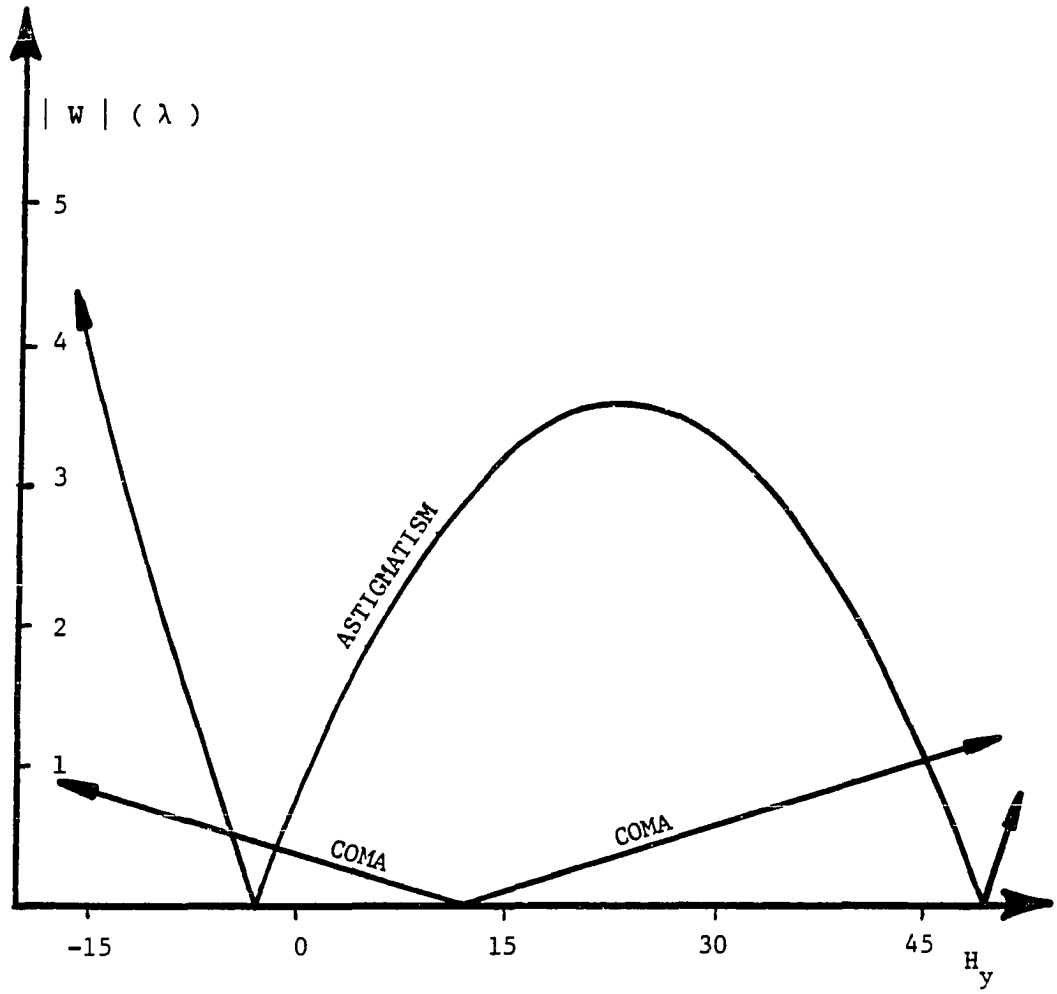

Figure 8.8. Aberration Magnitudes for System 4.

some accessible point in the field. It is not necessary that this common node fall at the center of the present field of view ($H_y = 0$), for the entire optical system may be tilted to center the field about the node. However, shifting the field toward positive field angles will place the secondary in a position to obscure the primary, so only negative values of H_y are practical. The tertiary mirror itself must be tilted a few degrees (or several field-heights, since the field-height is 0.3°) in either direction.

One likely candidate for a tertiary mirror would have aberration fields such as those shown in Figure 8.9. (The scale of the coma magnitude has been changed to improve the clarity of the plot.) Because the resulting common node of coma and astigmatism is the "outer" node of both aberrations, the fields cross at relatively shallow angles, giving low coefficients for the combined aberrations.

In order to ensure that both coma and astigmatism produce nodes at this "outer" crossing, the relative signs must be considered. On the basis of the discussion concerning the graphical interpretation of the theory, it is seen that the outer node will be attained when the signs of both the coma and astigmatism introduced by the tertiary are opposite those introduced by the two mirror system. Referring to Table 8.2, this means that the coma must be positive and the astigmatism negative. The signs of the aberrations of a reflective tertiary mirror are easily computed for any of the possible tertiary types, and are given in Table 8.3. From the table, it is clear that only a negative mirror will do the job required. Furthermore, this mirror has two significant drawbacks: 1)

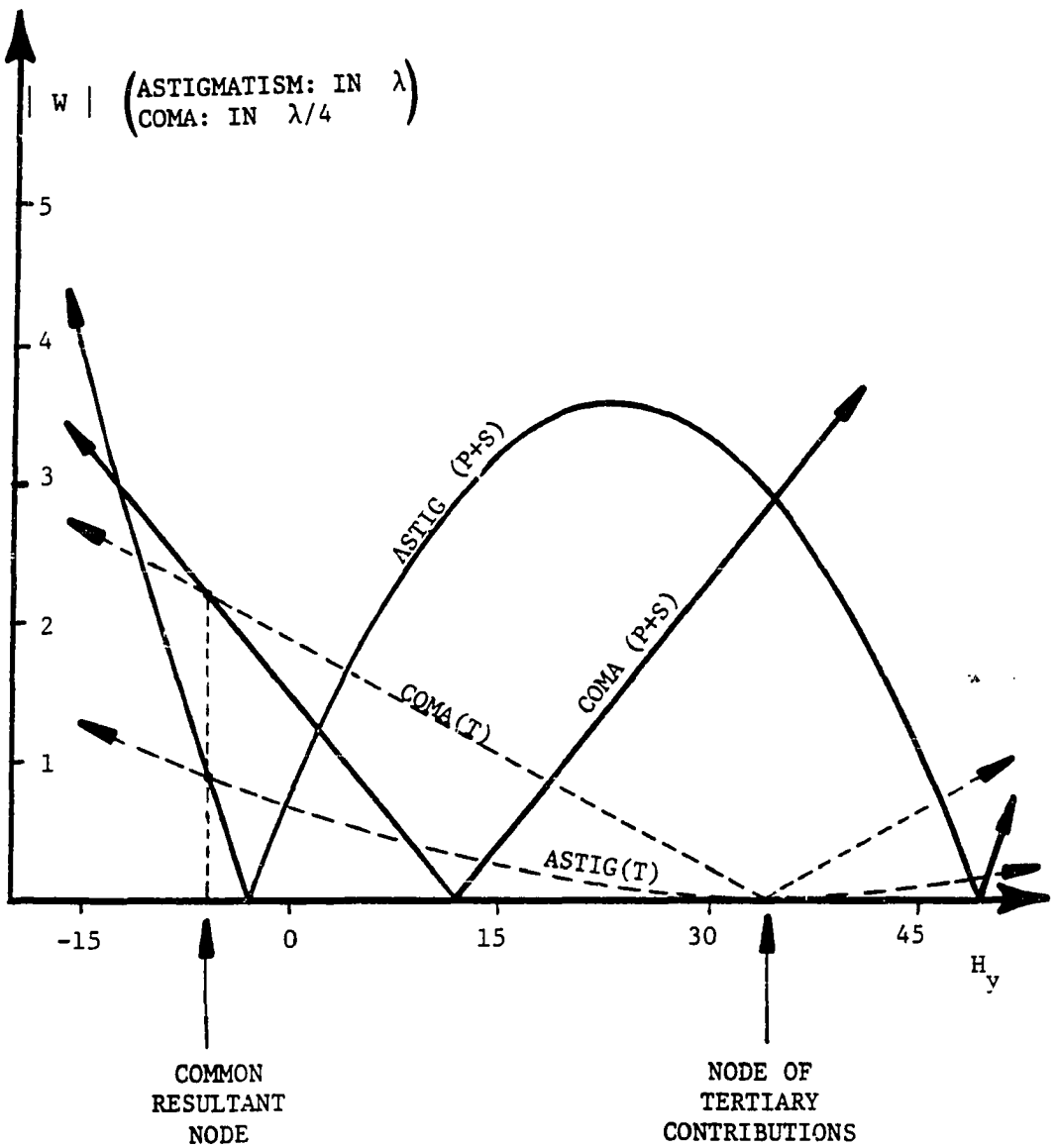

Figure 8.9. Aberration Magnitudes for a possible Tertiary Mirror.

Table 8.2 Aberration Coefficients for System 4.

SURFACE	W_{040}	W_{131}	W_{222}	W_{311}	W_{220M}
PRIMARY	.120020	-.063278	.008341	.000000	.004170
SECONDARY	-.079647	.030904	-.002998	-.000250	-.000210
TOTALS	.040373	-.032374	.005343	-.000250	.002070

Table 8.3. Signs of Coma and Astigmatism for Tertiary Mirrors of Several Types

TYPE OF SURFACE	LOCATION	CURVATURE	COMA (SIGN)	ASTIGMATISM (SIGN)
Convex	Inside Focus	Weaker than Image Centered	Positive	Negative
	Inside	Weaker than Pupil Centered	Negative	Positive
	Focus	Stronger than Pupil Centered	Positive	Positive
Concave	Outside	Weaker than Pupil Centered	Negative	Positive
		Stronger than Pupil Centered	Positive	Positive
	Focus	Image Centered	Zero	Positive
		Stronger than Image Centered	Negative	Positive

the f/number of the system is increased and 2) the Petzval curvature of the tertiary worsens the already backwards-curving field of the two mirror system.

Both of these problems are alleviated if a weak positive mirror is used as a tertiary, but the table shows that both the aberrations change sign. the result of this is that the inner node is obtained for both aberrations. To obtain a final common node at slightly negative values of H_y, the tertiary must have its local axis displaced in the negative H_y direction, as shown in Figure 8.10.

On the basis of the above discussion, a concave mirror of radius -70mm was inserted 32mm "downstream" from the secondary, and tilted 5°. ACCOSV was then used to optimize the system, using a merit function consisting of real-ray definitions of coma and astigmatism at the center of the field. The tertiary was allowed to tilt, thereby adjusting the position of its aberration contribution, and the entire telescope was tilted to keep the field of view centered on the "best" image position. The resulting system operates at f/5.7. The residual coma may be eliminated by aspherizing the secondary, and the spherical aberration then corrected by aspherizing the primary. The required conic constants for the primary and secondary are -2.763 and -36.927, respectively. Although the latter may sound large, it represents only about $\frac{1}{8}\lambda$ of aspheric departure, due to the flatness of the secondary. Figure 8.11 shows a layout of the system. Figure 8.12 shows spot diagrams for several points in the field of this system. (The scale shown is for the individual spot diagrams; the field is shown at an arbitrary scale.) It

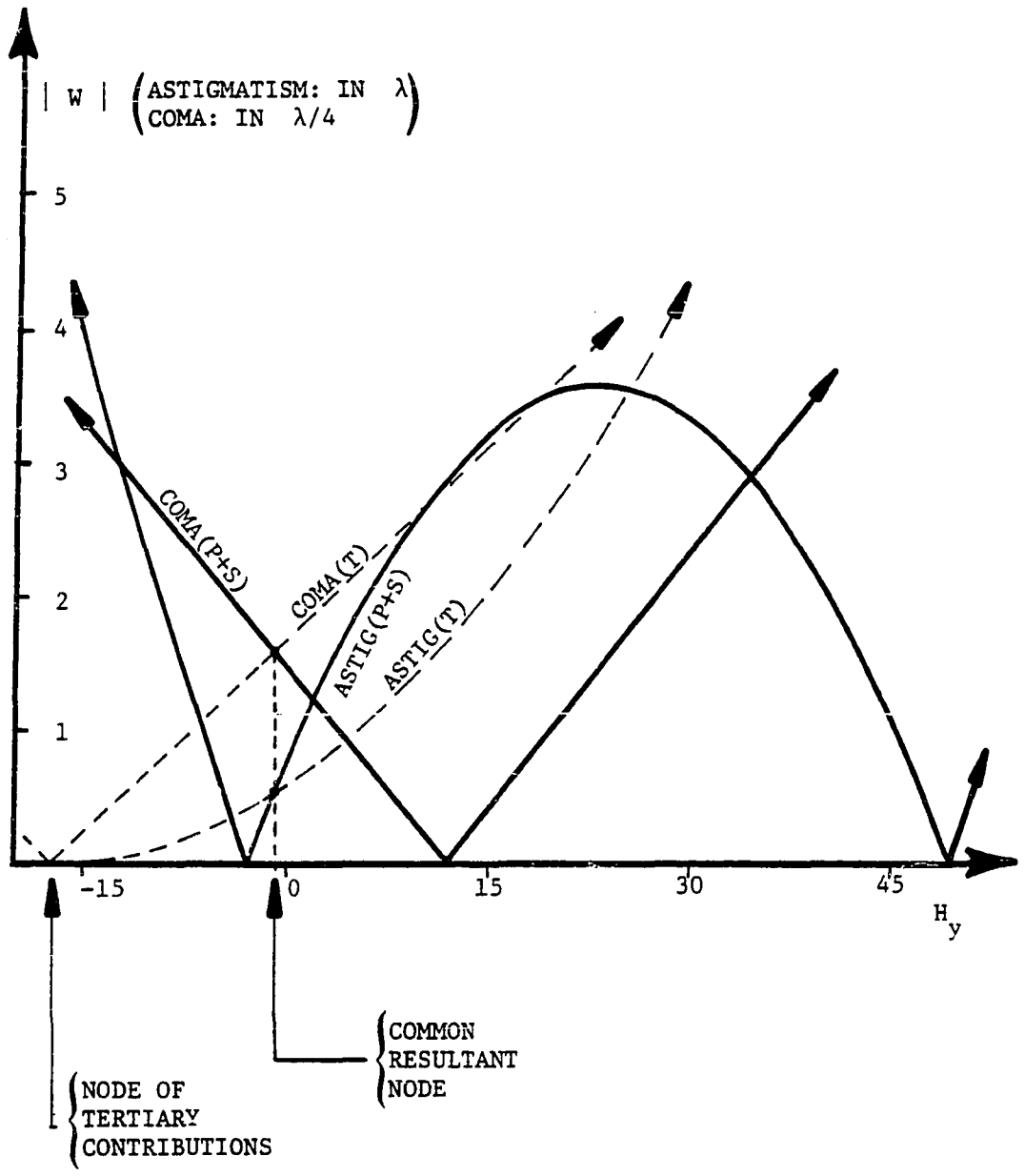

Figure 8.10. Aberration Magnitudes for the preferred Tertiary Mirror.

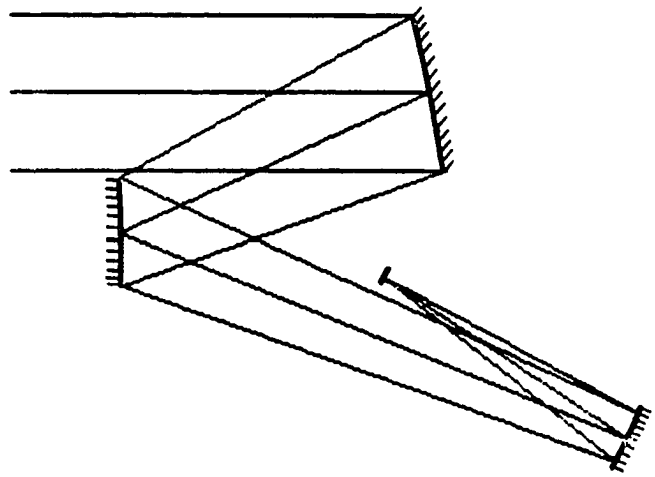

Figure 8.11. Layout of final Three Mirror System.

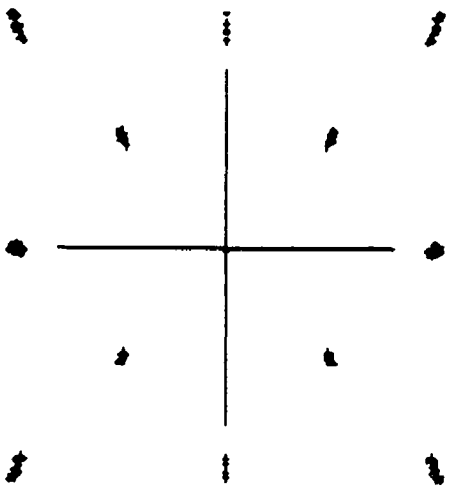

Figure 8.12. Spot Diagrams for Three Mirror System.

is interesting that the astigmatism varies linearly with the field, as the theory predicts. Also, note that the orientation of the astigmatism is not radial, as would be expected in a system with quadratic astigmatism. Because of these facts, it is difficult to balance the residual astigmatism against ordinary (field centered) astigmatism, so aspherizing the tertiary does very little to improve the performance of the system. With this in mind, it is instructive to look again at Figure 8.10. If, by varying the radius, position, and tilt angle of the tertiary, the two astigmatism curves can be made to be tangent to each other at the same field position where the coma curves cross, then the residual astigmatism would be greatly reduced, and would vary quadratically in the field. The residual coma, even if it is strong, remains of the ordinary kind, and may be eliminated using the aspheric coefficients of the surfaces. Unfortunately, it appears that this condition can be met only in the obscured, positive values of H_y, for this is the region in which the binodal astigmatism magnitude is downward curving. Perhaps, with this in mind, the two mirror system could be redesigned to place the node A_1 farther to the left, allowing such a solution to occur in an unobscured region of the field.

CHAPTER 9

FIELD AVERAGED WAVEFRONT VARIANCE

In a rotationally symmetric system, the aberrations show a radial dependence with the field position. It is therefore sufficient to sample the image field at relatively few field points, the distance from the field center being the only significant parameter. Due to the tendency of the aberrations of tilted and decentered systems to develop multiple nodes in the field, this is no longer a sufficient means of determining the overall image quality.

One of the advantages of using an analytic treatment of the aberrations of optical systems is that both the pupil and field dependences of the aberrations are known. This facilitates the computation of such quantities as the mean-square wavefront variance at arbitrary points in the field.

Because the field dependence is known explicitly, the mean square wavefront variance may be integrated over the field of view of the system. Dividing this quantity by the area of the field then yields the field averaged wavefront variance.

In this chapter, the field average of the mean square wavefront variance will be developed from the vector aberration theory of Chapter 4. It should be remembered that the values of the "wave aberration" coefficients derived from the transverse ray error

coefficients of ACCOSV do not represent the classical wave aberration function of geometrical optics, for they relate the aberration function to points on a flat pupil plane, rather than on a reference sphere. For this reason, inserting these coefficients (which are the coefficients used in the vector aberration program described in this work) into the equations derived in this chapter will not yield the classically defined wavefront variance. What results is the variance of the wavefront, as measured on a coordinate system which is distorted slightly from the classical reference sphere coordinates. Nevertheless, this quantity is still useful in that it varies in the same direction as the classical wave aberration variance, and vanishes at the same point that the function vanishes: when there is no aberration. Furthermore, the equations derived below are correct, in that insertion of the classical wave aberration coefficients will yield the classical wavefront variance. No further distinction will be made between the variance computed by the program and the classical wave aberration variance.

Calculation

Thompson (1980) derives the mean-square wavefront variance in terms of the vector aberration expansion, as a function of the field coordinates. Repeating it here without derivation, it is (to third order):

$$W_{ms} = (1/12)[W_{20} + W_{040} + S_{220M}]^2$$

$$+ (1/180)\, W_{040}^2$$

$$+ (1/24)|\mathbf{V}_{222}^2|^2$$

$$+ (1/4)|(2/3)\mathbf{V}_{131} + \mathbf{V}_{311}|^2$$

$$+ (1/72)|\mathbf{V}_{131}|^2, \tag{9.1}$$

where

$$S_{220M} = W_{220M}(\mathbf{H}\cdot\mathbf{H} - 2\mathbf{H}\cdot\mathbf{a}_{220M} + b_{220M} + \mathbf{a}_{220M}\cdot\mathbf{a}_{220M}) \tag{9.2}$$

is a scalar giving the defocus due to field curvature at this field point, and

$$\mathbf{V}_{222}^2 = W_{222}[(\mathbf{H}-\mathbf{a}_{222})(\mathbf{H}-\mathbf{a}_{222}) + \mathbf{b}_{222}^2], \tag{9.3}$$

$$\mathbf{V}_{131} = W_{131}(\mathbf{H}-\mathbf{a}_{131}), \tag{9.4}$$

and

$$\mathbf{V}_{311} = W_{311}(\mathbf{H}\cdot\mathbf{H})\mathbf{H} + (\mathbf{H}\cdot\mathbf{H})\mathbf{a}_{311}$$

$$+ 2(d_{311} + \mathbf{a}_{311}\cdot\mathbf{a}_{311})\mathbf{H}$$

$$+ (b_{311}{}^2 + \mathbf{a}_{311}{}^2)\mathbf{H}^*$$

$$+ c_{311} + (\mathbf{a}_{311}\cdot\mathbf{a}_{311})\mathbf{a}_{311}]. \qquad (9.5)$$

are vectors representing the aberration coefficients augmented by the appropriate vector power of the field variable. The quantity W_{20} is a coefficient of defocus corresponding to the longitudinal separation of the detector plane from the Gaussian image plane.

Noting that the area of the normalized field is $(1/\pi)$, the field averaged wavefront variance may be defined as

$$(W_{ms})_{avg} \equiv (1/\pi)\int_0^1 \int_0^{2\pi} W_{ms}(H,\theta)d\theta\ H\ dH. \qquad (9.6)$$

It remains only to carry out the dot products indicated in Equation (9.1), convert the equation into scalar notation, and perform the integral. This process is straightforward but tedious and only the result will be shown here. The reader is referred to Appendix A for details of the derivation. Although the field averaged variance derived in Appendix A and listed below is by no means in the simplest possible algebraic form, it is in a form which facilitates the computation of the average variance

with the computer program discussed Chapter 7. The intention here is simply to demonstrate that the average wavefront variance, calculated analytically from the third order theory, is a useful merit function for the design of unobscured reflective systems.

From the appendix, it is seen that

$$(W_{ms})_{avg} = (1/\pi)[\text{INTEGRAL 1} + \text{INTEGRAL 2} + \text{INTEGRAL 3} + \text{INTEGRAL 4'}], \tag{9.7}$$

where the values of the individual integrals are given below:

$$\text{Integral 1} \equiv (1/12)\{[W_{20}^2 + W_{20}W_{040} + W_{040}^2 + 2\,(W_{20} + W_{040})(W_{040})(b_{220M} + a_{220M}^2)] + W_{220M}^2(a_{220M}^4 + b_{220M}(B_{220M} + 2a_{220M}^2)) + (2/3)[(W_{20} + W_{040})W_{040} + W_{220M}^2(b_{220M} + a_{220M}^2)]\}, \tag{9.8}$$

$$\text{Integral 2} \equiv W_{040}^2/180, \tag{9.9}$$

$$\text{Integral 3} \equiv (1/4) + a_{222}^2 + 2b_{222}^2 + a_{222}^4 + 2a_{222}^2b_{222}^2 + (b_{222}^2)^2 + (4\pi/3)(a_{222}^2 + b_{222}^2), \tag{9.10}$$

$$\text{Integral } 4' \equiv I_{41}' + I_{42} + I_{43}, \tag{9.11}$$

where further,

$$I_{41}' \equiv [(4/9) + (1/72)]W_{131}^2[(1/3) + a_{131}^2], \tag{9.12}$$

$$I_{42} \equiv (4/3)W_{131}W_{311}((1/5) + (1/3)(2d_{311} - b_{311}^2) - a_{311}a_{131})$$

$$+ c_{311}a_{131} + a_{311}a_{131} + (\pi/3)(2b_{311}^2 + a_{311}a_{131})], \tag{9.13}$$

$$I_{43} \equiv w_{311}^2\{(1/7) + (1/5)(4d_{311} - 2b_{311}^2 + 3a_{311}^2)$$

$$+ (1/3)[2a_{311}c_{311} + 2a_{311}^4 + 4Q_1^2 + 4Q_1Q_2 + Q_2^2]$$

$$+ c_{311}^2 + 2c_{311}a_{311}^3 + a_{311}^6$$

$$(\pi/5)[4Q_2 + a_{311}^2]$$

$$+ (\pi/3)[2c_{311}a_{311} + 2a_{311}^4 + 8Q_1Q_2]\}, \tag{9.14}$$

$$Q_1 \equiv d_{311} + a_{311}^2, \tag{9.15}$$

and

$$Q_2 \equiv a_{311}^2 + b_{311}^2. \tag{9.16}$$

Except for the defocus correction represented by the W_{20} term, the above equations measure the field averaged variance against a reference sphere centered on the Gaussian image point. Figure 7.9 shows that in addition to the local distortion of the image field, the decentration of the Seidel distortion nodes causes a large transverse shift of the image field. In a finished design, this shift may be removed by a proper choice of the detector position. Therefore, the degradation of the merit function caused by this image shift is somewhat artificial. Examining Eq. (9.5), one sees that the field augmented distortion vector, V_{311}, contains a term $c_{311} + (a_{311}\cdot a_{311})a_{311}$, which is independent of H. Because c_{311} appears nowhere else in the equation, then the field independent term may be set to zero without affecting the local distortion by setting

$$c_{311} \equiv -(a_{311}\cdot a_{311})a_{311}. \tag{9.17}$$

This enables the average variance to be computed without regard to the image position, but including the local distortion of the image field.

It is also important to realize that the field averaged variance, as given above, does not include the effects of anamorphic and keystone distortion. Furthermore, in many applications, distortion is not considered a degradation of the image, for it may be removed later by image processing techniques. If it is desirable to do so, the average

variance may be calculated with total disregard to Seidel distortion by setting W_{311} to zero.

In Chapter 6, it was pointed out that a considerable longitudinal image shift may be introduced by "off axis" manifestations of the medial field curvature. This may also be removed by repositioning the detector, and presumably, the defocus coefficient W_{20} represents just that focal shift. However, the best focal position changes continually during the design process, so it cannot always be guaranteed that the detector position is the one which is the most desirble. One focal position which may be simulated analytically is the one in which the detector is shifted longitudinally and tilted, so that it is tangent to the medial surface. This closely resembles the Gaussian image plane in a symmetric system. Reference to Eq. (9.2), or to the discussion of medial field curvature in Chapter 4, shows that by setting the scalar b_{220M} and the vector $\mathbf{a}_{220M}$ to zero, the longitudinal and transverse separations of the medial focal surface from the image plane have been eliminated, thus leaving the image plane tangent to the medial surface. This is not quite the same as shifting and tilting the detector to obtain the tangent condition, because the medial focal surface is (to third order) paraboloidal, and having the detector plane tangent to the "side" of the paraboloid is not equivalent to having it tangent at the vertex of the paraboloid. Nevertheless, this is a useful approximation, for it removes the undesired field-constant defocus, and leaves an approximate measure of the field curvature. Naturally, if $\mathbf{a}_{220M}$ and b_{220M} are set to zero, the coefficient W_{20} represents a defocus from the tangent condition

described above.

Applications

As a test of the merit function, the above equations were used to calculate the field averaged wavefront variance for systems 3 and 4. The average variance of System 3 (the two spherical mirror Cassegrain system), including all the terms is 127 waves squared at .5876 μm. Eliminating the transverse image shift from the computation, the variance drops to 27.7 waves squared, demonstrating the importance of the transverse position of the detector. When all but the quadratic term of the field curvature is eliminated, the merit function drops to 6.5 waves. By removing Seidel distortion from the calculation entirely, the average variance is reduced to 1.6 waves squared. This now represents the image degradation due to spherical aberration, coma, astigmatism, and the quadratic term of medial field curvature.

System 4. is the partially optimized Cassegrain, with a secondary magnification of two. The ray fans for this system show that the transverse error has been reduced by about a factor of 25 from those of System 3. The field averaged wavefront variance for this system, including all the terms is about 1861 waves squared. However, most of this is caused by the extreme distortion caused by the large tilt angle of the secondary. Eliminating just the field shift term of the distortion reduces the average variance to 21 waves squared. Calculating the variance with the detector at the "tangent" position further reduces the variance to 4.7 waves squared. Finally, removing the local distortion of the field from the computation yields an average variance

of .007 waves squared, due mainly to the astigmatism remaining in the system.

Discussion

The field averaged mean square wavefront variance, as computed analytically from the aberration coefficients, is a relatively simple yet meaningful quantity expressing the overall image quality within the field of view of the system. Unlike estimates of the wavefront variance based on raytrace data, there is no need to sample the field at a discreet locations, for the field dependence is explicitly accounted for in the integration. Also, the effects of various aberrations (such as distortion and defocus) may be easily manipulated without actually shifting or tilting the detector plane during the optimization, thereby reducing the numbers of constraints and variables in the optimization process. It is a simple matter to print out the individual terms of the integral (Equation (9.7)), thus providing the designer with information as to the nature of the image degradation.

The accuracy and usefulness of the field averaged wavefront variance are limited by the fact that only the Seidel aberrations are considered. Thus, another merit function must be adopted when the third order aberrations are nearly balanced and the higher order aberrations become dominant.

Another analytically available quantity which might be of interest is the field variance of the mean square wavefront variance. This would give a measure of the change in image quality over the field of view of the system. Although its derivation and computation follows

in a straightforward manner from the derivation of the field averaged variance, it is considerably more complex due to the fact that the integrand is squared.

CHAPTER 10

SUMMARY AND CONCLUSIONS

In Chapter 2, the form of the image was derived from the Gaussian properties of the system. It was seen that keystone distortion may not be calculated by the summation of surface contributions, due to the fact that the distortion introduced at a surface is strongly dependent on the distortion introduced at previous surfaces. Although keystone distortion has terms in all powers of the field, it may be parameterized by the single number K. The anamorphic distortion of the system may be described by simply introducing a separate scaling factor for the y-direction. In Chapter 3, a set of parameters were developed which are convenient for propagating the Gaussian properties through the system.

Chapter 4 outlined the vector aberration theory of Thompson (1980), and developed the computational technique necessary to apply the theory to a system with large tilts and decentrations. The need for correcting the coefficients computed along the Local Axis of the surface, to be compatible with description of the aberrations along the ray path was recognized. This correction was discussed in Chapter 5, along with similar corrections for the anamorphic and keystone distortions of the object and pupil. (In this dissertation, these latter corrections are by choice approximate and are strictly correct only along the H_y axis.)

In Chapter 6, the corrections for the obliquity of the detector

plane on the Gaussian properties and aberrational properties were developed. The latter was simplified considerably by the concepts developed in Chapter 5. In Chapter 7, the vector theory was applied to the analysis of several systems. It may be concluded that the theory correctly models the Gaussian and Seidel properties of optical systems, but that this description becomes inadequate for the analysis of well corrected systems in which the Seidel aberrations have been eliminated, leaving the higher order aberrations dominant. Although the systems analyzed in Chapter 7 were all reflective, the theory applies equally well to refractive systems.

In Chapter 8, the vector aberration concept was applied to the optimization of an unobscured reflective optical system. Even though the theory describes only the low order properties of optical systems, the nodal concept of aberration fields proved to be extremely useful in the design process.

In Chapter 9, the field averaged mean square wavefront variance was developed, to third order. This was applied as a merit function to two optical systems, and the effects of distortion and defocus were studied from the point of view of this parameter.

Suggestions for Further Research

In this work, the Gaussian distortions were treated separately from the Seidel distortion, even though the latter develops terms similar to the Gaussian distortion terms in a system with tilts and decentrations. Although their origins are quite distinct, their effects are identical, and a method for studying their combined effect seems

desirable. This would be of great assistance in the design of systems such as mapping cameras in which distortion is of major importance.

Although the major effort of this work centered on the analysis, rather than the design of optical systems, the author feels that the major value of the vector aberration concept lies in the field of design. To adequately analyze a well corrected optical system requires aberration terms of fifth and higher order. Such a high order theory would be far more complicated than the third order theory described in this paper, owing partly to the fact that higher order aberrations are induced at a surface by the lower order aberrations of the incident wavefront, which is oblique to the axis of that surface. Although this analysis could be carried out, it is felt that the development of a highly accurate program to describe the imagery of well-corrected systems would not be worth the effort.

The real value of the theory described in this dissertation lies in the insight which it provides the designer. The aberration magnitude plots such as Figure 8.8 allow him to understand the interactions among the aberration contributions of the various surfaces and to relate them directly to the constructional parameters of the system. The presence of higher order aberrations merely changes the numerical values of the magnitudes of the various aberration types - the concept of matching magnitudes and orientations to produce a resultant node is unaffected. The author feels that a hybrid program which uses third order vector theory to predict the image behavior and then samples the field using real ray aberration definitions to produce magnitude and orientation plots would be an extremely useful design tool.

APPENDIX A

DERIVATION OF THE FIELD AVERAGED MEAN SQUARE WAVEFRONT VARIANCE.

In the derivation which follows, frequent use will be made of the fact that all tilts and decentrations have been confined to the y-z plane, simplifying the results considerably.

The mean square wavefront variance is given in the text to be

$$\begin{aligned} W_{ms} &= (1/12)(W_{20} + W_{040} + S_{220M})^2 \\ &\quad + (1/180)W_{040}^2 \\ &\quad + (1/24)|\mathbf{V}_{222}{}^2|^2 \\ &\quad + (1/4)|(2/3)\mathbf{V}_{131} + \mathbf{V}_{311}|^2 \\ &\quad + (1/72)|\mathbf{V}_{131}|^2, \end{aligned} \tag{9.1}$$

where

$$S_{220M} = W_{2220M}(\mathbf{H}\cdot\mathbf{H} - 2\mathbf{H}\cdot\mathbf{a}_{220M} + \mathbf{b}_{220M} + \mathbf{a}_{220M}\cdot\mathbf{a}_{220M}), \tag{9.2}$$

$$\mathbf{V}_{222}{}^2 = W_{222}[(\mathbf{H}-\mathbf{a}_{222})(\mathbf{H}-\mathbf{a}_{222}) + \mathbf{b}_{222}{}^2], \tag{9.3}$$

$$\mathbf{V}_{131} = W_{131}(\mathbf{H}-\mathbf{a}_{131}), \tag{9.4}$$

and

$$V_{311} = W_{311}[(\mathbf{H}\cdot\mathbf{H})\mathbf{H} + (\mathbf{H}\cdot\mathbf{a}_{311})\mathbf{H} + (\mathbf{H}\cdot\mathbf{H})\mathbf{a}_{311}$$
$$+ 2(d_{311} + \mathbf{a}_{311}\cdot\mathbf{a}_{311})\mathbf{H}$$
$$+ (b_{311}^2 + a_{311}^2)\mathbf{H}^*$$
$$+ c_{311} + (\mathbf{a}_{311}\cdot\mathbf{a}_{311})\mathbf{a}_{311}. \qquad (9.5)$$

The five terms in this expression, which will be denoted Term 1 through Term 5, respectively, are easiest considered separately.

Term 1

Performing the square in this term yields:

$$\text{Term 1} = (1/12)[W_{20}^2 + 2W_{20}W_{040} + 2W_{20}S_{220M}$$
$$+ W_{040}^2 + 2W_{040}S_{220M}$$
$$+ S_{220M}^2]. \qquad (A.1)$$

Consider the quantity S_{220M}, as given by Eq. (9.2). This is (in scalar notation),

$$S_{220M} = W_{220M}(H^2 - 2Ha_{220M}\cos(\theta-\theta_a) + b_{220M} + a_{220M}^2) \qquad (A.2)$$

Because all tilts and decentrations have been confined to the y-z plane, $\mathbf{a}_{220M}$ (given by Equation (4.14)) will also be along the H_y axis. It is therefore a signed constant times a vector whose angle is zero, so that $\cos(\theta-\theta_a)$ in Equation (A.2) may be replaced with $\cos\theta$. Substituting Equation (A.2) for S_{220M} in Eq. (A.1), performing the square, and collecting terms gives:

$$\begin{aligned}
\text{Term 1} = (1/12)\{&W_{20}^2 + W_{20}W_{040} + W_{040}^2 \\
&+ 2(W_{20} + W_{040})(W_{040})(b_{220M} + a_{220M}^2) \\
&+ W_{220M}^2(a_{220M}^4 + b_{220M}(b_{220M} + 2a_{220M}^2)) \\
&+ H^2[2(W_{20} + W_{040})(W_{040}) + \\
&\quad + 2(b_{220M} + a_{220M}^2)W_{220M}^2] \\
&+ H^4[W_{220M}^2] \\
&+ H\cos\theta\ [-4a_{220M}(W_{20} + W_{040})(W_{040}) \\
&\quad |-4a_{220M}(b_{220M} + a_{220M}^2) \\
&+ H^3\cos\theta\ [-4a_{220M}] \\
&+ H^2\cos^2\theta\ [4a_{220M}^2]\}
\end{aligned} \tag{A.3}$$

Define Integral 1 to be the field integral of this expression.

$$\text{Integral 1} = \int_0^1 \int_0^{2\pi} (\text{Term 1})\, d\theta\ (H)dH \tag{A.4}$$

Note that the θ-integral is independent of that in H, and also that the odd powers of $\cos\theta$ will integrate to zero. The integral of $\cos^2\theta$ will simply produce a factor of π. The remaining polynomial in H is easily integrated, yielding after simplification,

$$\text{Integral } 1 = (1/12)\{[W_{20}^2 + W_{20}W_{040} + W_{040}^2 + 2(W_{20} + W_{040})(W_{040})(b_{220M} + a_{220M}^2) + W_{220M}^2(a_{220M}^4 + b_{220M}(b_{220M} + 2a_{220M}^2))] + [(W_{20} + W_{040})W_{040} + W_{220M}^2(b_{220M} + a_{220M}^2)] + (1/5)W_{220M}^2 + (4\pi/3)a_{220M}^2\} \quad (A.5)$$

Term 2

The second term of the mean square wavefront variance is simple to integrate. The integral may be written at once:

$$\text{Integral } 2 = W_{040}^2/180 \quad (A.6)$$

Term 3

The third term in the wavefront variance may be written as

$$\text{Term } 3 = (1/24)(\mathbf{V}_{222}^2 \cdot \mathbf{V}_{222}^2). \quad (A.7)$$

Substituting Eq. (9.3) for $\mathbf{V}_{222}^2$, and performing the dot product yields

$$\text{Term } 3 = (1/24)W_{222}^2[(\mathbf{H}-\mathbf{a}_{222})^2 \cdot (\mathbf{H}-\mathbf{a}_{222})^2 + 2(\mathbf{H}-\mathbf{a}_{222})^2 \cdot \mathbf{b}_{222}^2 + \mathbf{b}_{222}^2 \cdot \mathbf{b}_{222}^2]. \quad (A.8)$$

This may be rewritten as

$$\text{Term 3} = (1/24)W_{222}{}^2[|\mathbf{H}^2 - 2\mathbf{a}_{222}\mathbf{H} + \mathbf{a}_{222}{}^2|^2 + 2(\mathbf{H}^2 - 2\mathbf{a}_{222}\mathbf{H} + \mathbf{a}_{222}{}^2)\cdot\mathbf{b}_{222}{}^2 + |\mathbf{b}_{222}{}^2|^2]. \tag{A.9}$$

Consider just the first term:

$$|\mathbf{H}^2 - 2\mathbf{a}_{222}\mathbf{H} + \mathbf{a}_{222}{}^2|^2 = |\mathbf{H}^2|^2 - 4\mathbf{H}^2\cdot\mathbf{a}_{222}\mathbf{H} + 2\mathbf{H}^2\cdot\mathbf{a}_{222}{}^2 + |\mathbf{a}_{222}\mathbf{H}|^2 4\mathbf{a}_{222}\mathbf{H}\cdot\mathbf{a}_{222}{}^2 + |\mathbf{a}_{222}{}^2|^2. \tag{A.10}$$

Using the simplification that the angle associated with the vector $\mathbf{a}_{222}$ is zero, this expression is easily put into scalar form:

$$|\mathbf{H}^2 - 2\mathbf{a}_{222}\mathbf{H} + \mathbf{a}_{222}{}^2|^2 = H^4 - 4H^3 a_{222}\cos\theta + 2H^2 a_{222}{}^2\cos 2\theta + a_{222}{}^2H^2 + 4a_{222}{}^3H\cos\theta + a_{222}{}^4. \tag{A.11}$$

Using the identity

$$\cos 2\theta = 2\cos^2 2\theta - 1, \tag{A.12}$$

this may be rewritten as

$$|\mathbf{H}^2 - 2a_{222}\mathbf{H} + \mathbf{a}_{222}{}^2|^2 = H^4 - 4H^3 a_{222}\cos(\theta) + 4H^2 a_{222}{}^2\cos^2\theta + 3a_{222}{}^2H^2 + 4a_{222}{}^3H\cos\theta + a_{222}{}^4. \quad (A.13)$$

Consider next the second term:

$$2(\mathbf{H}^2 - 2a_{222}\mathbf{H} + \mathbf{a}_{222}{}^2)\cdot\mathbf{b}_{222}{}^2 = 2(\mathbf{H}^2\cdot\mathbf{b}_{222}{}^2 - 2a_{222}\mathbf{H}\cdot\mathbf{b}_{222}{}^2 + \mathbf{a}_{222}{}^2\cdot\mathbf{b}_{222}{}^2). \quad (A.14)$$

Referring to Eq. (4.29), one sees that the vector $\mathbf{b}_{222}{}^2$ is in the Hy direction, so its angle is zero. (Note that this is not necessarily true of its square root vector, $\mathbf{b}_{222}$, by the remarks following Eq. (4.31).) With this in mind, the dot products are easily converted to scalar form, giving:

$$2(\mathbf{H}^2 - 2a_{222}\mathbf{H} + \mathbf{a}_{222}{}^2)\cdot\mathbf{b}_{222}{}^2 = 2(H^2 b_{222}{}^2\cos 2\theta - 2a_{222}b_{222}{}^2 H\cos\theta + a_{222}{}^2 b_{222}{}^2). \quad (A.15)$$

This may be rewritten using the double-angle relation to yield:

$$2(\mathbf{H}^2 - 2a_{222}\mathbf{H} + \mathbf{a}_{222}{}^2)\cdot\mathbf{b}_{222}{}^2 = 4H^2 b_{222}{}^2\cos^2\theta - 4a_{222}b_{222}{}^2 H\cos\theta + 2a_{222}{}^2 b_{222}{}^2 + 2b_{222}{}^2 H^2. \quad (A.16)$$

The last term of Term 3 is simply

$$|b_{222}{}^2|^2 = (b_{222}{}^2)^2. \tag{A.17}$$

Combining Equations (A.13), (A.16), and (A.17), and collecting terms gives

$$\begin{aligned}\text{Term 3} = (1/24)W_{222}{}^2[&H^4 + 3H^2(a_{222}{}^2 + 2b_{222}{}^2) \\ &+ a_{222}{}^4 + 2a_{222}{}^2b_{222}{}^2 + (b_{222}{}^2)^2 \\ &+ \cos^2\theta\,(4H^2a_{222}{}^2 + 4H^2b_{222}{}^2) \\ &+ (\text{terms in } \cos\theta)].\end{aligned} \tag{A.18}$$

Noting that the terms in $\cos\theta$ will integrate to zero, and that the factor of $\cos^2\theta$ will yield a factor of π in the integration, the integral of this is seen to be

$$\begin{aligned}\text{Integral 3} = [&(1/4) + a_{222}{}^2 + 2b_{222}{}^2 \\ &+ a_{222}{}^4 + 2a_{222}{}^2b_{222}{}^2 + (b_{222}{}^2)^2] \\ &+ (4\pi/3)(a_{222}{}^2 + b_{222}{}^2).\end{aligned} \tag{A.19}$$

Term 4

The fourth term of Eq. 9.1 may be written as

$$\text{Term 4} = (1/4)[(2/3)\mathbf{V}_{131} + \mathbf{V}_{311}]\cdot[(2/3)\mathbf{V}_{131} + \mathbf{V}_{311}]. \tag{A.20}$$

Expanding the dot product yields

$$\text{Term } 4 = (1/4)(4/9)|\mathbf{V}_{131}|^2 + (4/3)\mathbf{V}_{131}\cdot\mathbf{V}_{311} + |V_{311}|^2]. \tag{A.21}$$

Considering the individual terms individually, it is clear that

$$\begin{aligned}(4/9)|\mathbf{V}_{131}|^2 &= (4/9)(\mathbf{V}_{131}\cdot\mathbf{V}_{131}) \\ &= (4/9)W_{131}^2[(\mathbf{H} - \mathbf{a}_{131})\cdot(\mathbf{H} - \mathbf{a}_{131})] \\ &= (4/9)W_{131}^2[\mathbf{H}\cdot\mathbf{H} - 2\mathbf{H}\cdot\mathbf{a}_{131} + \mathbf{a}_{131}] \\ &= (4/9)W_{131}^2[H^2 - 2Ha_{131}\cos\theta + a_{131}^2]. \end{aligned} \tag{A.21}$$

The term which follows is:

$$\begin{aligned}(4/3)(\mathbf{V}_{131}\cdot\mathbf{V}_{311}) = (4/3)W_{131}W_{311}\{&(\mathbf{H} - \mathbf{a}_{131}) \\ &\cdot[(\mathbf{H}\cdot\mathbf{H})\mathbf{H} + (\mathbf{H}\cdot\mathbf{a}_{311})\mathbf{H} + (\mathbf{H}\cdot\mathbf{H})\mathbf{a}_{311} \\ &+ 2(d_{311} + \mathbf{a}_{311}\cdot\mathbf{a}_{311})\mathbf{H} + (\mathbf{b}_{311}^2 + \mathbf{a}_{311}^2)\mathbf{H}^* \\ &- \mathbf{c}_{311} + (\mathbf{a}_{311}\cdot\mathbf{a}_{311})\mathbf{a}_{311}]\}. \end{aligned} \tag{A.22}$$

Simplifying, and writing out the dot product yields:

$$\begin{aligned}(4/3)(\mathbf{V}_{131}\cdot\mathbf{V}_{311}) = (4/3)W_{131}W_{311}\{&H^4 + (\mathbf{H}\cdot\mathbf{a}_{311})H^2 \\ &+ 2(d_{311} + a_{311}^2)H^2 + [(\mathbf{b}_{311}^2 + \mathbf{a}_{311}^2)\mathbf{H}^*]\cdot\mathbf{H} \\ &- \mathbf{c}_{311}\cdot\mathbf{H} + a_{311}^2(\mathbf{a}_{311}\cdot\mathbf{H}) - H^2\mathbf{a}_{131}\cdot\mathbf{H} - (\mathbf{H}\cdot\mathbf{a}_{131}\cdot\mathbf{H}) \end{aligned}$$

$$- H^2 a_{311} a_{131} - 2(d_{311} + a_{311}^2)(\mathbf{H}\cdot\mathbf{a}_{131}) - [(\mathbf{B}_{311}^2 + \mathbf{a}_{311}^2)\mathbf{H}^*]\cdot\mathbf{a}_{131}$$
$$+ \mathbf{c}_{311}\cdot\mathbf{a}_{131} + a_{311}^3 a_{131}] \qquad (A.23)$$

Performing the vector multiplications and the remaining dot products, and writing this in scalar form gives

$$(4/3)(\mathbf{V}_{131}\cdot\mathbf{V}_{311}) = (4/3)W_{131}W_{311}[H^4 + H^3 a_{311}\cos\theta$$
$$+ 2(d_{311} + a_{311}^2)H^2 + b_{311}^2 H^2\cos 2\theta + a_{311}^2 H^2\cos 2\theta$$
$$- c_{311}H\cos\theta + a_{311}^3 H\cos\theta$$
$$- H^3 a_{131}\cos\theta - H^2 a_{311}a_{131}\cos^2\theta$$
$$- H^2 a_{311}a_{131} - 2(d_{311} + a_{311}^2)Ha_{131}\cos\theta$$
$$- b_{311}^2 Ha_{131}\cos(-\theta) - a_{311}^2 a_{131}H\cos(-\theta)$$
$$+ c_{311}a_{131} + a_{311}^3 a_{131}]. \qquad (A.24)$$

Writing $\cos(2\theta)$ in terms of $\cos^2\theta$ and collecting terms gives:

$$(4/3)(\mathbf{V}_{131}\cdot\mathbf{V}_{311}) = (4/3)W_{131}W_{311}[H^4$$
$$+ H^2[2d_{311} - b_{311}^2 - a_{311}a_{131}]$$
$$+ [c_{311}a_{131} + a_{311}^3 a_{131}]$$
$$+ H^2\cos^2\theta\,[2b_{311}^2 + a_{311}a_{131}]$$
$$+ (\text{terms in } \cos\theta)]. \qquad (A.25)$$

The last term of Term 4 is:

$$|\mathbf{V}_{311}|^2 = \mathbf{V}_{311}\cdot\mathbf{V}_{311}^{*} \tag{A.26}$$

Recalling Equation (9.5), this may be written out as

$$\begin{aligned}
|\mathbf{V}_{311}|^2 = W_{311}^2\{&H^2\mathbf{H}\cdot H^2\mathbf{H} + 2H^2\mathbf{H}\cdot(\mathbf{H}\cdot\mathbf{a}_{311})\mathbf{H} + 2H^2\mathbf{H}\cdot H^2\mathbf{a}_{311} \\
&+ 2H^2\mathbf{H}\cdot 2(d_{311} + a_{311}^2)\mathbf{H} + 2H^2\mathbf{H}\cdot(\mathbf{b}_{311}^2 + \mathbf{a}_{311}^2)\mathbf{H}^{*} \\
&+ 2H^2\mathbf{H}\cdot\mathbf{c}_{311} + 2H^2\mathbf{H}\cdot a_{311}^2\mathbf{a}_{311} + (\mathbf{H}\cdot\mathbf{a}_{311})\mathbf{H}\cdot(\mathbf{H}\cdot\mathbf{a}_{311})\mathbf{H} \\
&+ 2(\mathbf{H}\cdot\mathbf{a}_{311})\mathbf{H}\cdot H^2\mathbf{a}_{311} + 2(\mathbf{H}\cdot\mathbf{a}_{311})\mathbf{H}\cdot 2(d_{311} + a_{311}^2)\mathbf{H} \\
&+ 2(\mathbf{H}\cdot\mathbf{a}_{311})\mathbf{H}\cdot(\mathbf{b}_{311}^2 + a_{311}^2)\mathbf{H}^{*} + 2(\mathbf{H}\cdot\mathbf{a}_{311})\mathbf{H}\cdot\mathbf{c}_{311} \\
&+ 2(\mathbf{H}\cdot\mathbf{a}_{311})\mathbf{H}\cdot(a_{311}^2)\mathbf{a}_{311} + H^2\mathbf{a}_{311}\cdot H^2\mathbf{a}_{311} \\
&+ 2H^2\mathbf{a}_{311}\cdot 2(d_{311} + a_{311}^2)\mathbf{H} + 2H^2\mathbf{a}_{311}\cdot(\mathbf{b}_{311}^2 + \mathbf{a}_{311}^2)\mathbf{H}^{*} \\
&+ 2H^2\mathbf{a}_{311}\cdot\mathbf{c}_{311} + 2H^2\mathbf{a}_{311}\cdot a_{311}^2\mathbf{a}_{311} \\
&+ 4(d_{311} + a_{311}^2)^2H^2 + 4(d_{311} + a_{311}^2)\mathbf{H}\cdot(\mathbf{b}_{311}^2 + \mathbf{a}_{311}^2)\mathbf{H}^{*} \\
&+ 4(d_{311} + a_{311}^2)\mathbf{H}\cdot\mathbf{c}_{311} + 4(d_{311} + a_{311}^2)\mathbf{H}\cdot a_{311}^2\mathbf{a}_{311} \\
&+ (\mathbf{b}_{311}^2 + \mathbf{a}_{311}^2)\mathbf{H}\cdot(\mathbf{b}_{311}^2 + \mathbf{a}_{311}^2)\mathbf{H} \\
&+ 2(\mathbf{b}_{311}^2 + \mathbf{a}_{311}^2)\mathbf{H}\cdot\mathbf{c}_{311} \\
&+ 2(\mathbf{b}_{311}^2 + \mathbf{a}_{311}^2)\mathbf{H}\cdot a_{311}^2\mathbf{a}_{311} + c_{311}^2 + 2\mathbf{c}_{311}\cdot a_{311}^2\mathbf{a}_{311} \\
&+ a_{311}^6\}.
\end{aligned} \tag{A.27}$$

The dot products are easily evaluated since the vectors $\mathbf{a}_{311}$, $\mathbf{b}_{311}^2$, and $\mathbf{c}_{311}$ lie on the H_y axis. Performing the dot products, writing the double angle expressions in terms of $\cos^2\theta$, and collecting terms yields:

$$
\begin{aligned}
|V_{311}|^2 = W_{311}^2\{&H^6 + H^4[4d_{311}-2b_{311}^2 + 3a_{311}^2] \\
&+ H^2[2a_{311}c_{311} + 2a_{311}^4 + 4(d_{311} + a_{311}^2)^2 \\
&\quad + 4(d_{311} + a_{311}^2)(b_{311}^2 + a_{311}^2) \\
&\quad + (b_{311}^2 + a_{311}^2)^2] \\
&+ [c_{311}^2 + 2c_{311}a_{311}^3 + a_{311}^6] \\
&+ H^4\cos^2\theta\,[4(b_{311}^2 + a_{311}^2) + a_{311}^2] \\
&+ H^2\cos^2\theta\,[2c_{311}a_{311} + 2a_{311}^4 \\
&\quad + 8(d_{311} + a_{311}^2)(b_{311}^2 + a_{311}^2)] \\
&+ [\text{terms in } \cos\theta]\}. \qquad \text{(A.28)}
\end{aligned}
$$

The three terms which make up Term 4 have now been calculated. Copnsidering the complexity of Term 4, it is easiest to integrate each of the three terms individually. Equation (A.21) gives the first term. Its integral is

$$I_{41} = (4/9)W_{131}^2[(1/3) + a_{131}^2]. \qquad \text{(A.29)}$$

The second term in the integral is given by Eq. (A.25), and integrates to

$$
\begin{aligned}
I_{42} = (4/3)W_{131}W_{311}[&(1/5) + (1/3)(2d_{311} - b_{311}^2 - a_{311}a_{131}) \\
&+ c_{311}a_{131} + a_{311}^3a_{131} + (\pi/3)(2b_{311}^2 + a_{311}a_{131})] \qquad \text{(A.30)}
\end{aligned}
$$

The last term in the integral is given by (A.28). Its integral is

$$I_{43} = W_{311}^2\{(1/7) + 1/5(4d_{311} - 2b_{311}^2 + 3a_{311}^2)$$
$$+ (1/3)[2a_{311}c_{311} + 2a_{311}^4 + 4Q_1^2 + 4Q_1Q_2 + Q_2^2]$$
$$+ [c_{311}^2 + 2c_{311}a_{311}^3 + a_{311}^6]$$
$$+ (\pi/5)[4Q_2 + a_{311}^2]$$
$$+ (\pi/3)[2c_{311}a_{311} + 2a_{311}^4 + 8Q_1Q_2\}, \qquad (A.31)$$

Where the quantities Q_1 and Q_2 have been defined as follows:

$$Q_1 \equiv d_{311} + a_{311}^2 \qquad (A.32)$$

$$Q_2 \equiv a_{311}^2 + b_{311}^2. \qquad (A.33)$$

The integral of Term 4 may now be written out as simply

$$\text{Integral } 4 = 1/4\ [I_{41} + I_{42} + I_{43}] \qquad (A.34)$$

Term 5

The last term in the integral of the wavefront variance is

$$\text{Term } 5 = (1/72)|\mathbf{V}_{131}|.^2 \qquad (A.35)$$

The squared magnitude of $\mathbf{V}_{131}$ was calculated earlier, during computation of one of the terms of Term 4. Referring to Eq. (A.21), one sees that

Term 5 may be immediately written as

$$\text{Term } 5 = (1/72)W_{131}{}^2[H^2 - 2Ha_{131}\cos\theta + a_{131}{}^2] \qquad (A.36)$$

The integral of this is easily seen to be

$$\text{Integral } 5 = (1/72)W_{131}{}^2[(1/3) + a_{131}{}^2] \qquad (A.37)$$

Since this is identical in form to the quantity I_{41}, it is easiest to define

$$I_{41}{}' \equiv [(4/9) + (1/72)]W_{131}{}^2[(1/3) + a_{131}{}^2]. \qquad (A.38)$$

Using this quantity in place of I_{41} in the summation for Integral 4 gives Integral 4', and Integral 5 is now dropped.

The final integral may now be written:

$$(Wms)_{avg} = (1/\pi)[\text{Integral } 1 + \text{Integral } 2 + \text{Integral } 3 + \text{Integral } 4']. \qquad (A.39)$$

SELECTED BIBLIOGRAPHY

Buchdahl, H. A., Optical Aberration Coefficients, Oxford University Press, London (1954).

_____, An Introduction to Hamiltonian Optics, Cambridge University Press, London (1970).

Buchroeder, R. A., "Tilted Component Optical Systems," Ph.D. dissertation, Optical Sciences Center, University of Arizona (1976).

Burch, C. R., "On the Optical See-Saw Diagram," Mon. Not. R. Astron. Soc. 201, 159 (1942).

Conrady, A. E., "Decentered Lens Systems," Mon. Not. R. Astron. Soc. 79, 384 (1919).

Epstein, L. I., "The Aberrations of Slightly Decentered Optical Systems," J. Opt. Soc. Am. 39, 10, 847 (1949).

Hofman, Chr., and J. Kiebe, "Uber eine allgemein aus dem Eikonal ableitbare Abbildungsgleichung fur beliebig dezentierte Flachen aller Art, die eine Verallgemeinerung der Sturmschen Formeln fur darstellt, und der uber deren Anwendung zur Bestimmung aspharisher Flachen," Optik 22, 2, 95 (1965).

Hopkins, G. W., "Aberrational Analysis of Optical Systems: A Proximate Ray Trace Approach," Ph. D. dissertation, Optical Sciences Center, University of Arizona, (1976).

Hopkins, H. H., "A Transformation of Known Astigmatism Formulae," Proc. Phys. Soc. Lond., 58, 663 (1946).

_____, Wave Theory of Aberrations, Oxford University Press, London (1950).

_____, Applied Optics and Optical Engineering, V.9 ed. Shannon and Wyant, Academic Press (1983).

Korsch, D., "Reflective Schmidt Corrector," Appl. Opt. 13, 2005 (1974).

_____, "Aplantic Two-Mirror Telescope from Near-Normal to Grazing Incidence," Appl. Opt. 19, 499 (1980a).

Korsch, D., "Design and Optimization Technique for Three-Mirror Telescopes," App. Opt. 19, 3640 (1980b).

Linfoot, E. H., "On Decentered Aspheric Plates," Proc. Phys. Soc. Lond., 58, 65 (1946).

Prasad, J., G. Mitra, and P. K. Jain, "Aberrations of a System of Arbitrarily Inclined Planar Surfaces placed in Non-Collimated Light Beam," Nouv. Rev. Optique 6, 6, 345 (1975).

Rimmer, M., "Optical Aberration Coefficients," Appendix IV of the Ordeals II Program Manual, Tropel Inc., 52 West Ave., Fairport, New York, (1965).

Ruben, P. L., "Aberrations Arising from Decentrations and Tilts," J. Opt. Soc. Am. 54, 45 (1964).

Sands, P. J., "Off-Axis Aberration Coefficients," Ph. D. dissertation, Australian National University (1967).

Shearer, J., "Geometrical Optics of Concave Mirrors and of Combinations of Mirrors," Australian J. Sci. Res. A. 3, 532 (1950).

Thompson, K. P. "Aberration Fields of Tilted and Decentered Optical Systems," Ph. D. dissertation, Optical Sciences Center, University of Arizona (1980).

Ukita, Y., and T. Tsujiuchi, "On the Wave Aberrations of a Decentered Lens System with a Finite Aperture," J. Phys. Soc. Japan 9, 502, (1945).

Weinstein, W., "Wave-front Aberrations of Oblique Pencils in a Symmetrical Optical System: Refraction and Transfer Formulae," Proc. Phys. Soc. Lond. 62B, 726 (1949).

_____, "The Computation of Wave-front Aberrations of Oblique Pencils in a Symmetrical Optical System," Proc. Phys. Soc. Lond., 63B, 709 (1950).

Welford, W. T. Aberrations of the Symmetrical Optical System, Academic Press, New York, (1974).

Wynne, C. G., "Primary Aberrations and Conjugate Change," Proc. Phys. Soc. Lond., B65, 429 (1952).